Dnajc22 - a new susceptibility gene for salt-sensitive hypertension

Dissertation

zur

Erlangung des Doktorgrades (Dr. rer. nat.)

der

Mathematisch-Naturwissenschaftlichen Fakultät

der

Rheinischen Friedrich-Wilhelms-Universität Bonn

vorgelegt von

ANNA C. ASCHENBRENNER

aus Reinbek

Bonn 2013

Angefertigt mit Genehmigung der Mathematisch-Naturwissenschaftlichen Fakultät der Rheinischen Friedrich-Wilhelms-Universität Bonn

1. Gutachter: Prof. Dr. Michael Hoch

LIMES Institut, Programmeinheit Entwicklungsbiologie, Genetik & Molekulare Physiologie, Labor für Molekulare Entwicklungsbiologie, Universität Bonn

2. Gutachter: Prof. Dr. Waldemar Kolanus

LIMES Institut, Programmeinheit Molekulare Immun- und Zellbiologie, Labor für Immun- und Stammzellbiologie, Universität Bonn

Tag der Promotion: 24.06.2014

Erscheinungsjahr: 2015

Table of contents

Summary

The ability of an organism to maintain its osmotic balance is of fundamental importance to protect its cells from hyperosmotic stress. Proper function of the kidneys is key to this osmoregulation, as it controls the reabsorption and excretion and of electrolytes. If the organism is not capable of matching the renal secretion to its dietary intake, this will consequently affect blood pressure. Hypertension is a major risk factor for peripheral vascular disease, congestive heart failure, myocardial infarction, stroke, and overall mortality, affecting nearly one billion people worldwide. Deciphering the regulatory networks, molecular mechanisms, and identifying the genetic factors involved in osmoregulation and its pathological alterations is thereby of utmost importance to develop effective therapies for this enormous public health challenge.

In this present work, I describe *Dnajc22* as a new osmoregulator in mammals. DNAJC22 is an evolutionary highly conserved member of the J protein family, bearing a single ortholog in fruit fly, zebrafish, mouse, and human. No functional data for its importance in mammalian physiology had been published before. Expression analyses revealed that *Dnajc22* is primarily expressed in the liver, the intestine, and the kidneys. To be able to analyze the physiological function of DNAJC22 in mammals, a conditional *Dnajc22* mouse model was generated using a combination of recombineering and standard cloning techniques. *Dnajc22* knockout mice are viable and revealed no obvious major alterations on a morphological as well as histological level. While basic renal functions, such as glomerular filtration and water balance, seem unaffected in the *Dnajc22*-deficient animals, electrolyte handling is slightly disturbed in normal conditions and the peripheral blood pressure moderately increased. After receiving a high salt diet, urine analyses revealed that *Dnajc22* knockout mice are not able to cope with the electrolyte challenge as well as their wildtype littermates, as they secrete less sodium and chloride. Consequently they suffer from an elevated peripheral blood pressure.

In parallel to the *in vivo* analyses, I used murine cortical collecting duct cells (M-1) as a system to model the consequences of varying electrolyte changes on a cellular level to further examine the molecular mechanism of DNAJC22. These studies identified *Dnajc22* as a new player of the hyperosmotic stress response. Subjecting M-1 cells to various hyperosmotic stressors induced *Dnajc22* transcript levels – a response that persists at least for 24 hours and which could be abrogated by inhibiting sodium influx into the cell with amiloride.

To gain further insight into the molecular function of DNAJC22, studying subcellular localization of the protein in a heterologous expression situation demonstrated that

DNAJC22 is a transmembrane protein in the endoplasmic reticulum and with a fluorescence protease protection assay I could show that the J domain is facing the cytoplasm. J proteins are cochaperones that stimulate the ATPase activity of heat shock (HSP) 70 proteins through interaction with their J domain. As DNAJC22 is expressed in the epithelial cells of cortical renal tubules, the working hypothesis is that it may influence electrolyte transport in these cells: on the one hand it could serve as a quality control check point at the ER surveying transporter or channel assembly and their export to the Golgi, on the other hand DNAJC22 could influence clathrin-mediated endocytosis, thereby regulating transporter or channel activity via their abundance at the plasma membrane.

This work is the first description of the physiological function of mammalian DNAJC22. It is not only part of the hyperosmotic stress response in the cell, but also involved in the osmoregulation of the organism by influencing renal electrolyte handling and thus blood pressure. The present findings provide evidence that Dnajc22 is a susceptibility gene for salt-sensitive hypertension.

1 Introduction

1.1 Osmoregulation in the organism

Osmolality of the body fluids is tightly controlled in the organism in order to prevent extensive fluctuations in extra- and intracellular volumes, hence osmotic stress from its cells. Changes in plasma osmolality are registered by osmosensors in the central nervous system. Raising the extracellular osmolality, e.g. by loss of water or the dietary uptake of sodium chloride, leads to a loss of cell volume in the neurons of the hypothalamus, which react with the production of the hormone vasopressin and release thereof via their axon endings in the posterior pituitary gland into the blood stream. Vasopressin has a water-conserving effect on the renal collecting ducts in which it increases water permeability. More water is reabsorbed, the organism excretes higher concentrated urine, and consequently, the hyperosmotic plasma is counteracted by expanding the extracellular volume. Besides the vasopressin release, central osmosensors in the hypothalamus also trigger hyperosmotic thirst. In addition to increased water retention, the organism is prompted to replenish its body fluid[1,2].

The regulation of plasma osmolality is dependent on systemic salt homeostasis; hence the proper function of the kidney balancing electrolyte excretion and reabsorption is of fundamental importance.

1.1.1 The role of the kidney in osmoregulation

The basic function of the kidney is the filtration of the organism's blood and the reabsorption of valuable solutes as well the excretion of currently useless components and secretion of metabolic end products and xenobiotics (e.g. urea or drugs). It is essential for the maintenance of two major homeostatic balances in the organism: osmotic balance (fine-tuning volume and osmolality of the extracellular space) by controlling salt and water excretion and the acid-base balance by regulating proton and bicarbonate excretion[3].

The functional unit of the kidney is the nephron. It comprises the glomerulus, the renal tubule and the terminal collecting duct (Figure 1.01). The glomerulus is located in the cortex of the organ and consists of an intricate capillary bundle, which is nearly completely

engulfed by the beginning of the proximal tubule, forming Bowman's capsule. Over this filtration barrier made up of the vascular fenestrated endothelium, the extracellular basal membrane, and the podocytes on the side of the tubule, a specialized cell distinguished by its characteristic foot processes, the blood is filtrated to produce the primary urine in the tubule lumen. The renal tubule passes from the cortex into the medulla of the kidney and turns up again into the cortical region. It is subdivided into the proximal part, the loop of Henle (consisting of the thin descending and the thick ascending limb), the distal part, and the connecting tubule. Along its way through the tubule the primary urine is considerably modified as solutes are differentially reabsorbed and secreted in the mentioned segments.
In the cortex the distal tubules coalesce via connecting tubules in collecting ducts in which the urine composition is ultimately defined. The collecting ducts transverse the kidney one more time from cortex to medulla and end at the renal papilla. Here the urine drains into the calyx and eventually via the ureter into the bladder[3].

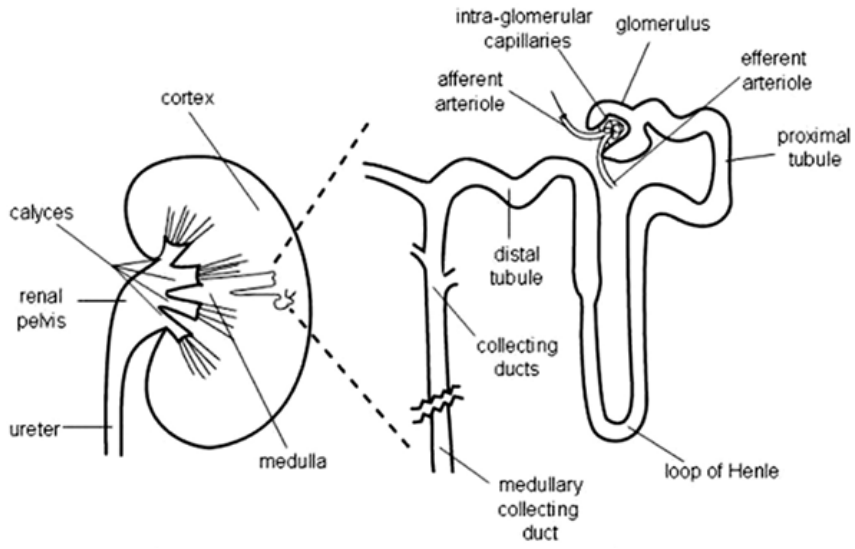

Figure 1.01 The kidney and the nephron
Schematic overview over the anatomy of the kidney and its functional unit, the nephron (modified from[4]).

Sodium

Sodium is freely filtered by the glomerulus and consequently reabsorbed in every part of the tubule. Over 99% of the filtrated sodium is retrieved under normal conditions[5].
The tubular epithelium consists of polar cells having a distinct apical site facing the tubular lumen and primary urine and a basolateral site adjacent to the interstitium and the vascular system of the organ[6]. The basolateral Na^+-K^+-ATPase actively exports sodium out of the cell into the blood creating a chemical sodium gradient over the epithelium. For every sodium ion, two potassium ions are imported into the cell. Due to back-diffusion of potassium out of the cell this is resulting in an electrical gradient. Taken together, this electrochemical

gradient is the driving force behind the sodium reabsorption establishing the basis for a passive sodium influx into the cell[5].

About 65% of the filtrated sodium is resorbed in the proximal tubule. One third is passively taken up via the Na^+/H^+-exchanger NHE3 (*Slc9a3*)[7] as well as via several symporters that use the sodium gradient to secondary actively reabsorb glucose and other substrates. The other two thirds follow passively on a paracellular route. This is on one hand due to electric potential differences, on the other hand due to the solvent drag of water that passively follows the osmotic gradient. Further 25% are taken up in the loop of Henle where sodium passes the apical plasma membrane of the tubule cells via the Na^+-$2Cl^-$-K^+-co-transporter (NKCC2, *Slc12a1*). Luminal sodium concentration decreases. Fine-tuning of the finally excreted amount occurs in the more distal parts of the nephron and the collecting duct. In the distal convoluted tubules sodium reabsorption is mediated by the electroneutral, thiazide-sensitive Na^+-Cl^--co-transporter (NCC, *Slc12a3*) and in the late portion of the distal convoluted tubule, the connecting tubule and the collecting duct via the amiloride-sensitive epithelial sodium channel (ENaC, *Scnn1a-c*)[5] (Figure 1.02).

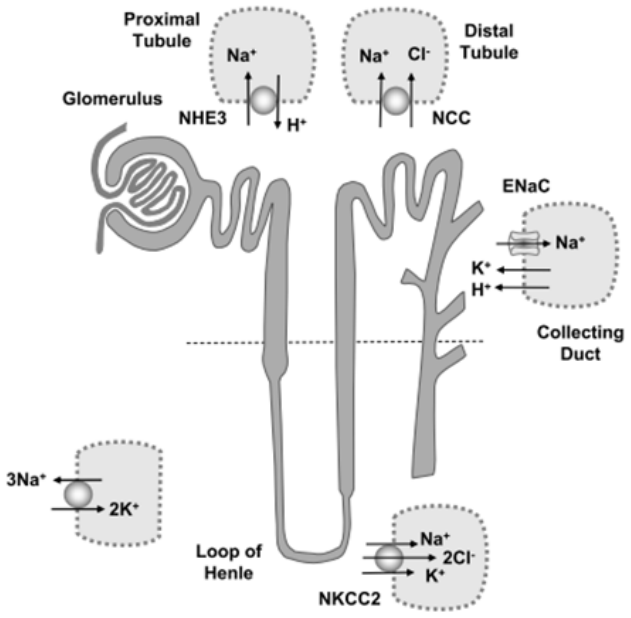

Figure 1.02 Sodium reabsorption in the nephron

NHE3 is located at the apical side of proximal tubule cells. In the thick ascending limb apical NKCC2 mediates sodium reabsorption and in the distal tubule NCC is expressed. ENaC are the predominant sodium channels in the collecting duct. The basolateral Na^+-K^+-ATPase generates the electrochemical gradient needed for sodium reabsorption in all segments of the nephron (modified from[8]).

Chloride

As for sodium, 95-99% of the filtrated chloride is reabsorbed. Chloride resorption is closely linked to that of sodium and water. About 50% is retrieved in the proximal tubule where it

diffuses passively via a paracellular route over the epithelium along its electrochemical gradient. In the thick ascending limb of the loop of Henle and in the distal tubule, chloride enters the cell secondary actively with the described sodium symporters. Chloride channels located at the basal membrane mediate the passive transport out of the cell into the interstititum[5].

Potassium

About 65% of the filtrated potassium gets resorbed in the proximal tubule, for the most part passively via the paracellular route. In the loop of Henle additional 15% leave the lumen in trans- and paracellular fashion. The final excreted amount is determined in the connecting tubule and collecting duct where potassium may be further resorbed or secreted as necessary. Type A intercalated cells can take up potassium via an apical H^+/K^+-ATPase and secretion via the renal outer medullary potassium channel (ROMK) is coupled to the sodium reabsorption (via ENaCs) in principal cells[9,10].

1.1.2 Hypertension due to dysfunctional osmoregulation

Combined research on mutations in humans as well as studies using animal models has provided insight into the different mechanisms and genes responsible for blood pressure maintenance. Many of these are involved in the regulation of salt and water reabsorption in the kidney[11,12].

Systemic osmoregulation has indeed a pivotal impact on blood pressure. Variations in osmolality are counteracted with adjustments in the extracellular volume. Hence, if the organism is not capable of matching the renal excretion to a heightened sodium chloride intake, this will lead to a compensatory extracellular volume expansion and therefore high blood pressure[13].

The importance of sodium reabsorption in the kidney for the maintenance of blood pressure has been demonstrated by several knockout mouse models as well as mutations in humans associated with blood pressure disorders. Loss of function of the renal sodium transporters NHE3[14–16] in the proximal tubule and thick ascending limb, NKCC2[17,18] in the thick ascending limb, NCC[19,20] in the distal tubule, and ENaC[21–24] in the distal tubule and collecting duct lead to a reduction in blood pressure. Mutations that provoke aberrant sodium retention can lead to hypertension as in pseudohypoaldosteronism type II (PHAII / familial hyperkalemic hypertension or Gordon's syndrome) and Liddle's syndrome. Gain of function mutations in the beta and gamma subunits of the ENaC result in the latter[25–27], whereas mutations in several genes have been associated with PHAII. The kinases WNK4[28–31] and WNK1[30–32] (with no lysine (K)) as well as Kelch-like 3 (KLHL3) and Cullin 3 (CUL3)[33,34] proved to regulate

proper channel trafficking to the plasma membrane or degradation thereof – all in all leading to an enhanced activity of NCC in the distal tubule. Further studies have also shown a role for dopamine in the regulation of sodium transport in the proximal tubulus[35].

In recent years it has become evident, that aside from the kidney, also the impact of blood sodium levels on the vascular system and the regulation of salt accumulation in the skin can have a crucial impact on the development of salt-sensitive hypertension[36,37]. Vascular endothelial cells react to elevated sodium in the blood via an ENaC-mediated pathway with an increase in stiffness and thereby vascular tone[36,38]. Excessive salt can accumulate in the interstitium of the skin, from where it is eliminated via the lymphatic system. Indeed, cells of the mononuclear phagocyte system are able to sense the hypertonicity and activate lymphangiogenesis via a signaling pathway comprising NFAT5 and VEGFC and thereby counteract salt-sensitive hypertension[37,39–41].

1.2 Cellular response to hyperosmotic stress

The functional building block of multicellular organisms – the cell – is constantly exposed to varying ion concentrations of its surrounding, however it is also dependent on the exchange and thereby communication with it. Many different ion channels and transporters mediate the flux of solutes over its enclosing plasma membrane, assuring compliance of their tightly controlled intracellular concentrations.

Osmolality is a measurement of the concentration of all osmotic active particles per mass and their total amount defines the osmotic pressure it exerts[42]. While being freely permeable to water, the plasma membrane of the cell is semipermeable to other substances and thereby enables the cell to maintain an intracellular concentration of solutes distinct from those in the extracellular surrounding.

When the extracellular space exceeds the osmolality within the cell, it is exposed to hyperosmotic stress. Due to the tonicity difference between intra- and extracellular space, water exits the cell and the cell volume decreases. At some point this state will turn critical due to nuclear condensation, DNA damage, and consequent cell cycle arrest as well as macromolecular crowding, protein aggregation and consequent interference with enzyme activities. The cell also faces mitochondrial depolarization and oxidative stress. In order to counteract these adversities, the cell has several molecular coping mechanisms at hand – including cytoskeletal rearrangements, up-regulation of osmolyte production as well as induction of molecular chaperones (such as heat shock proteins), transporters, and

antioxidant enzymes. If too much damage accumulates, the cell eventually undergoes apoptosis[43] (Figure 1.03).

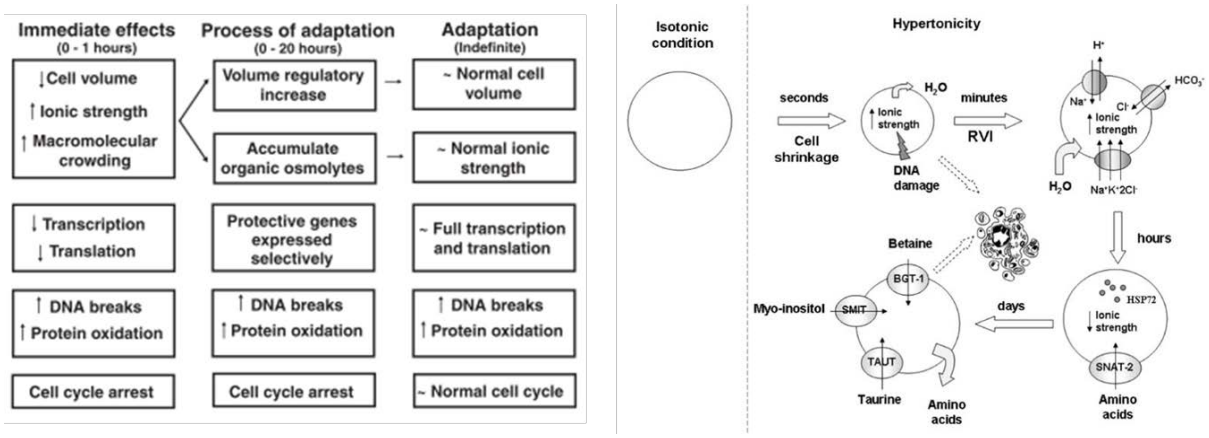

Figure 1.03 Cellular adaptation to hyperosmotic stress
(modified from[44,45])

Within minutes the cell responds to osmotic efflux of water with a regulatory volume increase mediated by the heightened import of potassium chloride as well as sodium chloride and the consequent re-influx of water. The inorganic ions enter the cell via already present transporters, such as the Na^+-K^+-$2Cl^-$ symporter (NKCC), the Na^+/H^+, and the $Cl^-/HCO3^-$ exchangers[46]. Later, the cell replaces these inorganic ions with osmolytes – small-organic molecules – to avoid harmful side effects of relatively high intracellular sodium, potassium, and chloride concentrations on its metabolism[45] (Figure 1.04). Altered intracellular ionic strength can impair the rates of enzymatically catalyzed reactions, cause macromolecules to denature or precipitate, and their concentration has an impact on the resting membrane potential as well as on ion gradients necessary for solute transport. Osmolytes, however, do not perturb cellular functions even at high concentrations[46]. Many of them can even act as chemical chaperones helping proteins sustain their structure and function[47]. Accumulation of these is achieved by the cell through direct synthesis and increased import thereof[48].

The transcription factor Nuclear factor of activated T-cells 5 (NFAT5) is considered one of the key regulators that gets activated under hyperosmotic stress and orchestrates many of the mentioned stress response mechanisms[49]. Upon activation it quickly up-regulates heat shock proteins[50,51]. Heat shock proteins protect the cell until they accumulate osmolytes. They help the cell to protect macromolecules from unfolding and aggregation[52] as well as to prevent apoptosis[53,54]. Induction of HSPs is succeeded by the up-regulation of osmolyte-producing enzymes, such as aldose reductase (AR) [55,56] for sorbitol, and osmolyte transporters, such as the betaine/γ-aminobutyric acid transporter (BGT1)[57,58], the

sodium/*myo*-inositol transporter (SMIT)[59,60], or the taurine transporter (TAUT)[2]. As a result, the cell is able to increase the amount of intracellular osmolytes and counteract the hyperosmotic stress.

1.3 DNAJC22 – a member of the J protein family

1.3.1 J proteins

J proteins are named after the first known member '*DnaJ*' from the bacterium *Escherichia coli*. All family members feature a so-called J domain – the functional protein domain determining this protein family. It is highly conserved between the family members, particularly the histidine, proline, and aspartate (HPD) tripeptide, which is crucial for J domain functionality[61,62].

J proteins assist the heat shock (HSP) 70 proteins as cochaperones. They can interact with specific clients, and are thereby involved in classical HSP functions such as protein folding, degradation, oligomerization or transport. More precisely, client-binding and release is an ATP-dependent cycle for the HSP70s. J proteins stimulate the ATPase activity of HSP70s through interaction with their J domain, thus help exert the heat shock proteins' functions. It has also been discovered that the J proteins can be the first to bind the client protein and target it to the HSP70 machinery[62].

J proteins have been classified into the three subfamilies – A, B, and C – based on the presence of additional functional protein domains[62–66] (Figure 1.4).

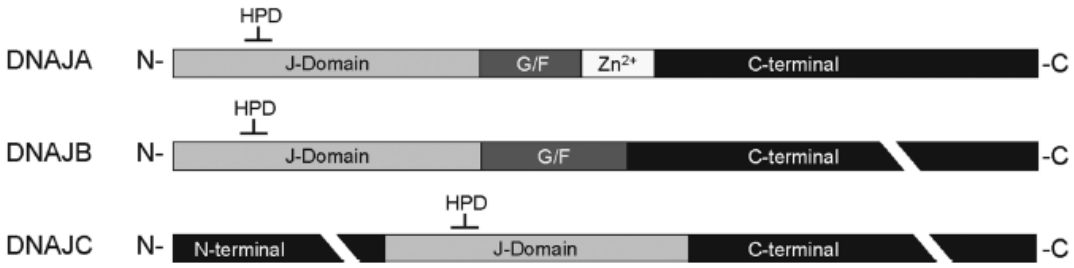

Figure 1.04 J protein subfamilies

J proteins are divided into three subfamilies A, B, or C depending on additional predicted protein domains. Subfamily A members are closely related to E. coli DnaJ. The N-terminal J domain is followed by a glycine/phenylalanine (G/F)-rich region, a cysteine-rich region, and a variable C-terminal part. Subfamily B members resemble subfamily A members but lack the cysteine-rich region. All other proteins containing a J domain belong to subfamily C (modified from[67]).

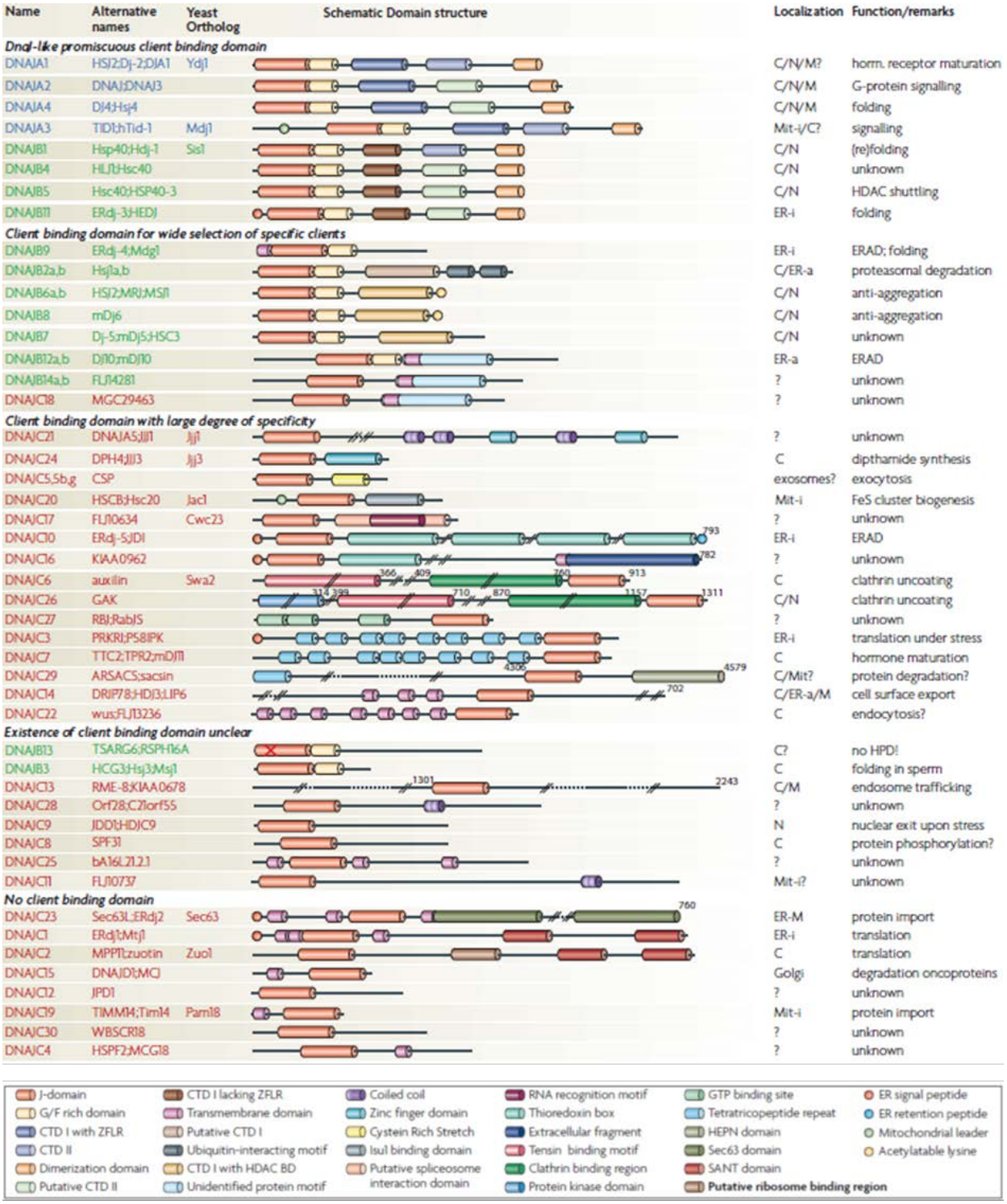

Figure 1.05 Diversity of human J proteins

Domain structure of human J proteins. Human and yeast J protein family members are clustered according to their known or presumed client-binding ability, and functional orthologs are connected by lines. For clarity, some domains and some differences between yeast and human orthologs are not shown. Abbreviations for intracellular localization: C – cytosol, N – nucleus, M – membrane-associated, Mit – mitochondrial, ER – endoplasmic reticulum, i – inside, a – associated. CBD – client binding domain, CTD – c terminal domain I, ERAD – ER associated degradation, HDAC – histone deacetylase, HEPN – higher eukaryotes and prokaryotes nucleotide-binding domain, SANT – Swi3, Ada2, N-CoR and TFIIIB domain, ZFLR – zinc finger like region (modified from[62]).

Class A J proteins are the closest orthologs of the family's founding member *DnaJ* from *Escherichia coli*. They possess an N-terminal J domain followed by a glycine and phenylalanine-rich region, a zinc finger motif, two client-binding domains and a C-terminal dimerization motif.
Class B J proteins feature the N-terminal J domain succeeded by the Gly-Phe-rich region as the A subfamily, but lack the zinc-finger domain.
All other proteins containing a J domain which do not fall into class A or B compose the C subfamily.

It should be noted that the subclassification of the J protein family members by the NCBI accepted nomenclature[65,68] is strictly based on predicted protein domains and may not match their actual function. In the most recent review of the protein family, Craig and Kampinga have therefore put more emphasis on the ability to bind clients (Figure 1.05). It is also questionable if the glycine and phenylalanine-rich region is of any functional relevance beyond being a flexible spacer between the other domains[62].
Whereas the number of different HSP70s in a cell is relatively low, there exists a high diversity of cochaperones. In humans, there are for example only eleven HSP70s, but 41 J proteins. The murine J protein family has 44 members. In contrast to the HSP70s, J proteins are structurally very diverse. It is believed that they account for the multifunctionality of the HSP70 machinery. By influencing localization and interaction with other factors and clients, the J proteins may determine the specificity and function of the HSP70 proteins[62,65,69].

1.3.2 The *Drosophila melanogaster* DNAJC22 ortholog Wurst

DNAJC22 function was first studied in the fruit fly *Drosophila melanogaster*, in which its ortholog Wurst was identified as a regulator of clathrin-mediated endocytosis in barrier epithelia[70].
In particular, it was shown to have a fundamental function in the development of the tracheal system – the respiratory organ of the fly. *Drosophila* Wurst influences tube size and regulates lumen clearance of the fly airways to enable breathing after hatching of the larvae. Mutants lacking the gene consequently die at the end of embryogenesis or as early L1 larvae[70,71].
Wurst is a multi-span transmembrane protein with a C-terminal J domain that was found to biochemically interact with heat shock cognate protein 70-4 (HSC70-4) and clathrin. Localization studies showed that Wurst recruits both proteins to the apical membrane. Endocytosis is impaired in the mutant as well as after knockdown via RNAi in S2 cells as shown via fluorescent dye uptake experiments[70]. It was therefore argued, that Wurst may

facilitate clathrin and HSC70-4 binding at the site of vesicle formation and that it stays present in the vesicles that enter the endosomal pathway[72].

Lung liquid clearance in mammals is dependent on the sodium gradient established by epithelial sodium channels (ENaC) located in the apical membrane of lung epithelial cells[73,74]. The orthologous pickpocket (PPK) genes 4 and 11 in *Drosophila* likewise play a role in tracheal lumen clearance[75]. Corroborated by genetic interaction experiments, they were proposed as potential cargo molecules[70,72].

1.3.3 DNAJC22 in vertebrates

A single ortholog of DNAJC22 has been identified in many vertebrate species[72,76]. Apart from its J domain, no other functional protein domain has been predicted. It is therefore a member of the C subfamily of J proteins. In this diverse subclass, it stands out when comparing the overall domain structures. Unlike the other J proteins, DNAJC22 is a unique multi-span transmembrane protein and in contrast to most of the other J proteins, its J domain is located at the C terminus.
Murine and human DNAJC22 are about 50% identical to *Drosophila* Wurst and show a similarity of 68%. Dividing the protein into the N-terminal part and the C-terminal J domain shows the especially strong conservation of the J domain (Figure 1.06).

	% id	% sim
complete protein		
D.m. vs. *M.m.*	49	67
D.m. vs. *H.s.*	50	68
M.m. vs. *H.s.*	83	89
N-terminal part		
D.m. vs. *M.m.*	48	66
D.m. vs. *H.s.*	53	71
M.m. vs. *H.s.*	82	89
J domain		
D.m. vs. *M.m.*	60	78
D.m. vs. *H.s.*	60	77
M.m. vs. *H.s.*	85	94

Figure 1.06 Sequence comparisons of *Drosophila*, murine, and human DNAJC22

DNAJC22 protein sequences of *Drosophila* (*D.m.*), mouse (*M.m.*) and human (*H.s.*) were blasted with the alignment tool from NCBI (bl2seq).

In fruit fly and human, both protein termini are predicted to reside in the cytoplasm. Yet for the murine protein, prediction tools for the transmembrane topology gave differing results of either five or six domains[77] (see Results 2.1.2). As a protein with an uneven number of transmembrane domains would have protein termini on opposite sides of the membrane, it will be important to know in which subcellular compartment the J domain is located.

Studies on the cellular heat stress response have shown that human DNAJC22 is not up-regulated in HeLa cells after exposure to heat[64].The so-called heat shock factors (HSFs) are the master regulators of transcription when overall transcription is silenced upon heat stress. Under these protein-damaging conditions, they mediate expression of polyubiquitin genes, cochaperones, transcriptional regulators, and signaling molecules to help maintain the cellular homeostasis[78]. A study investigating the target genes of HSFs showed that, in contrast to many other members of the J protein family, the *DNAJC22* promoter is not occupied by the heat shock factors (HSFs) upon heat stress.

No studies explaining the function of DNAJC22 in vertebrates have been published so far.

1.4 Aim of the thesis

The aim of this thesis was to elucidate the physiological role of mammalian *Dnajc22* using the mouse as a model organism.

Investigations in our laboratory had shown that the orthologous *wurst* gene in *Drosophila melanogaster* plays a fundamental role in barrier epithelia, as shown for the proper development and function of the tracheal system[70]. Yet until now, the function of mammalian *Dnajc22* has not been studied.

I planned to generate a mouse model lacking *Dnajc22* and investigate the consequences. These phenotypic analyses were to be further complemented by *in vitro* cell culture studies in order to be able to draw conclusions concerning the function of *Dnajc22* in mouse and possibly humans.

2 Results

2.1 Molecular analysis of DNAJC22

2.1.1 Subcellular distribution of overexpressed DNAJC22-GFP

In order to study the subcellular localization of murine DNAJC22, I overexpressed a GFP-tagged version of the protein in the murine kidney cell line M-1.

GFP signal was concentrated in a ring enclosing the nucleus and showed a reticulate distribution throughout the cytoplasm (Figure 2.01). Sometimes the structures of nuclear reticulum were seen as well (Figure 2.02 C).

DNAJC22-GFP does not seem to reside predominantly at the plasma membrane as there appears to be a gap of signal between the two transfected cells (Figure 2.01). Further, the co-staining with phalloidin, a marker for filamentous actin that is predominantly distributed at the plasma membrane of the depicted confluent cells, revealed no apparent colocalization (Figure 2.02 A). Yet, live co-staining with different cellular markers show an overlap with the ER, but not with mitochondria or lysosomes (Figure 2.02 B, C).

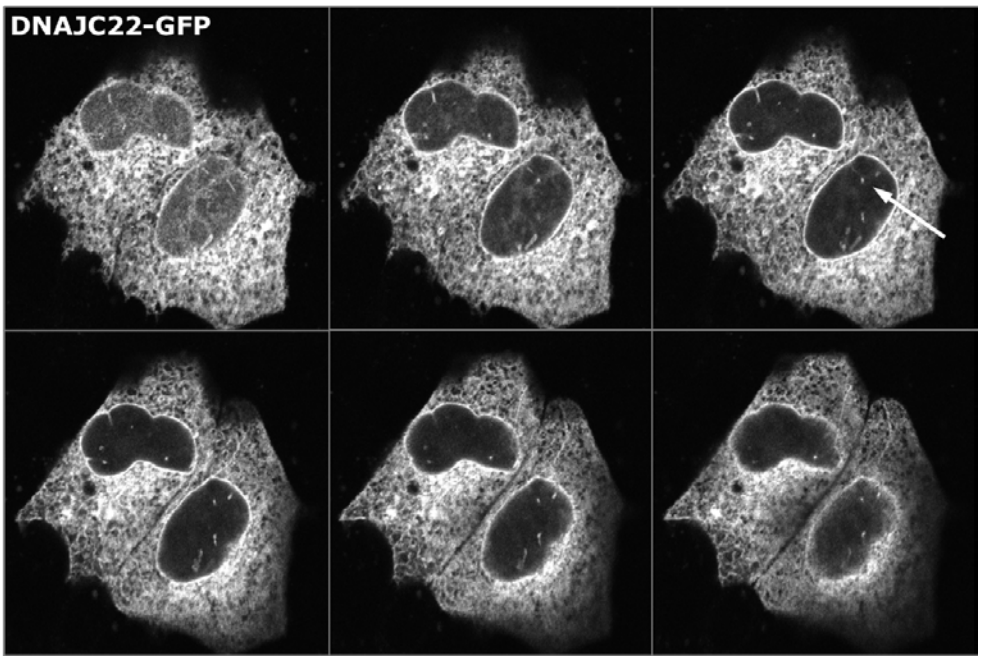

Figure 2.01 DNAJC22-GFP overexpressed in M-1 cells

Z stack of GFP signal showing signal of DNAJC22-GFP in the ER as well as the nuclear reticulum (arrow). Series of slices from top left to bottom right corner.

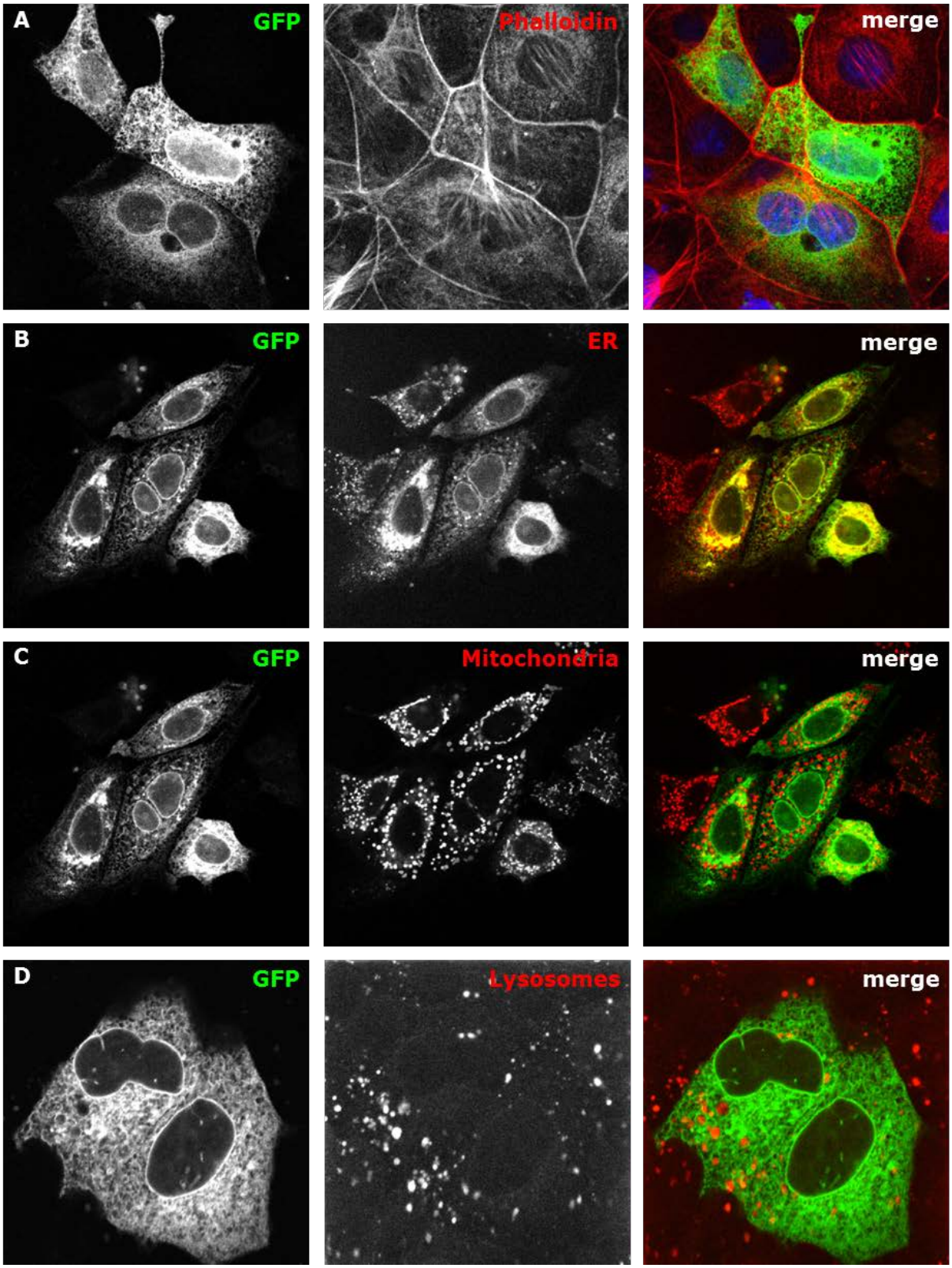

Figure 2.02 Co-staining of overexpressed DNAJC22-GFP with different subcellular markers in M-1 cells

A Phalloidin for filamentous actin visualization **B** ER-Tracker **C** MitoTracker **D** LysoTracker

2.1.2 Localization of the functional J domain

In my diploma thesis, I analyzed the transmembrane topology of DNAJC22[77]. While there was a clear prediction of six transmembrane domains for the *Drosophila* and human orthologs, Wurst and DNAJC22 respectively, different algorithms calculated ambiguous results for the murine protein. Either five or six transmembrane domains were predicted depending on the tool used. The hydrophobicity plot generated with the TMHMM algorithm indicated that the predicted fifth domain may actually consist of two (Figure 2.03 / The first hydrophobic region displayed is actually the predicted signal peptide.).

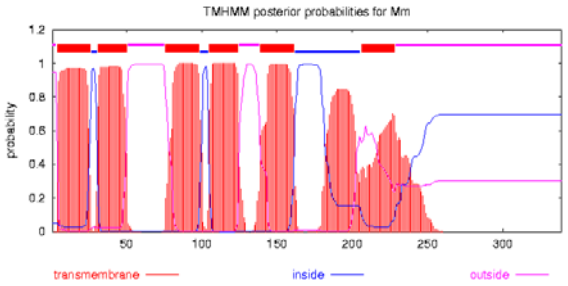

Figure 2.03 TMHMM 2.0 transmembrane domain prediction for murine DNAJC22[77]

In order to clarify the subcellular localization of the C-terminus of DNAJC22, I performed a fluorescence protease protection assay[79]. Locating the C-terminus of the protein is of essential importance as it contains the only predicted functional domain of the protein – the J domain.

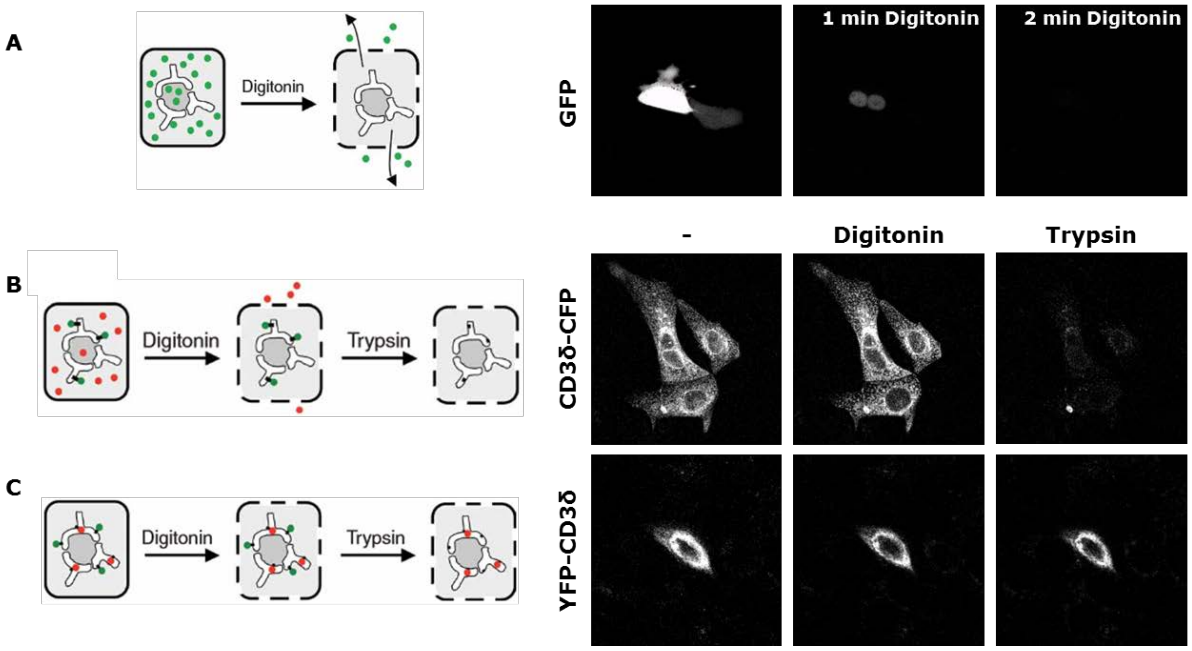

Figure 2.04 Principle of the fluorescence protease protection assay

Different overexpressed control constructs in M-1 cells show selective accessibility towards plasma membrane permeabilization by digitonin and proteolytic digest with trypsin. **A** Soluble GFP diffuses out of the cell upon digitonin treatment (first cytosolic and then nuclear GFP) **B** ER-resident transmembrane protein CD3δ-CFP is not affected by digitonin treatment, but CFP signal at the cytosolic C-terminus is lost upon addition of trypsin **C** Overexpressed YFP-CD3δ is not affected by either treatment showing ER luminal localization of the N-terminus including the tag (schematic pictures modified from[79])

Live M-1 cells overexpressing different GFP constructs were analyzed for the loss of GFP fluorescence after adding a protease to the cells with or without plasma membrane permeabilizing conditions. Protein topology can be inferred from the accessibility of the GFP-tag to the protease (Figure 2.04).

Addition of extracellular trypsin to M-1 cells heterologously expressing DNAJC22-GFP did not alter the fluorescent signal, showing an intracellular localization of the C-terminus of the protein (data not shown). Also, digitonin treatment did not diminish the signal, confirming a transmembrane or cellular compartment-enclosed localization since plasma membrane permeabilization alone did not lead to a loss of signal due to diffusion of the protein. However, a combined treatment with digitonin and trypsin led to a strong reduction in GFP signal disclosing the DNAJC22 C-terminus to be accessible by the protease via the cytoplasm (Figure 2.05).

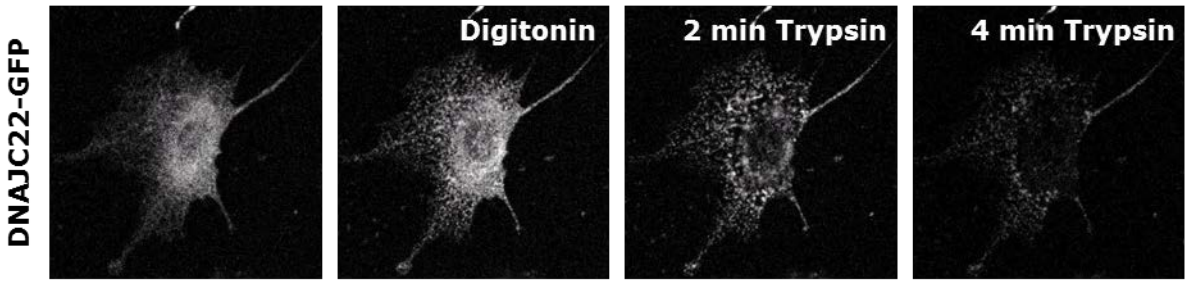

Figure 2.05 FPP assay for DNAJC22-GFP in living M-1 cells

Fluorescent signal is unaffected by plasma membrane permeabilization, yet addition of trypsin leads to loss of GFP fluorescence showing cytoplasmic localization of the DNAJC22 C-terminus.

Taken together, I could show that heterologously expressed DNAJC22 resides predominantly in the ER with its J domain facing the cytoplasm.

2.2 A *Dnajc22* knockout mouse model

2.2.1 Generation of the *Dnajc22* knockout mouse

The *Dnajc22* gene is located on chromosome 15 of the murine genome, consists of three exons and spans a genomic region of about 5.5 kilobases. The open reading frame is located on exon two and three, giving rise to a protein of 339 amino acids (see wildtype locus in the second lane of Figure 2.06).

For the generation of a conditional mouse model, loxP sites were inserted flanking the protein coding exons. Additionally, a reporter gene was chosen to be integrated in the 3' region of the gene to allow promoter studies after Cre-mediated excision of the floxed region (Figure 2.06 targeting construct in first lane). I was able to clone a great portion of the targeting vector during my diploma thesis which will be briefly summed up below[77]. The vector was then completed, extensively verified and used for gene targeting via homologous recombination in murine ES cells in the course of this thesis.

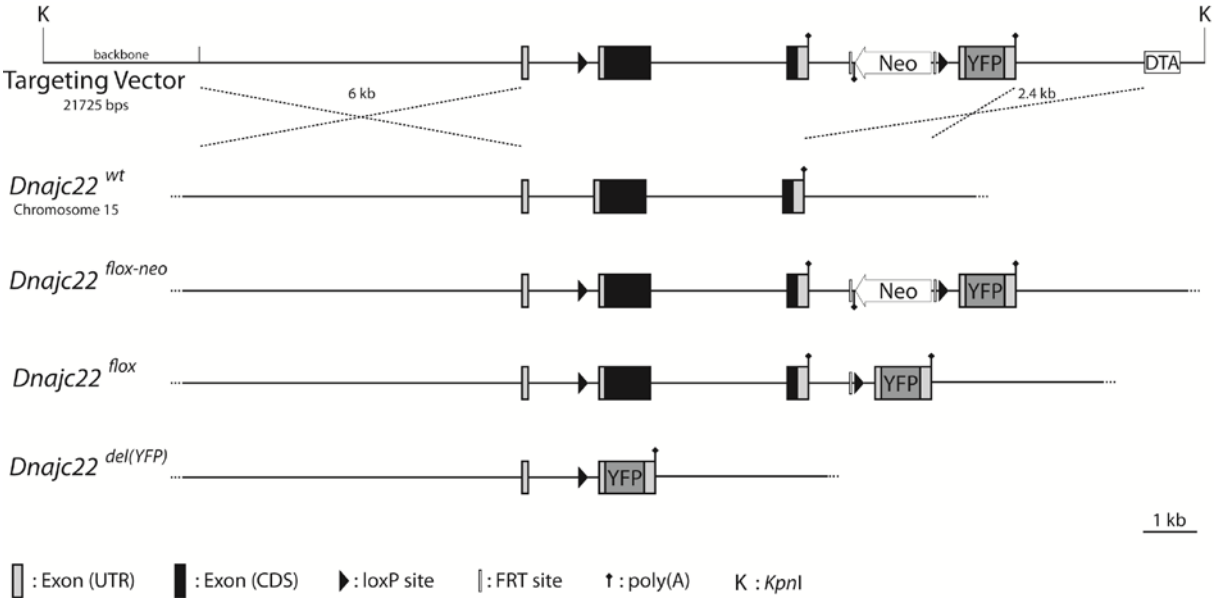

Figure 2.06 Targeting scheme for the *Dnajc22* knockout mouse

The wildtypic genomic locus of *Dnajc22* is depicted in the second lane with the designed targeting construct above and all the consequent possible alleles below. Exons 2+3 bear the open reading frame and are flanked by loxP sites (black triangles) in the floxed alleles. This region is removed by a Cre recombinase in the knockout allele (also designated del(YFP)), in which the reporter gene replaces the *Dnajc22* open reading frame. Note that the wildtypic UTRs of *Dnajc22* are retained in the reporter gene construct. The neomycin cassette is flanked by FRT sites (narrow empty boxes) and can be excised by a Flippase.

A suitable BAC was chosen and tested via Southern blot hybridization for the presence of the genomic *Dnajc22* locus[77], which was consequently retrieved via gap repair into the targeting vector making use of bacteria rendered competent for homologous recombination (Figure 2.07).

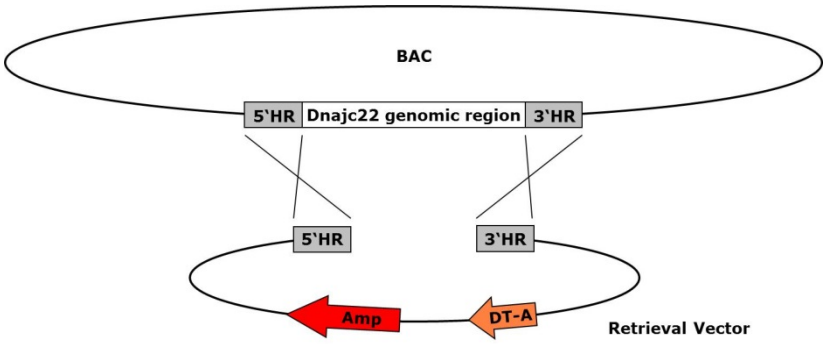

Figure 2.07 Retrieval of the genomic region of *Dnajc22* including the 5' and 3' homology arms needed for homologous recombination in ES cells

The linearized retrieval vector containing homologous regions to the *Dnajc22* locus was transformed into BAC-containing bacteria that were rendered recombineering-competent by the mini-phage λ. Gap repair yielded a new vector containing the retrieval vector backbone and the *Dnajc22* locus as an insert. (modified from[77])

Next, I inserted the 5' and 3' loxP sites, as well as the neomycin cassette for positive selection in ES cell culture, and the reporter gene YFP (Figure 2.08). For all of these steps, I cloned the DNA sequences to be exchanged in the targeting vector making use of SOE-PCRs and conventional cloning techniques with the help of restriction enzymes. The wildtype untranslated regions (light grey boxes) were fused to the reporter gene to mimic the expression of *Dnajc22* as closely as possible. To finally introduce either the 5' loxP site or the 3' loxP site, neomycin, and reporter gene, I employed the recombineering technique[80], as already introduced in my diploma thesis[77].

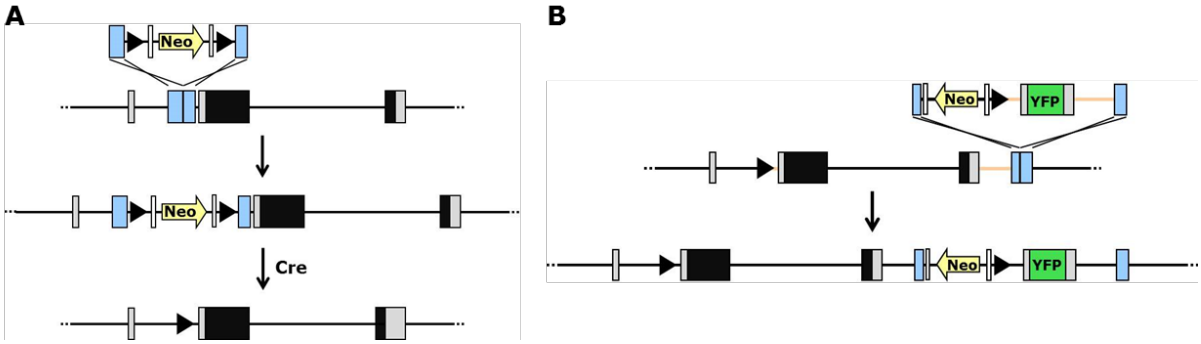

Figure 2.08 5' and 3' modification of the wildtype *Dnajc22* locus via recombineering

A Insertion of the first loxP site: A floxed neomycin/kanamycin resistance cassette is flanked by homologous arms (blue) to target recombination 5' of *Dnajc22* exon 2 in recombineering-competent bacteria containing the retrieval vector. Positive clones were selected on additional resistance to kanamycin. In a second step the resistance cassette was removed via Cre-mediated recombination leaving the one desired loxP in the locus. **B** The resulting intermediate vector containing the 5' loxP site was subjected to a recombineering step in which the 3' loxP site, neomycin resistance cassette and YFP reporter gene was inserted. Positive clones were again selected on double ampicillin/kanamycin resistance. (modified from[77])

The targeting construct was verified by several functional tests: the presence of the 5' loxP site was tested via PCR (Figure 2.09 A), the functionality of the loxP sites flanking the open reading frame of *Dnajc22* were checked by Cre-mediated excision in EL350 bacteria, the FRT sites flanking the neomycin cassette by FLP-mediated excision in EL250 bacteria (Figure 2.09 B). Moreover, the important parts of the construct (open reading frame, splice acceptor sites and the reporter gene YFP) were sequenced. The functionality of the reporter gene was verified by subcloning it into an expression vector and transiently overexpressing it in COS7 cells (Figure 2.09 C).

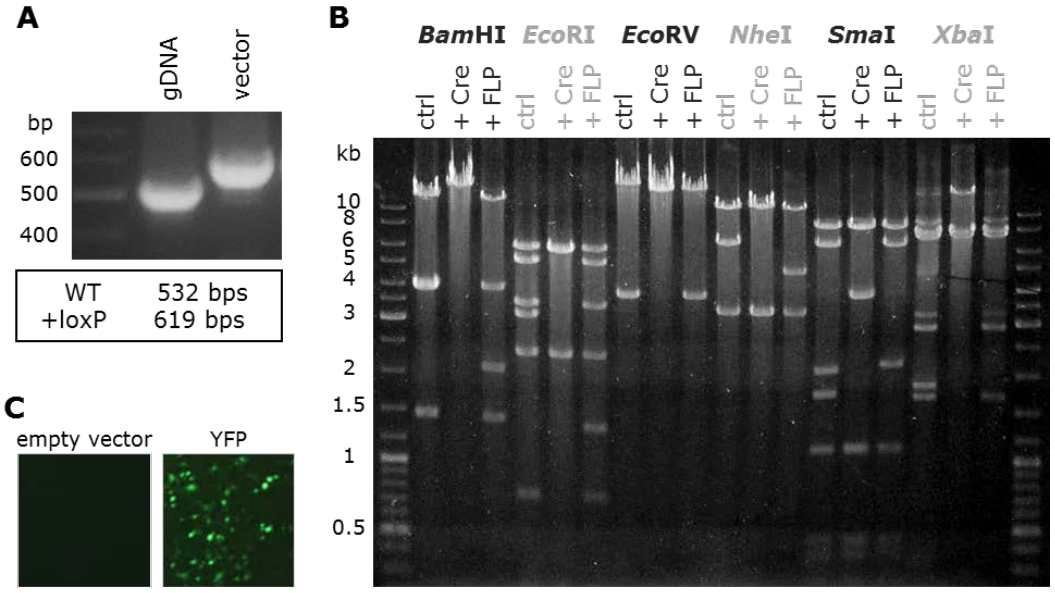

Figure 2.09 Verification of the targeting construct

A PCR to test for the presence of the 5' loxP site giving rise to a 87 base pair longer product for the targeting vector compared to wildtypic genomic DNA. **B** Restriction analysis of the targeting vector as well as Cre- or FLP-exposed vector. The expected band sizes can be found in Figure 2.10. **C** Transfection of COS-7 cells with either an empty vector control or the subcloned YFP reporter gene.

For the homologous recombination, I transfected murine embryonic stem cells with the *Kpn*I-linearized targeting vector. By the application of selection medium containing G418 only those cells in which the construct, including the neomycin cassette, inserted in the genome could give rise to clones. Cells bearing non-homologous integrated construct are thought to die due to expression of the diphtheria toxin (DTA). I picked about 750 clones and tested them both by two PCR strategies: a PCR over the 3' homology arm to test for correct integration and the 5'loxP

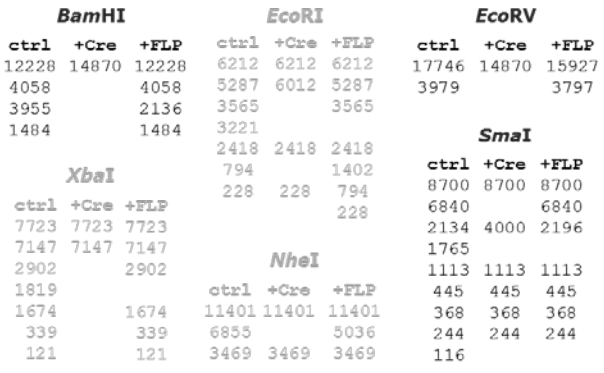

Figure 2.10 Expected results for the restriction analyses of the targeting vector as well as Cre- or FLP-exposed vector (Figure 2.9 B).

PCR, already utilized to verify the targeting construct itself, to test for the presence of the 5' loxP site. After testing ~300 clones, fourteen were positive in both of the PCRs (Figure 2.11 A,B). These clones were expanded and cryopreserved while further verifying them via Southern blot hybridization and examining their karyotype (Figure 2.11 C).

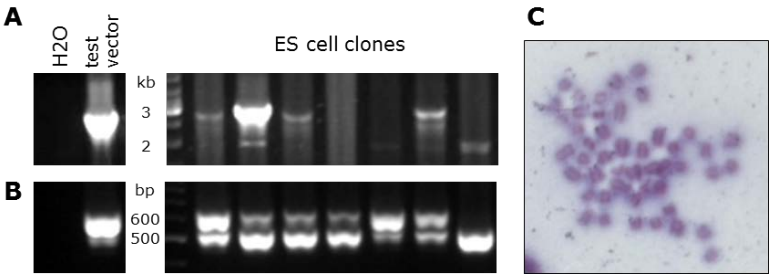

Figure 2.11 Selection of the homologous targeted ES cell clones

A 5'loxP PCR **B** Screening PCR over the 3' homology arm **C** Karyotype. Depicted are exemplary pictures.

Twelve clones showed the correct bands in the Southern blot hybridization using a 5' and an internal probe (Figure 2.12). Subsequently, two clones with an unaltered karyotype were selected for blastocyst injection and given to the transgenic service of the HET (Jürgen Schmidt) to carry out the procedure.

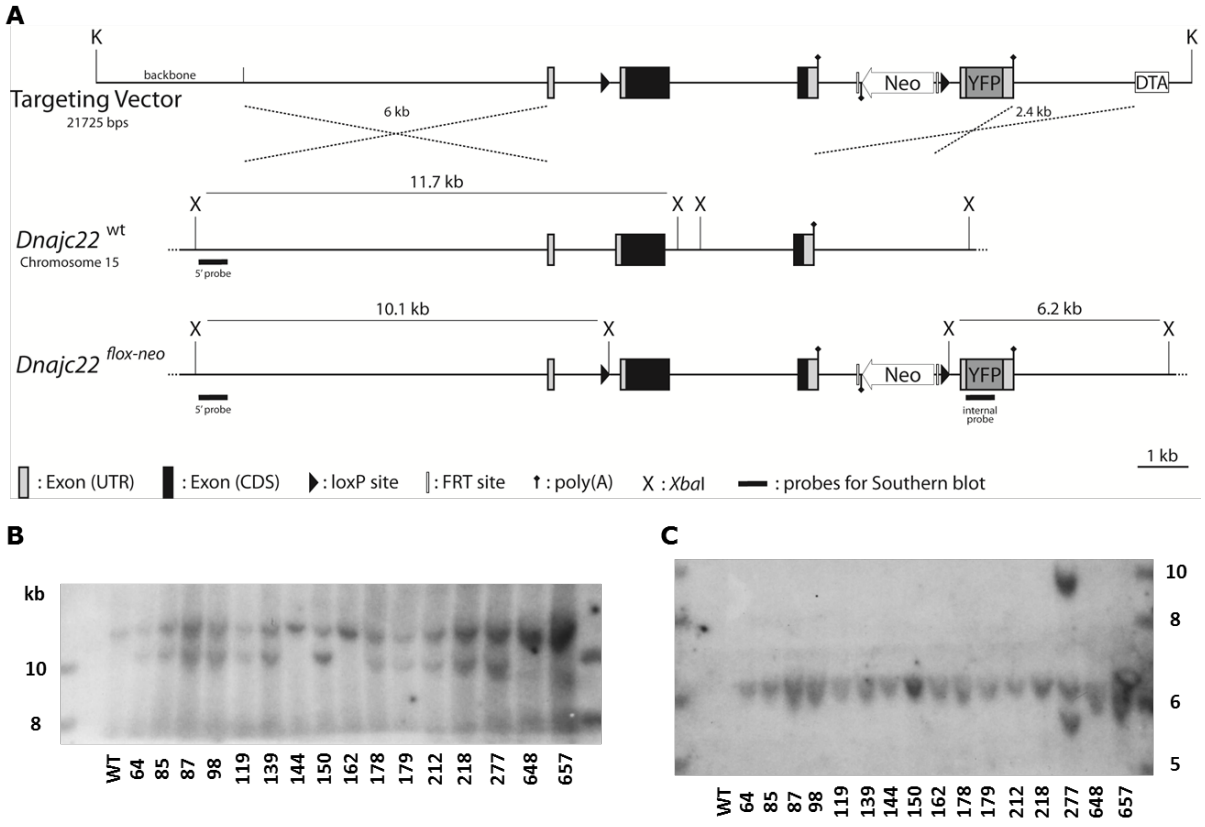

Figure 2.12 Verification of PCR double positive ES cell clones

A Targeting scheme for the wildtypic and recombined locus including relevant *Xba*I restriction sites used in the Southern blot procedure **B** Southern blot hybridization with external 5' probe on *Xba*I-digested genomic DNA **C** Southern blot hybridization with internal YFP probe on *Xba*I-digested genomic DNA

The transgenic ES cells (HM-1, agouti) were injected into blastocysts from wildtype (C57BL/6, black) mice and implanted into pseudopregnant foster mice. Two male offspring were obtained that were highly chimeric as seen by their brown fur color. They were backcrossed to C57BL/6 mice to test for germline transmission of the ES cells which can be observed by agouti fur color. One of the chimeras produced two female heterozygous transgenic animals (*Dnajc22*$^{+/flox\text{-}neo}$). The colony was further expanded and subsequently the *Dnajc22*$^{+/flox\text{-}neo}$ offspring was mated to PGK-Cre mice. The PGK-Cre mice express the Cre recombinase under the control of the PGK-1 promoter, thereby displaying an early and ubiquitous expression[81]. Cre-mediated excision of the floxed coding region of the *Dnajc22* gene produced *Dnajc22*$^{+/del(YFP)}$ mice.

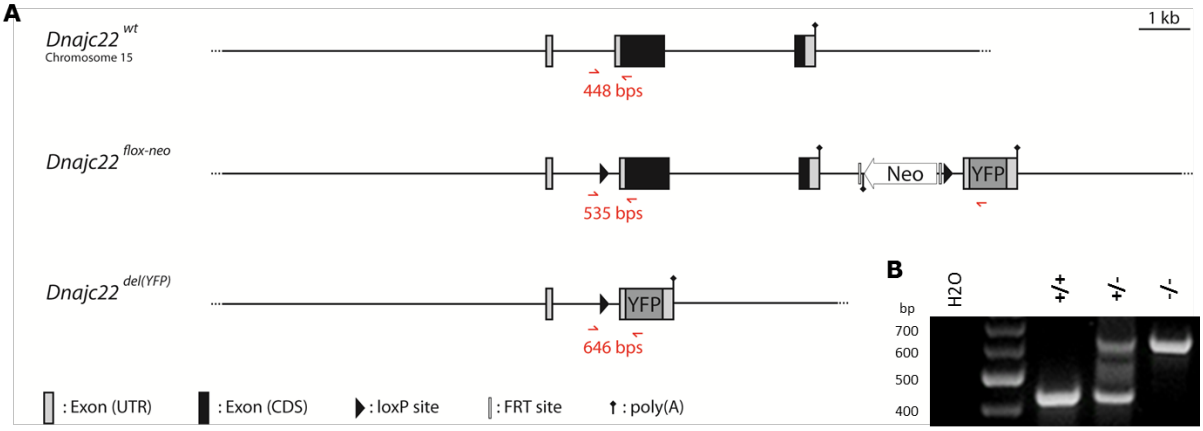

Figure 2.13 Genotyping strategy for *Dnajc22* mice

A *Dnajc22* alleles including binding sites of the PCR primer **B** Exemplary PCR result for wildtypic, heterozygous, and knockout *Dnajc22* mice (including water control)

Those heterozygous *Dnajc22*$^{+/del(YFP)}$ animals were viable, showed no obvious phenotype and were mated to each other in order to obtain homozygous *Dnajc22* knockout animals. I confirmed the knockout by various methods: Southern blot hybridization validated accuracy of the genotypes of the studied allelic combinations, northern blot hybridization showed the absence of wildtypic mRNA in the knockout as well as transcription of the reporter gene, and via Western blot I could demonstrate reporter gene expression on protein level.

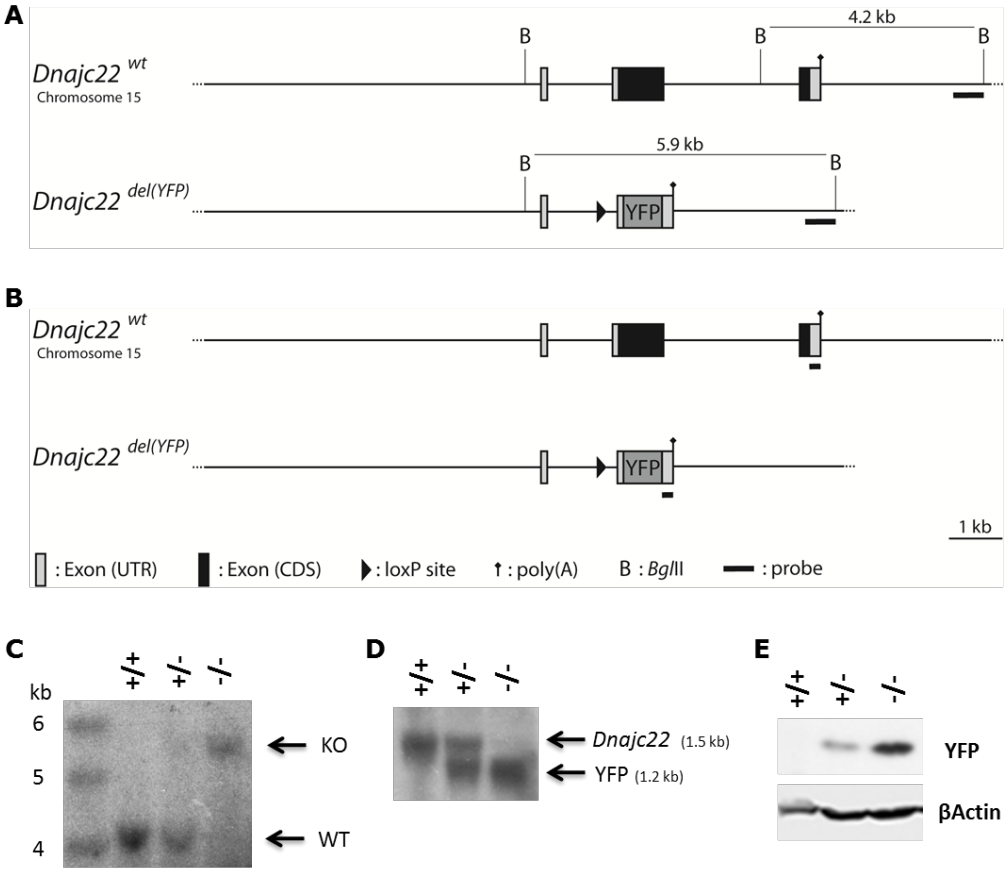

Figure 2.14 Verification of transgenic *Dnajc22* mice

A Scheme for the Southern blot hybridization showing the wildtypic and knockout allele including relevant *Bgl*II restriction sites used in the procedure **B** Scheme for the northern blot hybridization showing the wildtypic and knockout allele **C** Southern blot hybridization with external 3' probe on *Bgl*II-digested genomic DNA **D** Northern blot hybridization with a probe recognizing the 3' UTR and thereby recognizing wildtypic *Dnajc22* as well as the fusion YFP reporter transcript **E** Western blot for the YFP reporter protein on liver lysates (βActin used as loading control)

2.2.2 Basic phenotypic characterization of the *Dnajc22* mouse

The homozygous *Dnajc22* knockout mouse is viable and fertile, showing no obvious morphological alterations or changes in body weight (Figure 2.14 B). Heterozygous mice breed in nearly Mendelian ratios when mated with each other (Figure 2.14 A). Homozygous knockout mice are fertile and a homozygous mating produced a litter of normal size.

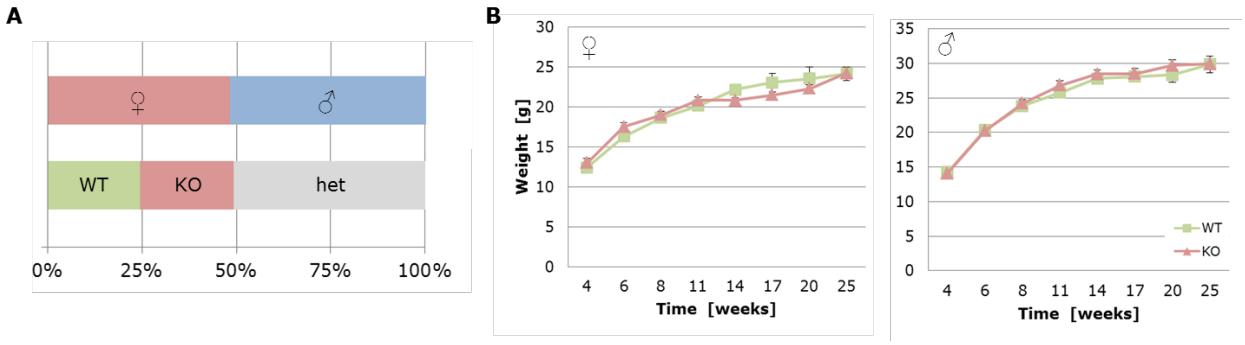

Figure 2.14 Basic breeding statistics.

A Almost equal birth of female and male offspring (48.2% and 51.8% respectively) and almost Mendelian birth ratio of genotypes from heterozygous matings (24.4% wildtype, 50.8% heterozygous, 24.9% knockout, n=631) **B** Body weight development over time of male (left) and female (right) mice. (n=4-25, ±SEM / WT: wildtype, KO: knockout, het: heterozygous).

I performed quantitative real-time PCR on several organs of adult male and female mice in order to explore the organs in which DNAJC22 may play a role in mammals. It is primarily expressed in kidneys, liver and intestine, whereas in many organs of the adult mouse it is expressed at low levels. Messenger RNA was barely or not at all detectable in heart and brain tissue (Figure 2.15).

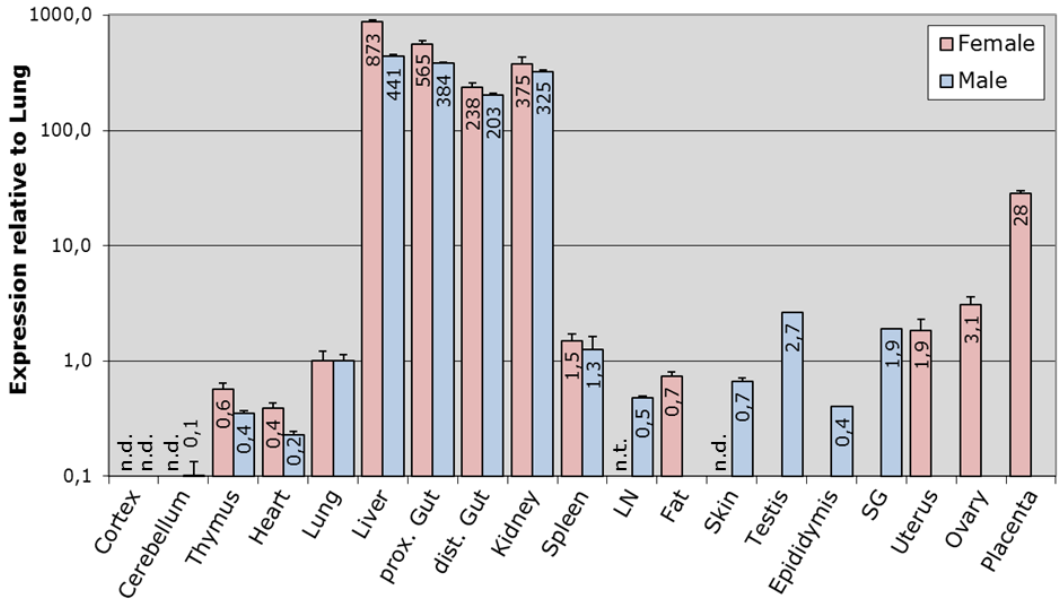

Figure 2.15 Quantitative real-time PCR on wildtype organ lysates

Dnajc22 mRNA expression levels in various adult female (red bars) and male (blue bars) organs relative to the lung. Transcript levels were normalized on the housekeeping gene *Hprt* and were plotted on a logarithmic scale. (n=1, ±STD, n.d.: non-detectable n.t.: not tested, prox.: proximal, dist.: distal, LN: lymph node, SG: seminal gland)

Using the heterozygous knockout mice (*Dnajc22*$^{+/del(YFP)}$) to study *Dnajc22* promoter activity by the presence of the reporter gene YFP, which is supposed to be expressed when *Dnajc22* is deleted, I could confirm the *Dnajc22* promoter activity in kidney, liver and intestine also on protein level by immunoblot as well as by immunohistochemical staining of cryosections (Figure 2.16-19).

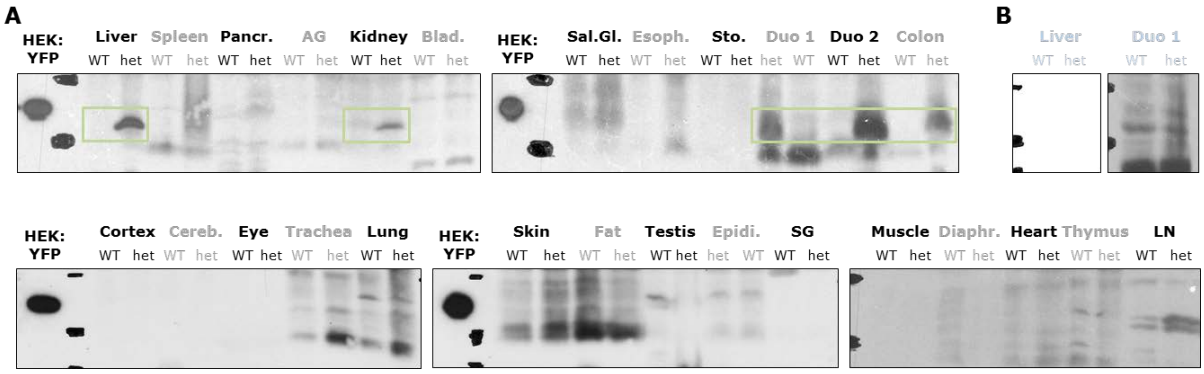

Figure 2.16 Tissue-specific *Dnajc22* promoter analysis by reporter gene expression analysis via Western blot

A Immunoblots show YFP expression levels in various organs of 6 week old *Dnajc22* wildtype and heterozygous littermates (green boxes). Overexpressed YFP in HEK293 cells served as a positive control. **B** Negative controls on liver and duodenum lysates in which the primary antibody was omitted. (Pancr.: pancreas, AG: adrenal gland, Blad.: bladder, Sal.Gl.: salivary gland, Esoph.: esophagus, Sto.: stomach, Duo 1: duodenum, Duo 2: jejunum, Cereb: cerebellum, Epidi.: epididymis, Diaphr.: diaphragm, LN: lymph node)

In the liver, the whole organ is homogeneously stained indicating expression in hepatocytes (Figure 2.17 A). This could also be confirmed by detecting the YFP fluorescence directly in primary hepatocytes via analysis by flow cytometry (Figure 2.17 B, data produced together with Dirk Wohlleber, AG Knolle).

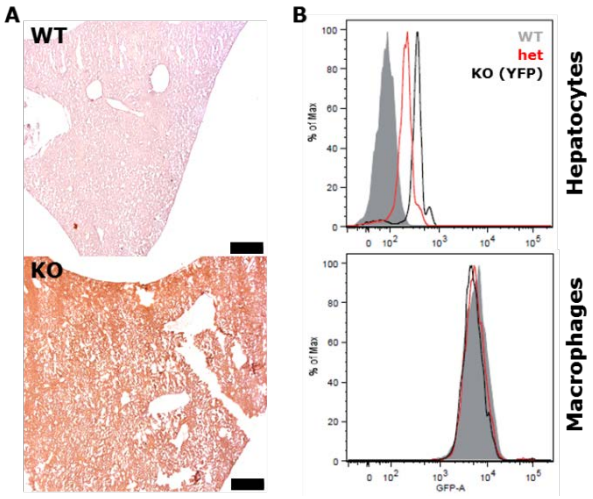

Figure 2.17 *Dnajc22* expression in the liver

A Cryosections of *Dnajc22* wildtype and knockout liver were stained against YFP (depicted in red/brown) and counterstained with hematoxylin (blue). (Scale bars represent 50µm) **B** Flow cytometry analysis of primary hepatocytes. YFP expression was detected in primary hepatocytes showing increasing fluorescence in samples from heterozygous and knockout animals. Co-staining for macrophages (i.e. Kupffer cells in the liver) revealed an overall greater autofluorescence but no positive YFP signal. (Data produced with Dirk Wohlleber, AG Knolle)

In the intestine, YFP staining could be detected at varying intensities in the epithelial cells of the mucosa, i.e. in villi as well as in crypts. Reporter gene expression was not detectable in submucosa, muscularis and serosa. Also, occasional lymph nodes in the sections showed no staining (Figure 2.18).

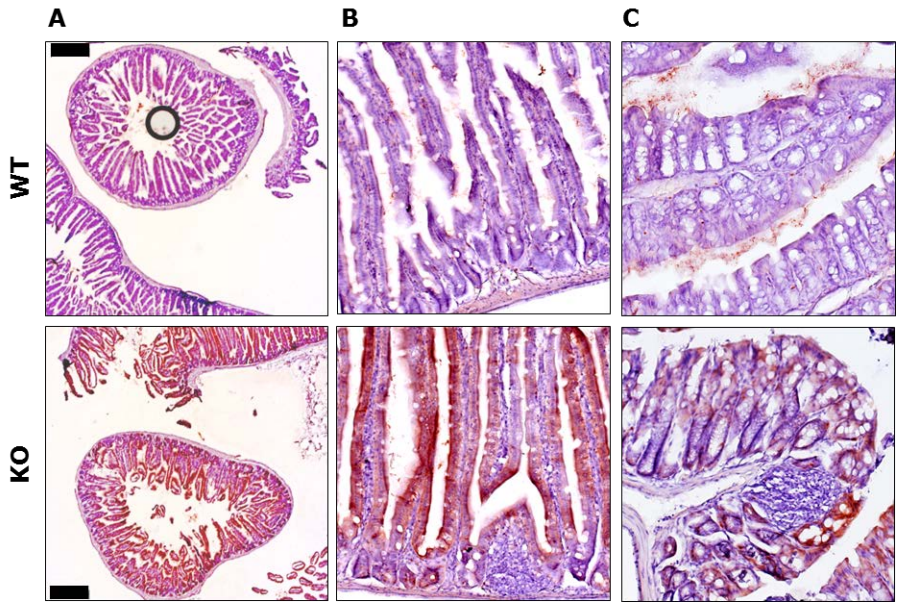

Figure 2.18 *Dnajc22* expression in the intestine

Cryosections of *Dnajc22* wildtype and knockout intestine were stained against YFP (depicted in red/brown) and counterstained with hematoxylin. **A** Duodenum (Scale bars represent 50µm) **B** Higher magnified picture of duodenum **C** Colon

In the kidney, the reporter gene is localized in the cortex of the organ. No detectable expression was found in the medulla. More precisely, YFP marked the epithelium of cortical tubules (Figure 2.19 A). Glomeruli were not YFP-positive (Figure 2.19 C). Further investigation showed that the stained tubules are phalloidin-positive in immunofluorescence staining, indicating that at least a part of the YFP expression is found in the proximal part of the nephron since its epithelium bears a brush border and therefore shows apical enrichment of actin (Figure 2.19 D). An *in situ* hybridization for *Dnajc22* made available by the GenitoUrinary Molecular Anatomy Project (GUDMAP) shows the same expression pattern (Figure 2.19 B). Based on their data mRNA is present in tubules of the renal cortex and outer stripe of the medulla (outer medullary portion of the loop of Henle). *Dnajc22* probe signal is reported to be absent from glomerular structures (capillary system, mesangium, visceral epithelium of mature renal corpuscule), inner medulla, inner stripe of the outer medulla, medullary collecting ducts, as well as cortical and medullary interstitium, vasculature, lymphatics and nerves[82,83].

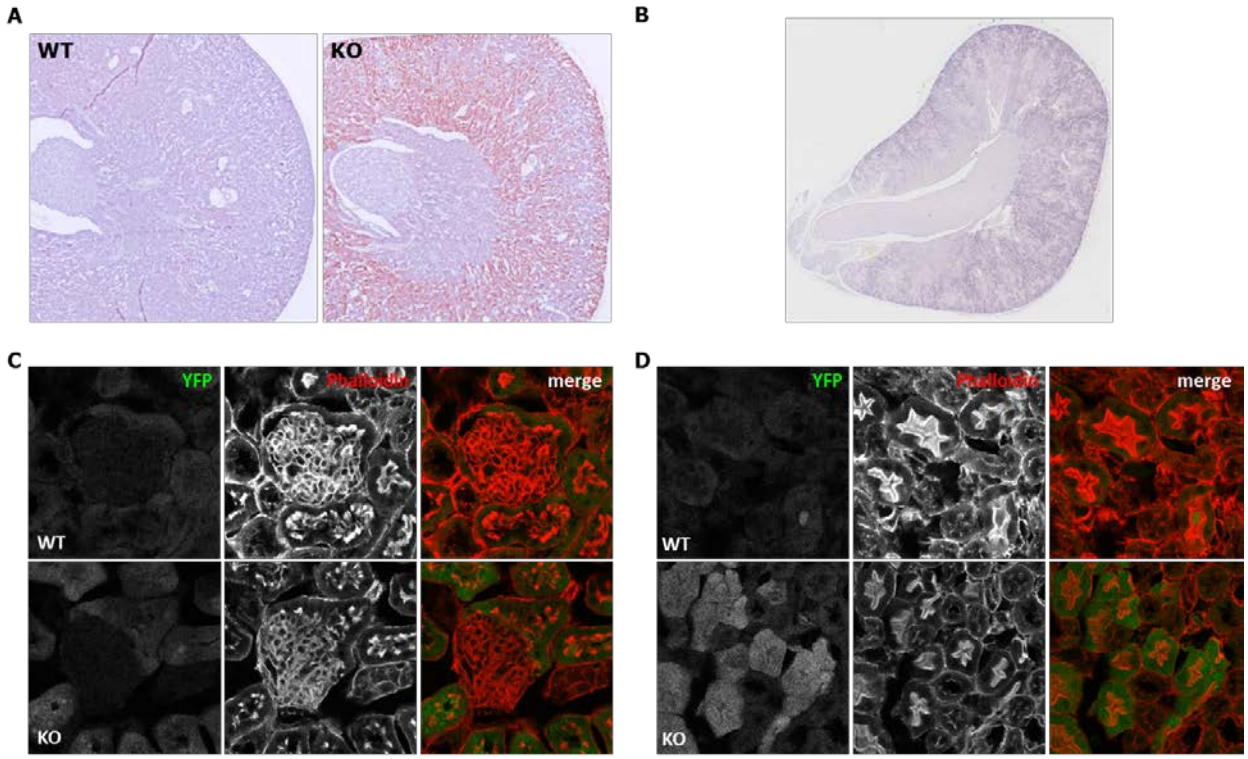

Figure 2.19 *Dnajc22* expression in the kidney

A Cryosections of *Dnajc22* wildtype and knockout kidneys were stained against YFP (depicted in red/brown) and counterstained with hematoxylin. **B** *Dnajc22 in situ* hybridization (GUDMAP project[82,83]) **C, D** Immunofluorescence staining for YFP (green) and the actin marker phalloidin showing magnifications from wildtype and knockout cortex (**C**) and outer medulla (**D**).

To assess kidney function I collected urine samples making use of metabolic cages. *Dnajc22*-deficient mice produced significantly less urine than their wildtype littermates. However they also drank less than the control animals. Consequently, the urinary osmolality of knockout mice were slightly elevated (Figure 2.20).

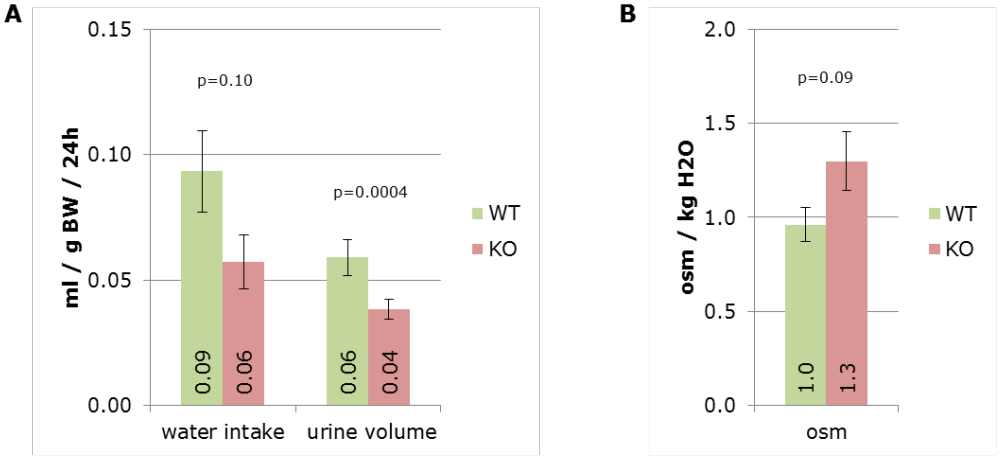

Figure 2.20 Water balance

Water intake and urine volume per gram body weight (g BW, **A**) and osmolality of urine (**B**) of wildtype (green) and *Dnajc22* knockout (red) mice (n=9-10, ±SEM, 6-20 week old males, p values calculated via unpaired student's t-test for comparison of WT vs. KO)

Urine levels of sodium, chloride, and potassium are slightly diminished in *Dnajc22* knockout mice (Figure 2.21 A), while serum levels were unchanged (Figure 2.21 B).

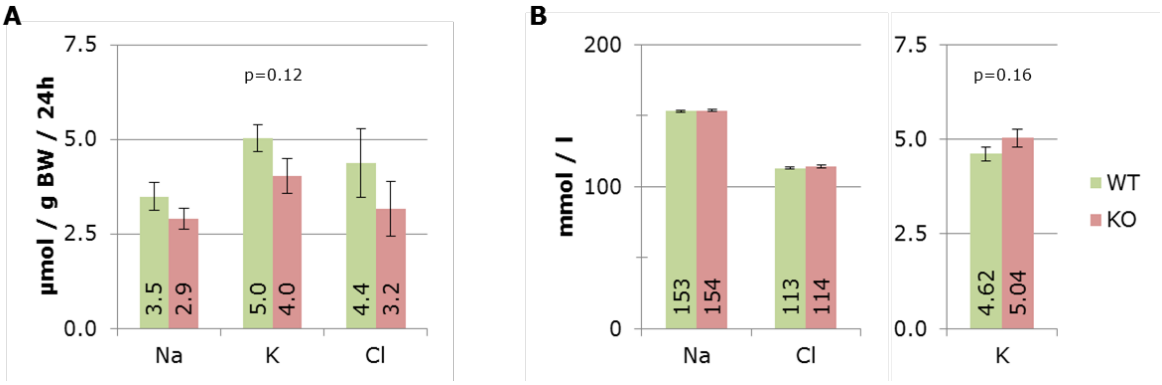

Figure 2.21 Electrolyte levels in urine and serum

A Sodium, chloride, and potassium excretion via the urine. (n=12-13, ±SEM, 6-20 week old males) **B** Sodium, chloride, and potassium concentrations in the serum (n=8-17, 2-12 months old males. ±SEM). Wildtype in green, knockout values in red. p values calculated via unpaired student's t-test for comparison of WT vs. KO.

By regulating osmolyte homeostasis and water balance, the kidney also has an impact on the regulation of blood pressure. The observed altered excretion of sodium and chloride raised the question if the possibly impaired kidney function has any implication for the maintenance of blood pressure in the *Dnajc22* knockout mice. Peripheral systolic and diastolic blood pressures were found to be slightly, yet insignificantly increased (9 mmHg difference of the means in systolic and 4 mmHg in diastolic pressure, Figure 2.22 A). The intraventricular measurements were unchanged (SBP -2 mmHg) or marginally lowered (DBP -3 mmHg) (Figure 2.22 B).

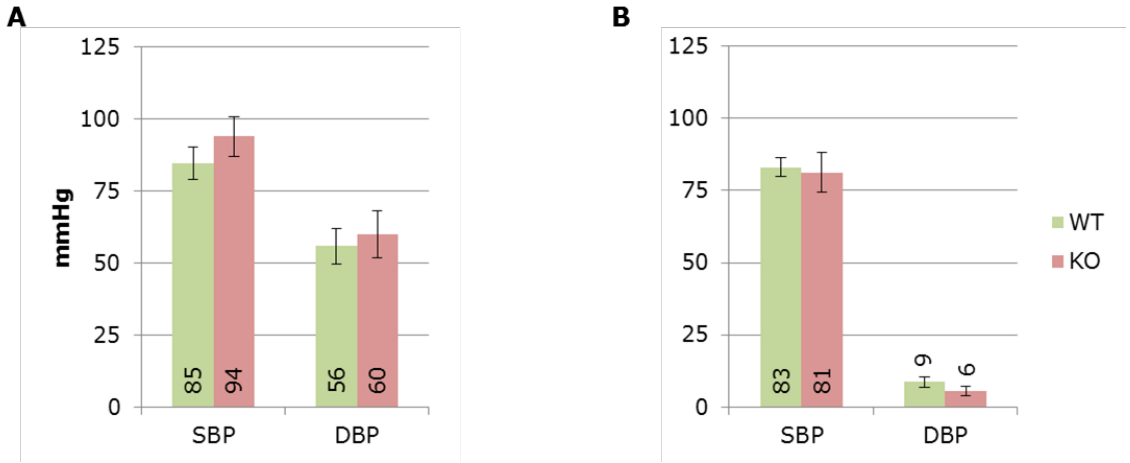

Figure 2.22 Blood pressure measurements

Systolic and diastolic peripheral (**A**, n=5) and intraventricular (**B**, n=4) blood pressure in *Dnajc22* wildtype (green) and knockout mice (red) (4-6 months old males, ±SEM, p value calculated via unpaired student's t-test, data produced with Paul Markowski, AG Knüfermann)

2.2.3 High salt diet challenge

Based on the observations of a moderate decrease of sodium and chloride excretion and the concomitant tendency to an increased blood pressure, I challenged the osmoregulatory function of *Dnajc22*-deficient mice by providing a diet with increased content in sodium chloride for two weeks. Again, urine electrolytes as well as blood pressure were analyzed in knockout animals and compared to wildtype littermates.

Whereas wildtype animals were able to increase their excretion of sodium and chloride in response to the elevated intake, *Dnajc22* knockout mice were not as effective in doing so (Figure 2.23). This observation was endorsed by looking at the statistical significances for the sodium values: in wildtypes the elevation of sodium excretion was significant (p=0.04) comparing the values before and after the diet, which was not the case for the knockout mice (p=0.12).

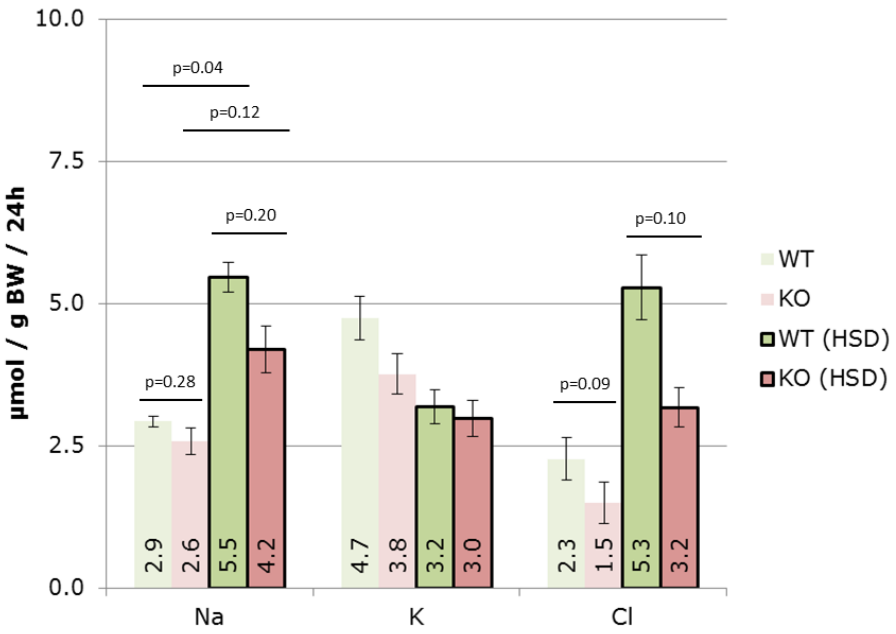

Figure 2.23 Urinary electrolytes before and after HSD

Sodium, potassium, and chloride secretion via the urine. Wildtype values before (light green) and after the diet (green), *Dnajc22* knockout values in red respectively (n=3-4, 7-13 week old males , ±SEM, p value calculated via unpaired student's t-test for comparison of WT vs. KO, via paired student's t-test for comparison of ctrl vs. HSD)

In line with these data, also peripheral blood pressure was elevated in the knockout animals compared to their littermates. After challenge with a two week high salt diet there was a clear difference between wildtype and *Dnajc22*-deficient mice, showing an increase of 14 mmHg in systolic and 16 mmHg in diastolic blood pressure (Figure 2.24 A). Intraventricular pressures were moderately increased at the end of the systole (+5 mmHg) and unchanged after diastole (Figure 2.24 C).

Comparing the differences between *Dnajc22* knockout mice and wildtype littermates showed that peripheral systolic blood pressure was elevated by +9 mmHg under normal conditions and +14 mmHg after high salt diet. The difference in peripheral diastolic blood pressure between knockout and control animals was +4 mmHg in the standard situation and +16 mmHg after the challenge. For intraventricular systolic blood pressure the deltas were -2 and +5 mmHg; for intraventricular diastolic blood pressure -3 and 0 mmHg. The dietary challenge with a high salt diet for two weeks heightened the phenotype in all of the four measures.

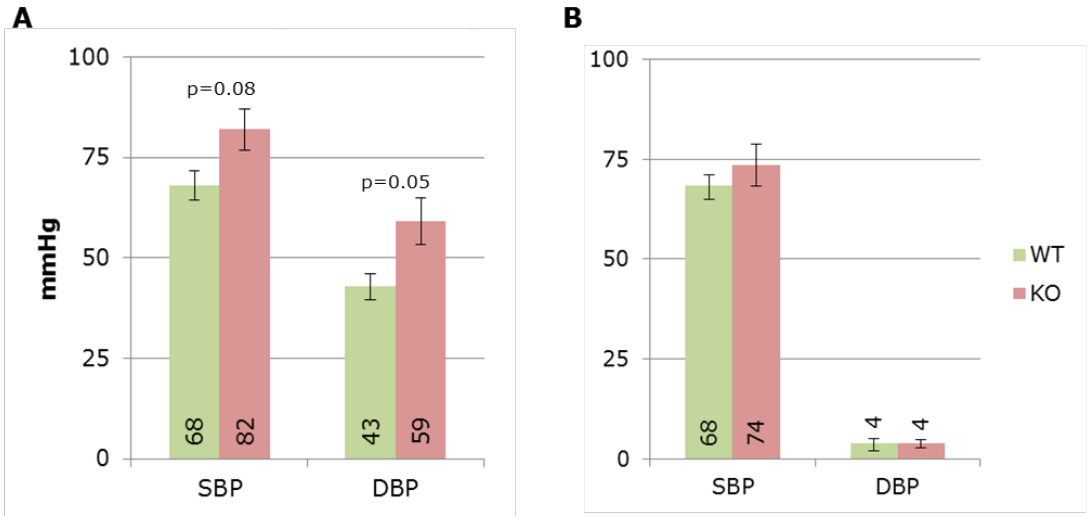

Figure 2.24 Blood pressure measurements after two weeks of high salt diet

Peripheral (**A**, n=5) and intraventricular (**B**, n=4) systolic and diastolic blood pressures in Dnajc22 wildtype (green) and knockout mice (red). (±SEM, 4-6 months old males, data produced with Paul Markowski, AG Knüfermann)

Analyzing transcript levels in kidneys from animals challenged with the high salt diet revealed that mRNA expression of the ENaC alpha and beta subunit (*Scnn1a* and *Scnn1b*) were significantly reduced. Transcript of the gamma subunit (*Scnn1g*) was unchanged. The mRNA level for *Hsp70* was found to be markedly decreased as well (Figure 2.25 A). Other sodium transporters such as NKCC2 (*Slc12a1*), NKCC1 (*Slc12a2*), and NCC (*Slc12a3*) along with further important tubular transporters were not significantly altered (Figure 2.25 B). Checking for possible compensatory expression of structurally similar members of class C J proteins showed no changes for *Dnajc4*, *12*, *14*, *15*, *19*, and *25* (Figure 2.25 C). *Dnajc22* transcript expression was analyzed with two different primer pairs: The C22/2 combination spans the second intron and binds to a region in the ORF, thus verifying the knockout situation. The C22/1 primer pair spans the first intron and binds sequences in the untranslated region, thereby also detecting the reporter-UTR-fusion transcript. Reporter gene expression was found to be more than twice as high as the expression of wildtype *Dnajc22* mice.

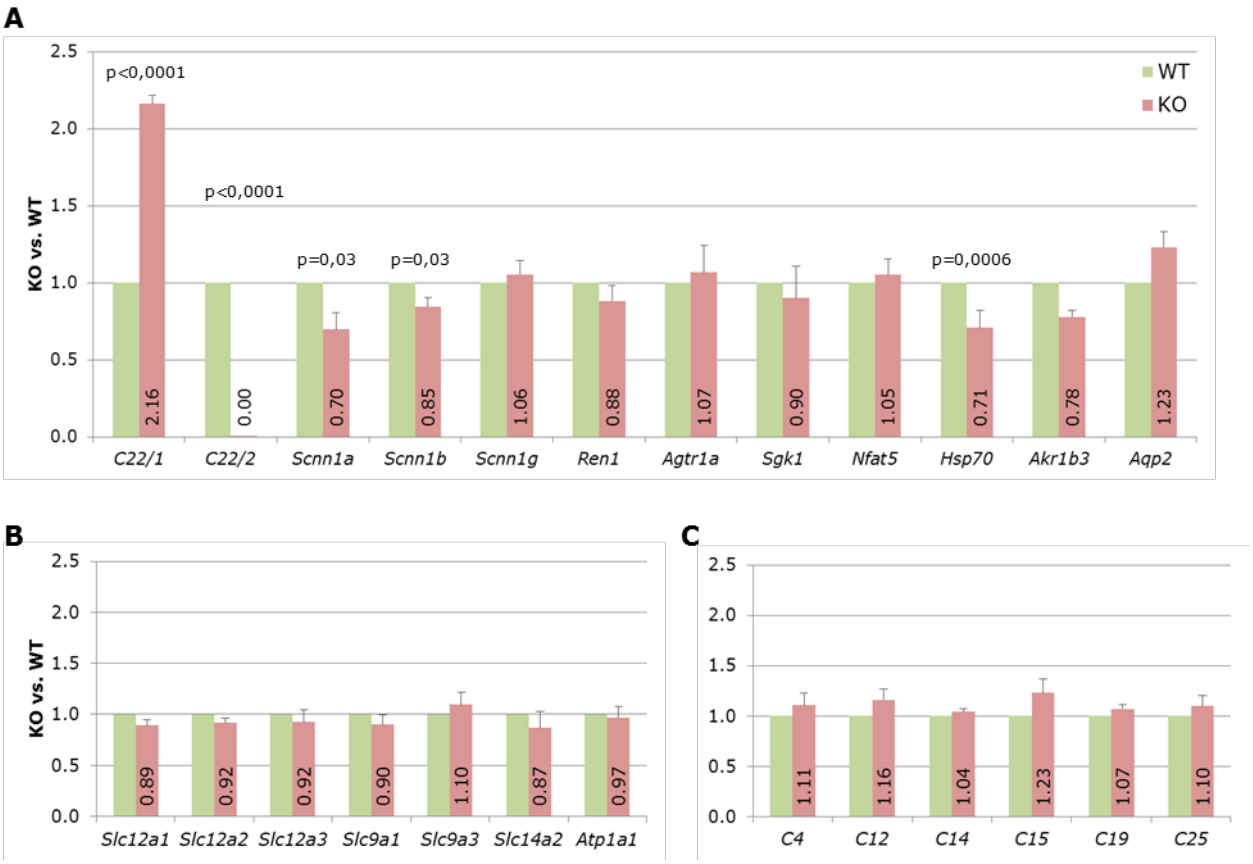

Figure 2.25 Quantitative real-time PCR on kidney lysates after high salt diet challenge

Relative expression levels of various transcripts in *Dnajc22* knockout (red) vs. wildtype (green) kidney samples after dietary challenge. Transcript levels were normalized on the housekeeping gene Hprt. **A** *Dnajc22*, ENaC subunits, and several genes relevant in hypertension **B** Selection of renal tubular solute transporters **C** Structurally similar J proteins from the C subclass. 'C' abbreviates 'Dnajc'. (n=4, +SEM, 4-6 months old males / *Scnn1a*: αENaC, *Scnn1b*: βENaC, *Scnn1g*: γENaC, *Ren1*: *Renin 1*, *Agt*: angiotensinogen, *Agtr1a*: angiotensin II receptor, type 1a, *Sgk1*: serum/glucocorticoid kinase 1, *Nfat5*: nuclear factor of activated T cells 5, *Hsp70*: heat shock protein 70, *Akrb3*: aldo-keto reductase family 1, member 3, *Aqp2*: aquaporin 2, *Slc12a1*: solute carrier family 12, member 1 (NKCC2), *Slc12a2*: solute carrier family 12, member 2 (NKCC1), *Slc12a3*: solute carrier family 12, member 3 (NCC), *Slc9a1*: solute carrier family 9, member 1 (NHE1), *Slc9a3*: solute carrier family 9, member 3 (NHE3), *Slc14a2*: solute carrier family 14 (urea transporter), member 2, *Atp1a1*: Na^+/K^+-ATPase, α 1 polypeptide).

Investigating the protein levels of αENaC and HSP70 revealed that both factors were slightly downregulated (Figure 2.26).

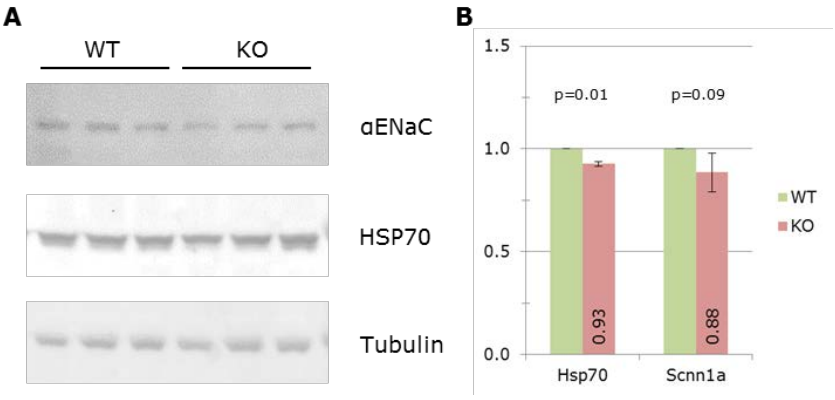

Figure 2.26 Analysis of αENaC and HSP70 protein levels in the kidney after HSD

A Western blot analyzing αENaC and HSP70 protein levels in total kidney lysates of 3 wildtype (WT) and 3 *Dnajc22* (KO) animals that received the high salt diet for two weeks. **B** Quantification of the results from **A** by normalization to Tubulin protein levels. (n=3, +SEM, 4-6 months old males)

2.3 Functional analysis of *Dnajc22* in M-1 cells

Since *Dnajc22* is involved in blood pressure control, I wanted to know whether *Dnajc22* responds to osmotic challenges *in vitro*. For this purpose, I studied the impact of altering the osmotic properties of the medium on the murine kidney cell line M-1.

Initial studies showed that increasing osmolality by addition of 100 mM sodium chloride to the standard medium led to an induction of *Dnajc22* transcript levels (Figure 2.27). The elevated abundance of transcript was seen in each experiment although values varied between four and over 25-fold, hence the large error bars and statistical non-significance. *Hsp70*[84] and the aldose reductase (*Akr1b3*)[55,56], both *Nfat5* target genes known to be up-regulated upon hyperosmotic stress, served as positive controls.

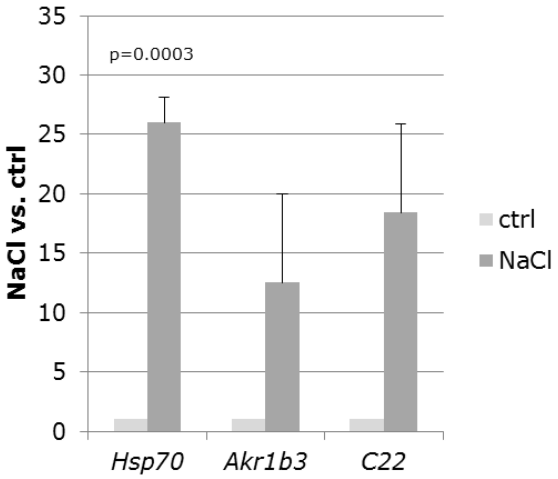

Figure 2.27 Gene expression analysis in M-1 cells after hyperosmotic challenge with sodium chloride

Quantitative real-time PCR on lysates of M-1 cells incubated with additional 100 mM sodium chloride for six hours compared to the controls. Expression levels were normalized to the housekeeping gene *Hprt*. (n=3, +SEM, p values calculated via unpaired student's t-test / ctrl: control, *Hsp70*: heat shock protein 70, *Akr1b3*: aldose reductase, *C22*: *Dnajc22*).

In primary cultures of mouse medullary thick ascending limb it had been shown that inhibition of the Na^+-K^+-$2Cl^-$ cotransporter type 2 (NKCC2) by the loop diuretic bumetanide reduces the elevation of *Nfat5* transcript levels and consequently its transcriptional activity in response to hypertonicity[85]. Therefore, I tested if the induction of *Dnajc22* mRNA could still be observed in a similar setting. Challenging the cells with sodium chloride under the presence of increasing concentrations of furosemide (a similar loop diuretic as bumetanide) led to a reduction of *Nfat5* transcript increase in response to sodium chloride induced hypertonicity as well as to a consequent diminished induction of its target genes *Hsp70* and aldose reductase. Yet *Dnajc22* transcript levels were nonetheless elevated by the addition of sodium chloride to the medium as in the absence of furosemide (Figure 2.28).

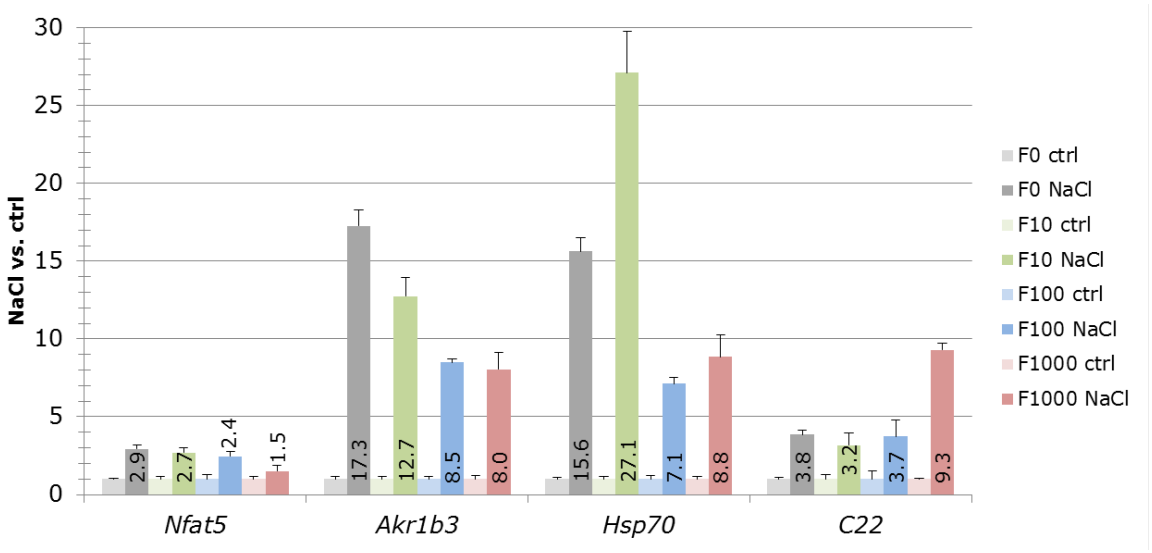

Figure 2.28 Gene expression analysis in M-1 cells after hyperosmotic challenge with sodium chloride under the presence of varying concentrations of furosemide

Quantitative real-time PCR on lysates of M-1 cells incubated with or without furosemide (10, 100 or 1000 µM) for one hour chased by addition of 100 mM sodium chloride or equivalent amount of water (ctrl: control) for six hours. Expression levels were normalized to the housekeeping gene *Hprt* and values are depicted as +NaCl vs. ctrl in each furosemide condition. (+SD, n=1 / ctrl: control, *Akr1b3*: aldose reductase, *C22*: *Dnajc22*).

In order to investigate whether the influx of sodium into the cell is responsible for the elevation of *Dnajc22* transcript levels, I inhibited the epithelial sodium channel (ENaC) with amiloride (Figure 2.29). This was indeed the case. Whereas *Dnajc22* was induced 2.2 fold in this experiments, no change was seen upon hyperosmotic challenge in the presence of amiloride (1.0 fold). Hsp70 transcript up-regulation served as a control for the successful hyperosmotic challenge. Notably, Hsp70 transcript was even diminished to 50% upon addition of sodium chloride in the presence of amiloride.

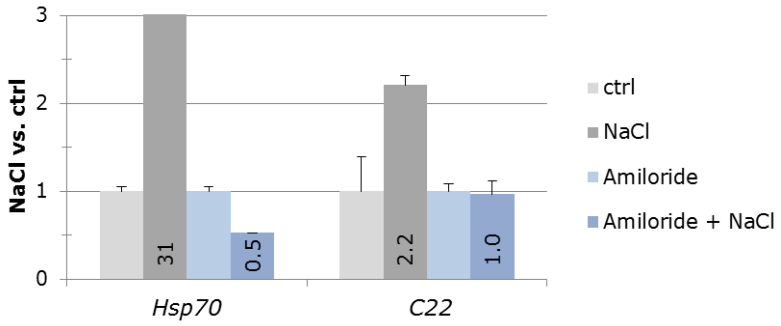

Figure 2.29 Gene expression analysis in M-1 cells after hyperosmotic challenge with sodium chloride in the presence of amiloride

Quantitative real-time PCR lysates of M-1 cells incubated with or without 5µM amiloride for one hour chased by addition of 100 mM sodium chloride or equivalent amount of water (ctrl) for six hours. Expression levels were normalized to the housekeeping gene *Gapdh*. Values are depicted as +NaCl vs. ctrl in each ±amiloride condition (+SD, n=1 / *C22*: *Dnajc22*).

Testing different solutes to subject the cells to hyperosmotic conditions revealed that this effect was not restricted to sodium chloride alone – also urea as well as mannitol was able to induce *Dnajc22* expression, though to a lesser extent (Figure 2.30). In this experiment *Dnajc22* was induced 3.8 fold by addition of sodium chloride. Raising the osmolality to a similar extent with urea and mannitol showed an increase of 2.5 and 1.4 fold respectively.

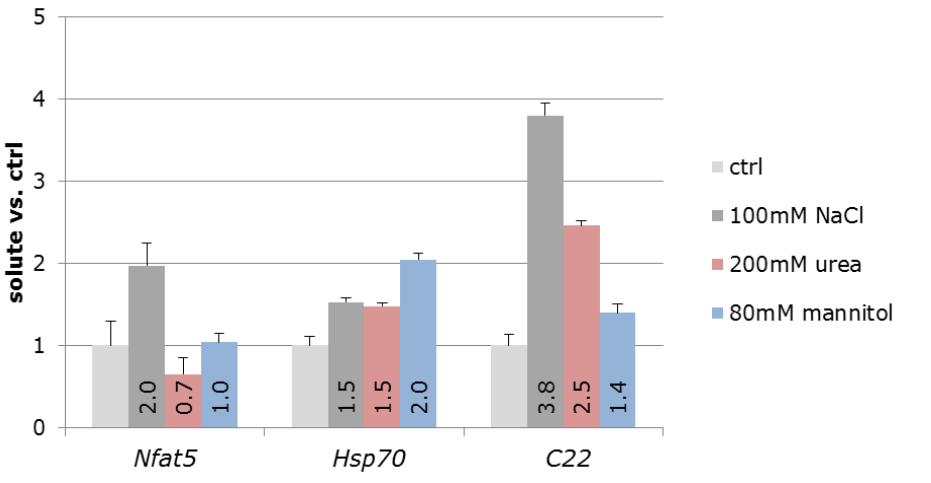

Figure 2.30 Gene expression analysis in M-1 cells after hyperosmotic challenge with different osmolytes

Quantitative real-time PCR lysates of M-1 cells incubated with different osmolytes or an equivalent amount of water (ctrl) for six hours. Expression levels were normalized to the housekeeping gene *Hprt*. Values are depicted relative to ctrl. (+SD, n=1 / *C22*: *Dnajc22*)

In order to further elucidate what triggers the observed transcript induction, I applied different kinds of sodium or chloride salts to the medium of the cells (Figure 2.31). As the addition of 100 mM sodium chloride approximately doubled the concentration already present in the medium, the other salts were added either in a concentration twice as a high as already present or in a concentration providing 100 mM of sodium or chloride. The higher concentrations of all tested salts dramatically induced *Hsp70* transcript levels. *Dnajc22*, however, was not affected by sodium bicarbonate in this setup. Compared to the 3.8 fold increase after challenge with sodium chloride, *Dnajc22* mRNA was induced 2.7 fold upon addition of 50 mM magnesium chloride and even 7.2 fold with potassium chloride.

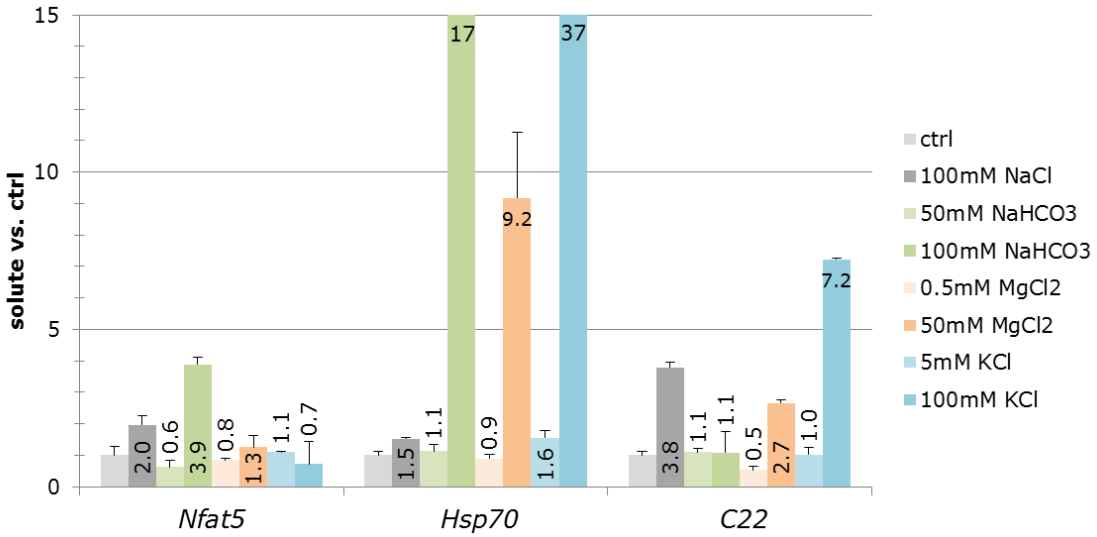

Figure 2.31 Gene expression analysis in M-1 cells after challenge with sodium bicarbonate, magnesium and potassium chloride

Quantitative real-time PCR lysates of M-1 cells incubated with different concentrations of the depicted salts or an equivalent amount of water (ctrl) for six hours. Concentrations were either twice the concentration from the standard medium (as adding 100mM sodium chloride nearly doubles the amount already present in the medium) or providing 100mM of either sodium or chloride. Expression levels were normalized to the housekeeping gene *Hprt*. Values are depicted relative to ctrl. (+SD, n=1 / *C22*: *Dnajc22*).

3 Discussion

This work was laid out to investigate the physiological role of mammalian *Dnajc22* using the mouse as a model organism.

Previous experiments on the ortholog Wurst in the fruit fly *Drosophila melanogaster* had described a function in barrier epithelia. Wurst proved to be involved in the proper development of the fly's airways – presumably by regulating members of the Ppk family (the orthologs of epithelial sodium channels in the fruit fly) via clathrin-mediated endocytosis)[70].

In my PhD thesis, I established a mouse model lacking the *Dnajc22* gene and examined its phenotype. I supplemented these data by conducting cell culture experiments to gain further insight into the possible molecular function of DNAJC22.

For many years, the creation of transgenes to alter the murine genome has been based on standard cloning techniques. Restriction endonucleases were used to cut DNA and assemble the different parts of a targeting vector by re-ligation thereof. By this means, the areas of possible manipulation in a genomic locus were confined to the recognition sites of the respective endonucleases as well as their uniqueness within the whole DNA construct. Recently, employing phage-based recombination functions (“recombineering”) in bacteria helped to overcome those complications. Transformation of the mini-phage λ renders bacteria competent for homologous recombination. Integrating or exchanging a certain DNA sequence in a construct can be achieved by adding short homologous arms at each end to target it to the site of choice. Transformation of this linear piece of DNA into recombination-competent bacteria bearing the target construct to be manipulated, leads to the desired alteration via homologous recombination[77,80,86,87].

The genomic locus of *Dnajc22* turned out to exhibit many restriction sites of usually seldom cutting restriction nucleases, which made the creation of a targeting strategy and design of a suitable targeting vector very challenging. By utilizing recombineering it was possible to overcome these limitations. After retrieving the genomic locus of *Dnajc22* via gap repair from a BAC, two cassettes were introduced by recombineering. The two cassettes themselves were produced by basic molecular biology techniques (PCR, fusion of single parts via SOE-PCR, and standard cloning procedures). The advantage in this approach was,

that it was possible to place the first cassette – containing the 5' loxP site – and the second cassette – containing the 3' loxP site, the neomycin resistance for negative selection during screening in ES cells, as well as the reporter gene – at the exact place of choice (see section 2.2.1)[77].

Dnajc22 knockout mice are viable, fertile and are born in nearly Mendelian ratio when bred heterozygously. Morphological and histological examinations revealed no obvious major alterations. Studying transcript levels of different tissues of the body identified the kidneys, liver and intestine as the main sites of expression in the mouse.

The YFP gene on the transgenic allele was genetically engineered to mimic the expression of *Dnajc22* as closely as possible. For this purpose the untranslated regions of *Dnajc22*, which are excised from the locus in case of Cre-mediated generation of the knockout allele, were added to the YFP sequence. Thus, YFP expression in the heterozygous or knockout mice can be used as a reporter gene to identify time and place of *Dnajc22* promoter activity. Indeed, I could confirm presence of YFP protein in the kidneys, liver and intestine though the overall low transcript levels in other tissues detected via quantitative real-time PCR did not translate into positive results in the YFP Western blot hybridization.

A somewhat puzzling observation along the way was that transcript levels of the reporter gene in knockout animals were significantly elevated when compared to those of the wildtype *Dnajc22* transcript. One possible explanation could be that this is a result of a response of the cell or organism to counteract the loss of *Dnajc22* transcript and protein. Another reason for this increase could be the absence of the second intron in the reporter gene including possible regulatory sequences that have a repressive effect on the *Dnajc22* promoter. This finding raises the question if the YFP reporter gene expression exactly reflects the endogenous *Dnajc22* expression levels. However, the difference on transcript level did not lead to an increase in potential false-positive results on the level of YFP protein expression.

3.1 *Dnajc22* prevents salt-sensitive hypertension

The kidneys are one of the three major sites of *Dnajc22* expression in the mouse. Since there were no evident differences in the morphological appearance of the organ in the *Dnajc22* knockout mouse, I examined whether there were any functional complications by analyzing the urine composition.

Defects in electrolyte handling could be reflected by changes in the water balance. Compared to control animals *Dnajc22* mice drank less and produced less, but more concentrated urine. Overall they seem able to produce urine output adjusted to their water intake. *Dnajc22*-deficient mice excreted similar amounts of protein via the urine (data not shown). It can be assumed that *Dnajc22* knockout animals have an intact glomerular filtration barrier. This matter is also supported by the fact that no *in situ* staining as well as no reporter gene expression could be observed in glomeruli arguing for no functional impairment by the loss of *Dnajc22*.

A more detailed analysis of various electrolytes showed moderate, but non-significant changes in sodium and chloride under normal conditions (see section 2.2.2). Since the ability of the kidneys to maintain the osmotic balance of the organism has a direct impact on the extracellular volume in the body, it can thereby also affect blood pressure. The lower sodium and chloride excretion values under normal conditions in *Dnajc22*-deficient mice prompted me to investigate the blood pressure. Under normal conditions *Dnajc22* knockouts have a slightly higher (though non-significant) peripheral blood pressure than their wildtype littermates. Repeated analysis after challenging the mice with a high salt diet for two weeks revealed that *Dnajc22* knockout mice are indeed prone to develop hypertension. Urine analyses indicated that they were not able to cope with the electrolyte challenge as well as their wildtype littermates, as they secreted less sodium as well as less chloride (see section 2.2.3).

Decreased sodium and chloride excretion argues for retention of these two electrolytes due to increased reabsorption. In these lines, loss of *Dnajc22* seems to have a positive effect on the apical sodium transporters of the nephron. Since *Dnajc22* is expressed in the kidney, it may act as a negative regulator of a channel itself, regulating its activity or presence at the plasma membrane, or a positive regulator of another channel inhibitor. Thus, down-regulation of sodium reuptake from the urine will fail when needed. Such a signaling network becomes even more evident in a situation of augmented dietary salt intake, when the kidney should normally enhance sodium chloride excretion by reducing its reabsorption. It could well be that this process is abolished in the *Dnajc22* knockout mouse, such that the organism continues to reabsorb sodium chloride to a greater extent than it should at the expense of hypertension.

It is still debatable in which part of the nephron, *Dnajc22* may influence sodium transport. *Dnajc22* is expressed in the cortex and outer medulla (see section 2.2.2).

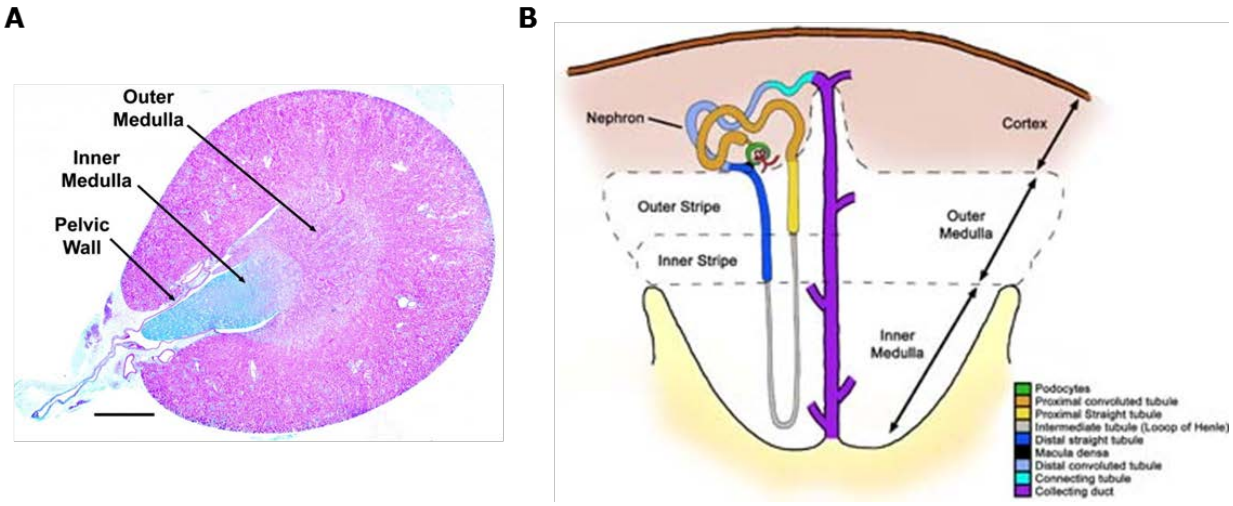

Figure 3.01 Schematic organization of the mammalian kidney

A Alcian blue staining of a coronal slice from rat kidney. Scale bar = 2mm (modified from[88]) **B** Schematic overview over the localization of different nephron segments within the kidney (modified from[89])

The *in situ* data for *Dnajc22* as well as YFP co-staining with phalloidin suggest expression in proximal tubule segments. Its cortical expression pattern resembles that of other proximal expressed proteins, such as Aldolase B and Megalin (Figure 3.02 C+D). The sodium transporters NKCC2 (*Slc12a1)*, NCC (*Slc12a3*), and ENaC (*Scnn1b+g*) (Figure 3.02 E-H) are most prominently expressed in the thick ascending limb, distal tubule, and distal tubule/connecting tubule/collecting duct respectively. Co-expression with *Dnajc22* has yet to be verified. Likely no overlapping expression can be found with Aquaporin 2 (Figure 3.02 I) marking the collecting duct.

3.1.1 Sodium handling in the distal nephron and collecting duct

The data obtained in *Drosophila melanogaster* hinted to a possible functional interaction between Wurst and the fruit fly orthologs of the mammalian epithelial sodium channels (ENaC)[70]. Following this hypothesis is intriguing because proper ENaC function is not only related to liquid clearance of the lung[24,73,90], but has also been strongly associated with disorders in blood pressure regulation[91]. Loss of function through missense mutations in one of the three subunits of the channel leads to pseudohypoaldosteronism type I[21–24], an autosomal recessive disorder characterized by salt wasting, hyperkalemia and metabolic

acidosis, whereas gain of function results in Liddle's syndrome[25–27]. In Liddle's syndrome patients, mutations in the C-terminal region of the beta or gamma subunit abolish interaction with the E3 ubiquitin ligase NEDD4. As a result ENaCs are no longer a target for degradation causing increased abundance at the plasma membrane and thereby promoting continued sodium reabsorption[92–94].

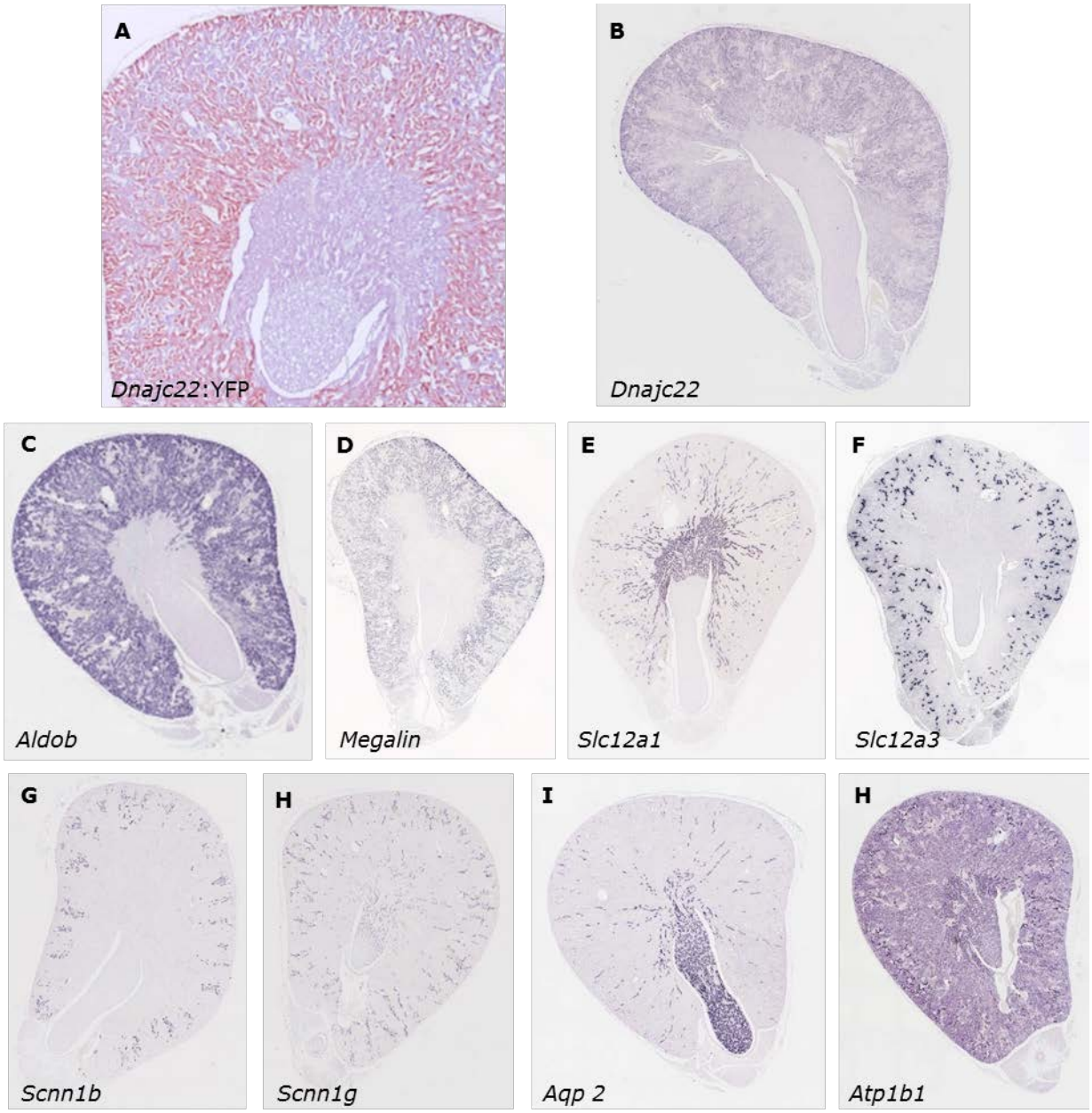

Figure 3.02 Expression patterns of *Dnajc22* and various typical renal genes

A Immunohistochemistry staining for YFP in the kidney of a D*najc22* knockout mouse showing *Dnajc22* promoter activity **B-H** *in situ* hybridization for the depicted genes (data from the GUDMAP project[82,83]). *Aldob* and *Megalin* are expressed in the proximal tubule. *Slc12a1* is most prominent in the thick ascending limb. *Slc12a3* is a marker of the distal tubule. *Scnn1b+g* are present in the distal and connecting tubule as well as the cortical collecting ducts. *Aqp2* is expressed in the collecting ducts. *Aldob:* Aldolase B, *Slc12a1*: solute carrier family 12, member 1 (NKCC2), *Slc12a3*: solute carrier family 12, member 3 (NCC), *Scnn1b*: βENaC, *Scnn1g*: γENaC, *Aqp2*: aquaporin 2, *Atp1b1*: Na^+/K^+-ATPase, β 1 polypeptide

As in the mouse model for Liddle's syndrome[27], *Dnajc22* knockout mice develop normally and show no changes in serum levels of sodium, potassium, or chloride under normal conditions. Another similarity is the development of hypertension upon receiving a high salt diet. Mice heterozygous for the Liddle mutation show a 15 mmHg systolic and 8 mmHg diastolic increase in blood pressure compared to their wildtype littermates; *Dnajc22*-deficient mice a 14 mmHg and 16 mmHg increase respectively. On the contrary, *Dnajc22* knockout mice do not develop hypokalemia due to loss of potassium via the urine. Sodium absorption by ENaC in the collecting duct is electronically coupled to potassium secretion.
This finding questions the functional interaction of DNAJC22 and ENaC in the collecting duct.

Interestingly, *Dnajc22* knockout mice also share phenotypic features with recently reported conditional *Nedd4L* knockout mice, in which the deficiency was induced in adult animals in a nephron-specific manner[95]. These *Nedd4L*$^{(Pax8/LC1)}$ knockout mice also show no apparent phenotype under normal conditions, but develop hypercalciuria and hypertension on high salt diet (10 mmHg increase compared to wildtype littermates when recorded at night). Studying protein expression in the kidney revealed an increased expression of NCC, but not all ENaC subunits. Furthermore, the observed hypertension could be reduced by a NCC-inhibiting thiazide (but not ENaC-inhibiting amiloride) treatment. This result was rather unexpected, since ENaCs are known to be down-regulated by NEDD4 – the process that is impaired in Liddle's syndrome. Yet, ENaC activity in the distal nephron and cortical collecting duct was found to be diminished. Although there was an increased expression of β- and γENaC, these were mainly found cytoplasmic, αENaC was down-regulated on transcript level and unchanged on protein level[95].
As seen in the *Nedd4L*$^{(Pax8/LC1)}$ knockout mice , the kidney often responds to alterations in the activity of single sodium transporters with compensatory changes in the expression levels of other sodium transporters attempting to maintain sodium balance[96]. Another example is the kidney-specific (KS) knockout of the kinase-defective isoform of WNK1 that is expressed in the distal convoluted tubule. The *KS-Wnk1* knockout mouse also displays up-regulated NCC, while all three ENaC subunits are down-regulated[97].
In humans, elevated NCC activity causes pseudohypoaldosteronism type II (PHAII)[30]. Besides hypertension, hyperkalemia is a typical symptom of PHAII patients. *Nedd4L*$^{(Pax8/LC1)}$ knockout mice, however, were able to maintain their Na^+/K^+ balance and showed no signs of hyperkalemia. Potassium excretion in the collecting duct is coupled to ENaC-mediated sodium absorption as the electrochemical driving force. Protein levels of the apical K^+ channel ROMK were revealed to be up-regulated in the collecting duct as well as in the connecting tubule, the distal convoluted tubule, and the thick ascending limb explaining the lack of hyperkalemia with heightened K^+ secretion via the urine[95].

I obtained similar results studying kidneys from *Dnajc22* knockout mice that have been fed a high salt diet: quantitative real-time data showed a significant reduction in *Scnn1a* mRNA

(and *Scnn1b*) while no difference on protein level could be seen (see section 2.2.3). Reduced *Scnn1a* mRNA levels may arise from low plasma aldosterone levels as seen in *Nedd4L*$^{(Pax8/LC1)}$ knockout mice. Considering these features, enhanced NCC activity might contribute to the observed salt-sensitive hypertension in *Dnajc22* knockout mice while diminished ENaC activity in the final parts of the nephron is a sign of compensation.

Thinking in lines of the theoretical functional interaction of DNAJC22 and ENaC, the question remains if this interaction is also true in the mammalian system. Heterologous expression of human DNAJC22 in human embryonic kidney cells leads to a reduction of the overall αENaC protein level (unpublished data by Tamara Krsmanovic). This finding supports the theory of DNAJC22 being an inhibitory factor for proper ENaC function. Comparable observations have been made for NEDD4-2 and WNK4, overexpression of which led to a reduction in ENaC levels in the renal A6 cell line from *Xenopus laevis*[98]. Murine models studying NEDD4-2 and WNK4 have proven that this interaction may not translate into the most prominent feature of the physiological phenotype[29,95].
A direct connection between DNAJC22 and ENaC could have explained the salt-sensitive hypertension by an aberrant increase in channel activity in the distal nephron parts and the collecting duct. However this does seem unlikely in the *Dnajc22* knockout mouse based on the comparison with the phenotype of the *Nedd4L*$^{(Pax8/LC1)}$ knockout mouse[95]. On the one hand, one could argue that the interaction simply does not happen because *Dnajc22* may not be expressed in the same parts of the nephron. From *Dnajc22 in situ* and YFP reporter histochemistry no expression seems apparent in the collecting duct although localization to the distal convoluted tubule and connecting tubule in the cortex cannot be excluded. On the other hand, low ENaC activity could be a compensatory mechanism due to up-regulation of a different sodium transporter earlier in the nephron.

ENaC function is crucial for lung liquid clearance at birth. Knockout mice for the alpha subunit of the channel are perinatal lethal as they die from respiratory distress[73]. *Dnajc22* knockout mice are born at Mendelian ratios indicating no embryonic lethality. After birth they develop normal as there are no differences in body weight. Close observation of newborn pups show no breathing problems or cyanotic conditions. Also, examining lung wet/dry weight ratios shortly before and after birth as a measure for lung water content indicate no disturbance of lung liquid clearance in *Dnajc22*-deficient animals (Figure 3.03). These observations indicate that there is likely no functional interaction between DNAJC22 and αENaC in lung. Since knockout models for the beta and gamma subunits show by far less obvious lung phenotypes[23,24], an interaction of DNAJC22 with these subunits cannot be excluded.

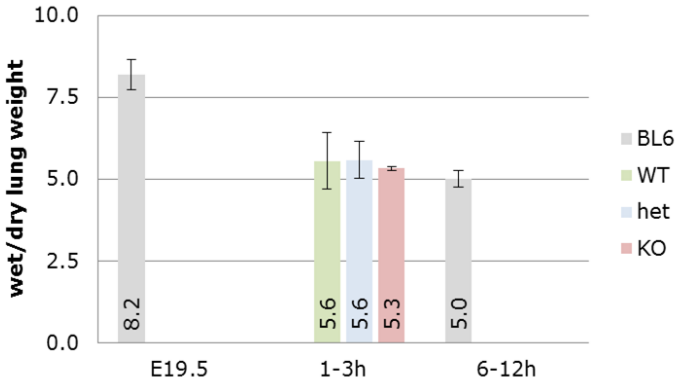

Figure 3.03 Lung liquid clearance in *Dnajc22* knockout mice

Wet-to-dry lung weight measures of one litter 1-3h after birth (4 wildtype (WT), 3 heterozygous (het), and 2 knockout (KO) animals) as well as E19.5 embryos (n=11) or newborn pups (n=14) from C57BL/7 wildtype mice (BL6).

ENaC also promotes sodium transport in the colon[99], where *Dnajc22* and ENaC are co-expressed. Altered intestinal ENaC function has been associated with diarrhea[100]. *Dnajc22* knockout mice neither show significantly increased colon length (WT 7.5 cm ±1.0 vs. KO 7.4 cm ±0.9, p value = 0.9, n= 4-7) nor signs of diarrhea. Measurements of transepithelial amiloride-sensitive potential differences will be helpful to see if loss of *Dnajc22* influences ENaC activity.

Taken together, a functional interaction between DNAJC22 and ENaC seems unlikely. The current physiological data obtained in the *Dnajc22* mouse model does not sufficiently support an interaction between DNAJC22 and ENaC, albeit it cannot be neglected. After all, the *Dnajc22* knockout mice suffer from sodium retention and salt-sensitive hypertension as the mouse model for Liddle's syndrome.

Another renal sodium channel in the distal tubule, that has been associated with hypertension, is the sodium-chloride symporter NCC. Mutations in regulatory proteins that result in inappropriately high NCC activity, such as the kinases WNK1[30,32,101], WNK4[28,30,101] as well as the KLHL3/CUL3 ubiquitin-protein ligase complex[33,34], have been identified in patients with pseudohypoaldosteronism type II. NEDD4 has initially been implicated to contribute to the pathogenesis of Liddle's syndrome[102]. Later studies showed that it can also act as a repressor on other channels than ENaC, namely NCC, as seen by the PHAII-like phenotype in *Nedd4L*$^{(Pax8/LC1)}$ knockout mice[95].

PHAII patients suffer from hypertension, hyperkalemia, and hypercalciuria. So far, electrolyte concentrations in the serum of *Dnajc22*-deficient mice challenged with high salt diet have not been analyzed. Measurements of urinary calcium concentrations were

hampered by often being below the detection limit. Though it must be noted, that wildtypic values were not measurable more frequently.
Dnajc22 knockout may well be a new model for PHAII. Further studies are needed to prove if loss of DNAJC22 increases NCC activity.

Although localization of DNAJC22 in the thick ascending limb and/or distal tubule is not impossible the current expression data clearly favors a more prominent role in the proximal part of the nephron.

3.1.2 Sodium handling in the proximal nephron

Most blood pressure regulation disorders have been attributed to changes in electrolyte transporter or channel activities in the more distal parts of the nephron and collecting ducts. In the light of the fact, that changes in sodium reabsorption in the proximal parts of the tubule can be compensated later on, it seems questionable to what extent sodium transport in the proximal tubule can influence blood pressure regulation. Nevertheless, altered sodium handling in the proximal parts of the nephron can ultimately affect blood pressure[103].

Loss of function of the predominant proximal sodium transporter NHE3 leads to a reduction in blood pressure[14–16]. An increase in NHE3 abundance and activity can be observed upon abrogation of dopamine signaling in the proximal tubule – such as in mice deficient for the dopamine producing enzyme aromatic amino acid decarboxylase (AADC)[104] or one of the dopamine receptors[105].
Stimulation of dopamine receptors inhibits proximal sodium reabsorption[105]. NHE3 activity and protein abundance at the apical membrane are decreased[106] and the basolateral Na^+-K^+-ATPase is down-regulated via endocytosis[103]. In a situation, in which the organism has to cope with an increase in dietary sodium intake, more than half of the sodium excretion is a consequence of activation of the renal dopaminergic system[103]. Dopamine receptor knockout mice develop hypertension[105]. A mutation in the dopamine receptor D1 has also been found to be responsible for the elevated blood pressure found in spontaneously hypertensive rats[107].
Additionally, constitutively active variants of the G protein-coupled receptor kinase type 4 (GRK4) have been associated with essential and/or salt-sensitive hypertension in several ethnic groups. Dopamine receptor 1 and 3 are hyper-phosphorylated by this kinase, subsequently desensitized, and internalized[35]. Additionally expression of the angiotensin II receptor type 1 (AT_1R) is increased by GRK4, which further increases sodium transport in the proximal tubule via stimulation of the Na^+-K^+-ATPase[103].

Salt-sensitive hypertension in *Dnajc22* knockout mice may be explained by altered proximal sodium handling: DNAJC22 could be a positive regulator of the dopamine receptor or dopamine synthesis. Therefore loss of DNAJC22 would be accompanied with a decrease in the natriuretic effect of dopamine. During high dietary sodium intake, the dopaminergic system would be less effective in promoting sodium excretion. It is also thinkable that DNAJC22 may be a negative regulator of GRK4, AT_1R or the Na^+-K^+-ATPase. Since all sodium reabsorption is secondary active transport, apical sodium entry into the cell is dependent on activity of the Na^+-K^+-ATPase. It is known that increased expression of Na^+-K^+-ATPase in the proximal tubule stimulates NHE3 activity[108]. Yet, the role of the Na^+-K^+-ATPase in the development of hypertension is not completely understood[103].

3.1.3 Chloride and blood pressure regulation

Chloride reabsorption is closely linked to that of sodium. While it is taken up on a paracellular route along electrochemical gradients in the proximal tubule, basolateral chloride channels (CLC-K) in the more distal parts of the nephron are secondarily linked to sodium reabsorption. In the thin ascending limb, ClC-K1 is essential for urine concentration and in the thick ascending limb as well as the distal tubule crucial for efficient sodium chloride reabsorption in concerted action with NKCC2 and ROMK[109,110].
Genetic polymorphisms in CLC-K channels resulting in gain of function may be associated with hypertension[111–113]. However, different studies could not reproduce the result in other cohorts so that the association remains controversially discussed[114,115].

Moreover, Pendrin (*Slc26a4*), a Cl^-/base exchanger in the cortical collecting duct, has been shown to be sensitive to dietary salt intake. Dietary chloride restriction leads to an up-regulation of the transporter and consequently chloride retention in a limiting situation[116,117]. Additionally, SLC26A6 mediates Cl^-/HCO_3^- exchange in the proximal tubule, thereby facilitating transcellular sodium chloride absorption[118]. Misregulation of SLC26A6 has been associated with increased blood pressure in spontaneous hypertensive rats[119].

Gain of function mutations in both transporters conceivably may lead to sodium chloride retention and thus play a role in the pathogenesis of hypertension. Yet, functional evidence in humans for an association to blood pressure regulation is still missing[118].
Dnajc22 knockout mice show defects in chloride excretion, especially when challenged with a high salt diet. On the lines of the discussed hypotheses for sodium handling, an additional or alternative explanation for the salt-sensitive hypertension in *Dnajc22*–deficient animals could be that DNAJC22 may be a negative regulator of apical chloride transport. In case of an elevated dietary chloride intake, loss of DNAJC22 could prevent the down-regulation of

chloride transport activity leading to undesired chloride retention. If DNAJC22 directly affects chloride transporters or if this finding is only secondary to an alteration in sodium handling remains to be clarified.

3.1.4 Systemic blood pressure regulation

Aside from possible disturbances in the local regulation of electrolyte transporters in the epithelial cells of the nephron, blood pressure is controlled by systemic mechanism, such as the renin-angiotensin system.

Renin is secreted by the kidney and cleaves angiotensinogen to angiotensin I. Subsequently produced angiotensin II will elicit the secretion of aldosterone from the adrenal glands, which in turn increases sodium retention via action on NCC and ENaC activity in the distal nephron and collecting duct[12]. Hence, Renin elevates blood pressure by reducing sodium excretion in the kidney. Transcript levels of *Renin* were unchanged in the kidneys of *Dnajc22*-deficient mice (after high salt diet) compared to the wildtype controls. The observed sodium retention is therefore not an effect of altered *Renin* levels.
The mineralcorticoid aldosterone, which is released from the adrenal glands upon angiotensin II stimulation, elevates transcript levels of β and γENaC in the collecting duct. The finding, that *Scnn1g* levels in the kidneys of *Dnajc22* knockout mice (after high salt diet) were unchanged and *Scnnn1b* levels even reduced, argues against altered blood pressure due to elevated levels of aldosterone.
These findings suggest that the observed salt-sensitive hypertension in *Dnajc22*-deficient mice is not a consequence of an abnormal increased activity of the renin-angiotensin system.

Hypertension can also be mediated by alterations in further downstream mediators of the renin-angiotensin pathway as well as changes in peripheral vasoconstrictory mechanisms, the heart, or regulatory circuits of the central nervous system. Recent findings have even described a role for cells of the mononuclear phagocyte system (MPS) in the skin on the development of hypertension[39,40].
There was no reporter gene expression evident in the vascular endothelium. *Dnajc22* transcript levels in macrophages are very low under normal conditions. It remains a matter of investigation if expression can be substantially up-regulated under certain conditions in tissues apart from the kidneys, liver and intestine.
Although other hypothesis should not generally be neglected, considering the strong renal expression pattern of *Dnajc22* I concentrated on a renal-immanent explanation for osmoregulation.

The presented results were obtained using a ubiquitous *Dnajc22* knockout model. I should like to point out again that the *Dnajc22* mouse was originally generated by introduction of a conditional knockout allele flanking the open reading frame with loxP sites. This transgenic line was then initially bred with the PGK-Cre line, in which the PGK promoter drives Cre recombinase expression necessary for the excision of the floxed *Dnajc22* sequence from a very early moment onwards in embryonic development[81]. In case of a lethal phenotype after a complete loss of function, the conditional knockout allows the generation of less severe tissue-specific deletions.

In contrast to the *Drosophila wurst* mutant, the complete knockout of murine *Dnajc22* is not embryonic lethal. *Dnajc22*–deficient mice are even viable up to old age (over two years). Yet, the conditional mouse model still bears important advantages for future experiments: crossing the conditional *Dnajc22* allele to different Cre lines offers the possibility to eliminate *Dnajc22* solely from certain cell and tissue types or at certain time points of choice depending on the promoter used to express the Cre recombinase. This will help to further decipher the *Dnajc22* knockout phenotype, pinpoint what organ, tissue or cell type is relying on proper *Dnajc22* function, and its impact for the metabolic well-being of the whole organism.

For example, recent studies showed that Liddle's syndrome might not predominantly result from a renal malfunction of osmoregulation, but also a volume expansion resulting from increased sodium absorption in the distal colon[27,120], the stiffening effect of ENaC signaling on vascular endothelium[38] as well as ENaC hyperactivity in the brain[121] have to be taken into account in explaining the syndrome's clinical features[95].

A kidney-specific *Dnajc22* knockout will clarify if the observed phenotype originates from impaired renal function or if loss of *Dnajc22* from other tissues contributes to the observed alterations. Using Cre lines for different parts of the nephron will help to elucidate which segment is most important for DNAJC22 function[122].

Another functional approach to clarify the site of action is the utilization of available inhibitors for the different sodium channels in the kidney. Conducting the dietary high salt challenge accompanied by the administration of one of the inhibitors will reveal which channel is responsible for the development of hypertension in the *Dnajc22* mouse model. Amiloride inhibits ENaC, thiazides act on NCC and bumetanide or furosemide on NKCC2. Telemetric blood pressure assessment would be of value in such an experiment, because apart from being able to record diurnal rhythms, the reaction of the animals to the inhibitor can be resolved in a time-specific manner.

By generation of a mouse model for *Dnajc22* and investigation of the physiological consequences of the loss of function, I discovered that *Dnajc22* plays a crucial role in body salt homeostasis and that it is a susceptibility gene for salt-sensitive hypertension.

3.2 *Dnajc22* is a new player in the hyperosmotic stress response of the cell

Since *Dnajc22* is involved blood pressure control, I wanted to know whether it responds to osmotic challenges on a cellular level.

Dnajc22 transcript is only found in low amounts in the murine cell line M-1. This cell line is derived from cortical collecting ducts mirroring the murine *in vivo* expression data for *Dnajc22,* which was not detectable in this part of the kidney. However, subjecting the cells to hyperosmotic conditions – a situation to which the cell generally reacts with inhibition of transcription and translation[44] – led to an increase in *Dnajc22* mRNA levels.

Coping with hyperosmotic stress is predominantly orchestrated by the transcription factor NFAT5[49]. Examination of the *Dnajc22* promoter region revealed two potential binding sites -88 bp (5'-GGAAAGCTTC-3') and -2598 bp (5'-GGAAACCTAG-3') upstream of the first exon of *Dnajc22* that fit the NFAT5 consensus sequence 5'-GGAAANN(C/T)N(C/T)-3' (N=any base)[123]. Thus, regulation of *Dnajc22* through action of NFAT5 may be possible.

Inhibition of NKCC2 with bumetanide had been reported to reduce elevation of *Nfat5* transcript levels in response to hyperosmotic conditions[85]. Addition of sodium chloride to the cell culture medium in the presence of furosemide (a similar loop diuretic as bumetanide) also blunted the response of *Nfat5* induction as well as its target genes *Hsp70* and aldose reductase (*Akr1b3*) in M-1 cells. Yet, *Dnajc22* transcription was not affected by furosemide indicating that another signaling pathway independent from NFAT5 leads to the observed increase upon hyperosmotic stress.

Second, *Dnajc22* up-regulation upon stimulation with sodium chloride is not completely abrogated in a NFAT5-deficient setting. Online available microarray data comparing the genetic response to hypertonicity in mouse embryonic fibroblasts (MEFs) of wildtype or *Nfat5* knockout mice showed that in contrast to the known NFAT5 target gene *Akr1b3*, *Dnajc22* levels still increase in *Nfat5* knockout MEFs after hypertonic stress compared to untreated control cells[124] (Figure 3.04).

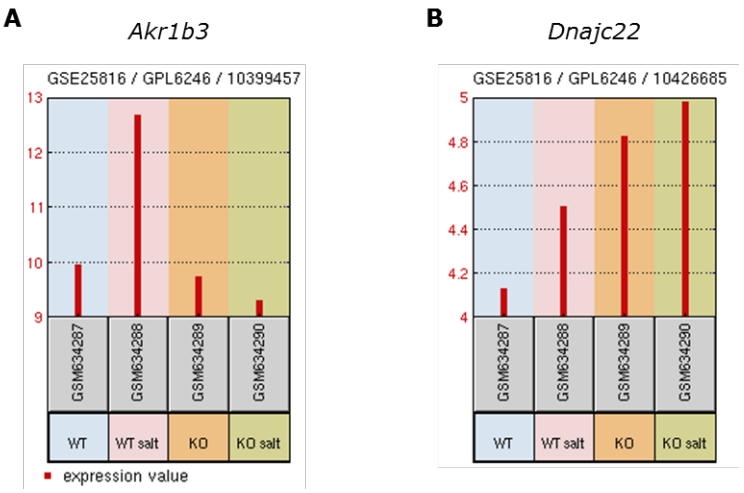

Figure 3.04 Gene expression changes in *Nfat5*-deficient MEFs under isotonic and hypertonic conditions

Aldose reductase (**A**) and *Dnajc22* (**B**) expression in mouse embryonic fibroblasts (MEFs) from wildtype (WT) and *Nfat5* knockout (KO) mice cultured in isotonic or hypertonic (salt / 75mM sodium chloride) medium for one day (data retrieved from[124]).

A third indication arguing against the sole regulation of Dnajc22 by NFAT5 is the discrepancy in distribution in the murine kidney. Here, expression of osmosensitive genes, such as Nfat5 and Akr1b3, follow the osmotic gradient and are predominantly expressed in the medulla[125]. This is the complete opposite pattern of that of *Dnajc22*, questioning a possible transcriptional regulation by NFAT5 in the in vivo situation in the kidney (Figure 3.05).

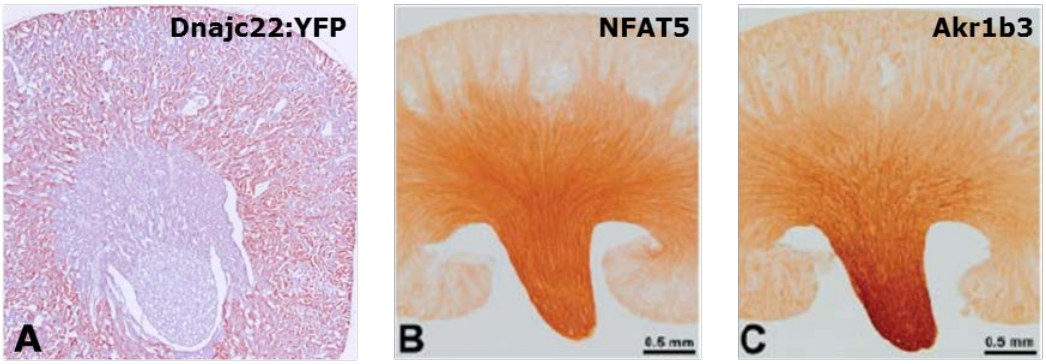

Figure 3.05 Renal expression of *Dnajc22* and osmosensitive genes

Immunostaining of the YFP reporter in the kidney of a *Dnajc22* knockout mouse (**A**) as well as immunostaining of NFAT5 (**B**) and aldose reductase (**C**) in kidneys from wildtype animals (modified from[125]).

Overexpression of wildtypic or a dominant-negative form of NFAT5 will help to clarify, if *Dnajc22* expression is regulated by this transcription factor. A second option would be the analysis of *Dnajc22* transcript induction after siRNA-mediated knockdown of Nfat5.

Several other transcription factors have been implicated to respond to hyperosmotic stress including ATF3, ATF4, c-Fos, c-Jun, Egr-1, Egr-3, HIF1α, HSF1, NF-κB, STAT1, or STAT3[44]. Further experiments to determine which factors evoke the tonicity-sensitive effects on *Dnajc22* transcription will shed light on the signaling pathway leading to the activation. This may in turn indicate a possible effector function of elevated *Dnajc22* levels.

My experiments revealed that *Dnajc22* mRNA is also induced by other hyperosmotic stressors than sodium chloride. Mannitol is another hyperosmotic substance. Exposure of M-1 cells to mannitol-containing medium of similar osmolality as used in the sodium chloride condition increased *Dnajc22* transcript levels as well, albeit to a lesser extent.
Interestingly, also urea affected *Dnajc22* transcription (in a similar dimension as sodium chloride). Membrane permeability of urea is comparable to that of water. Hence subjecting cells to higher urea concentration exposes them to hypertonicity, but urea does not create a gradient across the plasma membrane. Osmosis does not occur and the cell is not confronted with subsequent volume changes[126,127]. Sodium chloride and urea differ in their osmotic action and impose cellular stress by distinct signaling pathways. Whereas NFAT5 and HSP70 are the main factors helping the cell to cope with hypertonic stress, they are dispensable in case of urea stress[128]. Nfat5 and its target genes Akr1b3 (AR), Slc6a12 (BGT1), or Slc6a6 (TAUT) have been found to be unaffected or even down-regulated upon urea stress[129,130]. Urea can either act as a stressor inducing oxidative stress[131], cell cycle arrest, and apoptosis[132,133], or at lower concentrations also as a growth-promoting factor via multiple signaling pathways[128,134,135]. As urea stress-induced transcription has also been found to be mediated by EGF receptor signaling[136]. It will be interesting to know if activation of the pathway with the ligand itself will trigger *Dnajc22* transcription as well. On the contrary, subjecting cells to urea stress in the presence of an EGF receptor signaling inhibitor (such as AG-1478) will show if this can blunt *Dnajc22* induction[137].

The diminished response to mannitol raises the question if *Dnajc22* transcript levels are indeed regulated by hyperosmotic substances in general or if the seen effect is specific for sodium chloride. Testing more hyperosmotic chemicals like sucrose or raffinose may further elucidate the nature of *Dnajc22* transcription stimulants and clarify if up-regulation of *Dnajc22* coincides with changes in cell volume. Glycerol is another membrane-permeable solute as urea and examination of its effect on *Dnajc22* mRNA levels will show if hypertonicity alone, without affecting cell volume, is sufficient for induction.

Hyperosmotically induced macromolecular crowding upon loss of cell volume as well as the fact that high concentrations of urea denature proteins might suggest that these conditions may elicit an unfolded protein response (UPR) in the cell. UPR is initiated upon ER stress and many molecular chaperones are up-regulated to help the cells cope with the misfolded

proteins either by refolding or channeling them to degradation[138]. DNAJC22 is a cochaperone and by protein classification potentially involved in standard HSP-related functions such as protein folding[62]. Yet although being localized at the endoplasmic reticulum (ER), DNAJC22 is not a typical UPR cochaperone. Inducing ER stress in human embryonic kidney cells with tunicamycin or thapsigargin does not induce *Dnajc22* (data not shown). In line with this finding, it was shown that neither urea nor sodium chloride produce ER stress and the UPR[139] and consequently also GRP78, one of the hallmark HSPs of ER stress, is not up-regulated upon hyperosmotic stress[140].

Testing other salts than sodium chloride showed that *Dnajc22* is also induced by magnesium chloride and potassium chloride, but not by sodium bicarbonate.
My results are consistent with previous findings showing that potassium chloride is a more potent inducer of hyperosmotic stress than sodium chloride[141]. Comparing the composition of the different salts analyzed leads to the hypothesis that chloride may be the trigger of the hyperosmotic effect on *Dnajc22* transcription. Sodium acetate, sodium gluconate and chloride choline are other substances that could be tested to further elucidate the nature of the stimulant that leads to *Dnajc22* induction.
In contrast to furosemide, amiloride abrogated the induction of *Dnajc22* expression in response to hypertonic stress induced by sodium chloride. Amiloride is known as a specific inhibitor of ENaC-mediated sodium transport, but inhibits various other sodium transporters as well – though at higher concentrations[142]. This finding indicates that sodium entry into the cell is crucial for the observed effect in case of stimulation with sodium chloride. It will be interesting to see if amiloride can blunt the response to potassium chloride as well.

So far, only one other J protein has been reported to be regulated by hypertonicity. *Dnajb4* mRNA was induced by sodium chloride and raffinose, but not by urea in murine inner medullary collecting duct (mIMCD) cells. Based on the inhibitors studied this effect is not mediated by NFAT5[143]. *Dnajb4* was characterized as an immediate-early gene, since elevated transcript level could be detected as early as one hour after induction, persisted at four, but was gone at eight hours. On the contrary, *Dnajc22* transcript was found to be increased six hours after stimulation, an effect that was still present after 24 hours (data not shown).

Hyperosmolar stress is the first stimulus identified to regulate *Dnajc22* expression. It is not part of the immediate-early response, but induced in the process of adaptation. Many osmoprotective factors persist in high levels when a cell chronically adapts to hypertonic conditions[44]. How long *Dnajc22* remains up-regulated is yet to be determined, but since elevated mRNA levels are still present after 24 hours it is likely part of the long-term adaptation.

Helpful tools for the further elucidation of the cellular function of DNAJC22 will be the generation of genetically modified M-1 cell lines. Utilizing TALEN technology[144,145] or the CRISPR/Cas system[146,147] it is possible to introduce specific double-strand breaks in the genome, that can either result in mutations due to errors during non-homologous end joining repair or that can be used to generate transgenes by modifying the genome via homologous recombination at the site of the double-strand break.

A *Dnajc22*-deficient cell line may clarify the function of DNAJC22 during hyperosmotic stress. Comparison of this line with wildtype M-1 or *Dnajc22* overexpressing cells will reveal if DNAJC22 function has any impact on hyperosmolar stress susceptibility. Furthermore, equipping the endogenous protein with a tag will allow monitoring protein expression and localization in a non-overexpression situation. This cell line will also be of great value in the search for possible interaction partners of DNAJC22. For immunoprecipitation experiments coupled with the analysis by mass spectrometry, having this cell line at hand is a great advantage compared to the artificial overexpression situation. Moreover the DNAJC22-deficient line may serve as a negative control to sort out unspecifically bound proteins. It will be interesting to see, if any changes in localization can be observed upon salt challenge. In addition, the tagged protein will be useful to identify potential interaction partners by facilitating pull-down experiments that may be followed by mass spec analysis. Moreover, it will be possible to generate and study mutant forms of DNAJC22, such as a protein variant lacking the J domain, a potentially functional mutant by altering the catalytic tripeptide HPD in the J domain, and other deletion variants of the protein.

3.3 DNAJC22 – a new osmoregulator

Owing to the vast diversity of J proteins, the HSP70 machinery is able to carry out a variety of specific functions in the cell[62]. It is known to regulate exocytosis and endocytosis[148] as well as quality control of trafficked proteins. Aberrantly or not yet properly folded proteins can be retained in or at the endoplasmic reticulum either for ER-associated degradation (ERAD) or they can be refolded and released on the way to their destination[62].

Drosophila Wurst has been described to play a role in clathrin-mediated endocytosis[70].

In fact, many of the described electrolyte transporters of the mammalian kidney are regulated by internalization. When the organism encounters an elevated intake in dietary sodium, it counteracts reabsorption by redistributing the relevant sodium transporters or channels to an intracellular pool (e.g. ENaC in the distal tubule and collecting duct[149]).

Impeding the renal cell's ability to down-regulate sodium uptake will lead to aberrant sodium retention and hence promote salt-sensitive hypertension.

Heterologous expression of a C-terminally GFP-tagged DNAJC22 variant in M-1 cells is localized in the endoplasmic reticulum. By performing a fluorescence protease protection assay, I could show that the C-terminal J domain is facing the cytoplasm (see section 2.1).
DNAJC14 is one of the few J proteins of the C subfamily that shares structural similarities with the DNAJC22 protein: it features several transmembrane domains as well the J domain at the C-terminus, and it is located in the ER with the J domain facing the cytoplasm. It has been reported to represent a quality control check point for several G protein coupled receptors (GPCRs), such as the D1 dopamine receptor[150] or the chemokine receptor CCR5[151], retaining them in the ER and preventing premature transport to the Golgi. It has also been suggested that DNAJC14 is involved in the oligomerization of receptors as well as the formation receptor complexes with its accessory G protein[151,152].

In the light of these findings, one can hypothesize about an analogous molecular function of DNAJC22 in the regulation of dopamine signaling in the proximal nephron. Dopamine signaling inhibits sodium reuptake by decreasing activity of the apical sodium transporter NHE3 as well as by down-regulation of the basolateral Na^+-K^+-ATPase via clathrin-mediated endocytosis (see section 3.1.2). On the other hand, arguing in lines of a direct function for DNAJC22 in clathrin-mediated endocytosis, it could contribute to the inhibitory impact of the pathway on sodium reabsorption by assisting in the internalization of the Na^+-K^+-ATPase.
On the other hand, it may well be, that DNAJC22 is able to interact with GPCRs in the ER – similarly to DNAJC14. In this scenario, *Dnajc22*-deficiency could lead to a decreased assembly and/or exit of receptor out of the ER and possibly decreased presence at the plasma membrane, which would abrogate the inhibitory effect of dopaminergic signaling. In both cases, loss of DNAJC22 would hinder the cell to down-regulate sodium reabsorption when needed, hence promoting hypertension.

The Na^+-K^+-ATPase consists of two subunits and is assembled in the ER as well. Instead of a role of DNAJC22 in the clathrin-mediated endocytosis of ENaC, a DNAJC22-mediated regulation of the Na^+-K^+-ATPase – directly or potentially via interference with the dopaminergic signaling pathway – would rather be in line with the obtained expression data for *Dnajc22* as well as with an explanation of the phenotype based on signaling events in the proximal tubule of the kidney. It will be interesting to investigate, if this hypothesis holds true. A mechanistical interaction between DNAJC22 and the Na^+-K^+-ATPase remains to be clarified.

However, applying the concept of DNAJC22 as a quality control checkpoint at the ER, it may be also possible that it interacts with other sodium transporters that are consequently

retained and prevented from transport to the Golgi. Loss of function would lead to enhanced trafficking of such sodium transporters to the plasma membrane resulting in abnormal sodium reabsorption and consequently perturbation of blood pressure regulation.

Aside from the kidney, *Dnajc22* is also expressed in the intestine and the liver. It will be exciting to see what function DNAJC22 carries out in these organs – especially in the context of osmotic stress. Both organs are metabolically very active organs and the intestinal epithelial cells as well as the hepatocytes are subjected to variable osmotic conditions under physiological situations by the dietary metabolites. In fact the liver is hyperosmolar compared to serum. Lymphoid tissue is another example [153].

Furthermore, it will be interesting to investigate if expression of *Dnajc22* can be induced in any other tissue or cell type. Hyperosmotic stress has been primarily studied in renal cells, but in recent years also other cell types have been studied[45]. Hyperosmotic microenvironments may also arise in pathological situations such as at the site of inflammation or in a tumor[43].

Recently, protein levels of DNAJC22 has been reported to be reduced in colorectal cancer tissue compared to normal controls[154] though no functional data was provided. My own transcript expression studies showed increasing transcript levels during development (data not shown). Expression of DNAJC22 seems to be a feature of differentiated epithelial cells. It may well be that the protein is involved in tumorigenesis as a tumor suppressor.

3.4 Potential implications for human diseases

Hypertension is a major risk factor for peripheral vascular disease, congestive heart failure, myocardial infarction, stroke, and overall mortality[155]. According to the 2013 World Health Statistics report published by the World Health Organization (WHO), the global prevalence of raised blood pressure is about 25% in adults over the age of 25. The number of nearly one billion affected people shows the importance of this public health challenge worldwide[156].

High dietary salt intake has often been proclaimed to be detrimental in hypertensive patients. However a reduction in salt intake has not yet been confirmed as an effective measure to lower blood pressure – presumably due to the fact that not every patient with high blood pressure is also necessarily salt-sensitive[157]. In fact, also harmful effects of this approach have been reported (inverse salt-sensitivity)[158]. Dietary salt restriction as part of a general treatment plan is therefore still controversially discussed[155].

In this present work, I have identified murine *Dnajc22* as a susceptibility gene for salt-sensitive hypertension. Regarding the high evolutionary conservation between *Dnajc22* and its human homolog, the question arises if DNAJC22 is affecting blood pressure in humans as well.
Data from a recent study on genetic variants influencing blood pressure and cardiovascular risk[159] showed no association of these traits with DNAJC22 (data analyzed by Stefanie Heilmann from the Institute of Human Genetics, University of Bonn). Narrowing down the patient collective to be analyzed specifically to salt-sensitive hypertensive subjects and compare these with normotensive people may raise the chances of finding associated genetic variants in the DNAJC22 locus.

Differentiating between salt-sensitive and salt-resistant hypertension is important because salt-sensitivity is, also independent of blood pressure, a risk factor for cardiovascular morbidity, and mortality as well as other diseases[160]. Knowledge about this parameter would be beneficial for optimizing an individual therapy plan. Unfortunately, practicable routine testing methods are not yet developed[155]. It is thinkable that genetic variation in the DNAJC22 locus could be a marker for salt-sensitivity and that in the future predictive genomics will help the disease management as a diagnostic tool[160].

As proper DNAJC22 function protects from the development of salt-sensitive hypertension, learning about interaction partners and the molecular mechanisms influencing its actions will help to understand its role in blood pressure regulation. Identifying ways to stimulate its function may provide an alternative starting point for antihypertensive therapy – be it either by a stimulant or by inhibiting a factor that negatively regulates DNAJC22.

Blood pressure is regulated by complex interactions between genetic and environmental factors. Disturbances in renal epithelial electrolyte transport mechanisms have been identified in many cases of salt-sensitive hypertension. Whereas mutations in some genes lead to detrimental effects already under normal circumstances, these rare monogenic forms of hypertension explain only a very low percentage of the elevated blood pressure seen in salt-sensitive patients[161]. There are still many factors to be identified – one of which may be DNAJC22.

4 Materials

4.1 General materials

4.1.3 Technical equipment

Autoclave	H+P Varioklav Dampfsterilisator EP-2
Bacterial incubator	Innova 44 New Brunswick scientific
Balances	BL 1500S + BP 211D Sartorius
Cetrifuges	5415 D + 5415 R Eppendorf
	Megafuge 1.0R Heraeus
	Avanti J-20 XP + JA-10 Rotor Beckmann Coulter
	Biofuge primo R + Multifuge 3L-R Heraeus
Confocal microscope	LSM710, Zeiss
Cryostat	Leica
Electroporation console	E.coli Pulser Bio-Rad
	Biorad Gene Pulser Xcell
Electrophoresis equipment	Bio-Rad
Homogenizer	Precellys, Peqlab
Incubation shaker	Unitron Infors HT
	Innova 4230 New Brunswick Scientific
Metabolic cages	Techniplast
Microwave	Panasonic
RealTime PCR machine	iCycler, BioRad
Spectrophotometer	NanoDrop2000, Thermoscientific
Thermal Cycler	MJ Research PTC 150 Peltier Minicycler Bio-Rad
	MJ Research PTC 200 Peltier Bio-Rad
Thermomixer	5436 + compact + comfort Eppendorf
UV cross linker	Stratalinker 2400, Stratagene
UV hand lamp	Konrad Benda Laborgeräte
Vortexer	Vortex Genie2, Scientific Industries
Water bath	Julabo SW22

4.1.2 Consumables

1.5 / 2 ml reaction tubes	Eppendorf
Cover slips	VWR
Electroporation cuvette 0.8 cm	BioRad

Falcons	Sarstedt
Microscope slides	VWR
Nitrocellulose membrane	Amersham
O.C.T. TissueTek	Sakura
Plastic wares	Greiner
Sephadex G50 columns	GE Healthcare
Superfrost Plus adhesive microscope slides, ThermoScientific	
X-ray films	Fuji Medical X-Ray Film Super RX

4.2 Buffers, solutions, media

All buffers, solution and media were prepared with double distilled water (ddH_2O). The pH was adjusted with NaOH or HCl, if not described otherwise. Stock solutions are concentrated as indicated. Solutions, not being stored at room temperature, have their storage temperature depicted. All percentages correspond to mass per volume.

4.2.1 General buffers and solutions

Agarose

0.8-1.5% agarose (Roth) in 1x TAE

Ampicillin

100 mg/ml stock in ddH_2O, use 1:1,000 (100 µg/ml), store at -20 °C

Blocking solution

5% milk powder (Roth) in 1x TBST

10x DNA Loading Dye

40 % sucrose (saccharose), 0.2 % Orange G, 0.2 % Xylencyanol

Fixating solution / Histofix

4% paraformaldehyde in PBS (Roth)

Glycerol Solutions

10% and 50% glycerol (v/v) is dissolved in ddH2O and autoclaved prior to utilization.

Laird buffer

0.1 M Tris (pH 8.0), 0.2 % SDS, 0.2 M NaCl, 5 mM EDTA

20x PBS

2.6 M NaCl, 140 mM Na_2HPO_4, 60 mM NaH_2PO_4 (pH 7.0)

Proteinase K Buffer

100 mM Tris (pH 8.5), 5 mM EDTA, 0.2 % SDS, 200 mM NaCl, 200 µg/ml RNase A, 200 µg/ml Proteinase K

RIPA buffer

150 mM NaCl, 1 % IPEGAL CA-630, 0.5 % sodium deoxycholate, 0.1 % SDS, 50 mM Tris-HCl (pH 8.0)

5x SDS-PAGE loading buffer

100 mM Tris, 3% SDS, 10% Glycerol, 0.1% Bromphenolblue, 2 % β-Mercaptoethanol (pH 6.8)

10x SDS-PAGE running buffer

250 mM Tris/HCl, 1.92 M Glycine, 1 % SDS

Sephadex G50

30 g Sephadex G50, 300 ml TE buffer

incubation over night at room temperature, replace excess TE buffer with fresh buffer (1:1), autoclave for 20 min at 120°C

20x SSC

3 M NaCl, 0.3 M trisodium citrate

SYBR Safe

1:10000 in agarose gel

TAE

40 mM Tris-Acetat (pH 8,0), 1 mM EDTA, autoclave for 20 min at 120°C

TBST

0,01 M Tris-HCl (pH 7.5), 0,15 M NaCl, 0.01% Tween20

TE

10 mM Tris-HCL (pH 8,0), 1 mM EDTA, autoclave for 20 min at 120°C

Transfer buffer

25 mM Tris, 150 mM Glycine, 10 % Methanol

4.2.2 Solutions and chemicals

Alkalische Shrimp-Phosphatase (SAP)	Roche
Amiloride	Sigma
Complete protease inhibitors	Roche
DAPI-Fluoromount G	Biozol
Dexamethasone	Sigma
Digitonin	Invitrogen
2-log DNA ladder, 1kb DNA ladder	NEB
ER-Tracker	Invitrogen
Ethanol	Roth
Furosemide	Sigma
G418	Invitrogen
GoTaq	Promega
Hematoxylin	Merck
Isopropanol	Roth
LysoTracker	Invitrogen
Methanol	Roth
MitoTracker	Invitrogen
NovaRed	Vector Laboratories

PCR Nucleotide Mix	Roche
Phalloidin-TRITC	Invitrogen
Pfu Polymerase	Fermentas
Precision Plus Protein All Blue Standard	BioRad
Proteinase K	Sigma
QuickHyb	Stratagene
Restriction endonucleases	NEB
RNase A	Sigma
Saccharose	Roth
T4 DNA Ligase	Roche
T4 Polynucleotide kinase	Roche
Trypsin	Sigma + Invitrogen

4.2.3 Solutions for isolation of DNA from bacteria

Solution I

50 mM glucose, 25 mM Tris-Cl (pH 8.0), 10 mM EDTA (pH 8.0),
Solution I is autoclaved and stored at 4°C.

Solution II

0.2 N NaOH (freshly diluted from a 10 N stock), 1% (w/v) SDS
Solution II is freshly prepared. and used at room temperature.

Solution III

3 M potassium acetate, 5M glacial acetic acid, in ddH_2O
The solution is stored at 4°C and cooled on ice just before utilization.

4.2.4 Media

4.2.4.1 Media for bacterial culture

LB Medium

Dissolve 25 g/l LB broth powder in ddH_2O and autoclave the solution.

LB Agar Plates

Dissolve 25 g LB broth powder and 15 g agar technical in 1 l ddH_2O and autoclave the solution. Let cool down to 60°C, add antibiotics, and pour the liquid agar into 10cm dishes.

4.2.4.2 Media for cell culture

M-1 1:1 mixture of DMEM : Ham's F12, 5% FBS, 2 mM L-glutamine, 5 µM dexamethasone

HM-1 GMEM, 10 % ES-FBS, 1 % L-glutamine, 1 % non-essential-amino-acids, 1 % aodium pyruvate, 1 % penicillin/streptomycin, 0.1 % β-mercaptoethanol, 0.1 % LIF (provided by AG Willecke)

gelantine	1 % in ES-H_2O, autoclaved, mixed, then autoclaved again working solution: 0.1%
ES-trypsin	10 % chicken serum, 5 % of 2.5 % trypsin, 6.33 mM EDTA in ES-PBS (pH 8.0, autoclaved), in ES-PBS

4.4 Kits

BCA Protein Assay	Pierce
ECL Western Blotting Substrate	Pierce
iQ™ SYBR Green Supermix	BioRad
Multiprime-DNA labelling system	Amersham
NucleoSpin Extract II	Macherey-Nagel
NucleoSpin RNA II	Macherey-Nagel
Nucleobond PC 100 (Midi)	Macherey-Nagel
Nucleobond PC 500 (Maxi)	Macherey-Nagel
QuantiTect, Reverse Transcription Kit	Qiagen

4.5 Antibodies

4.5.1 Primary antibodies

Antibody	Species	Method	Company
Actin	mouse	WB (1:5000)	Novus Biologicals
GFP	mouse	WB (1:800)	Santa Cruz
GFP	rabbit	IHC (1:400)	Invitrogen
HSP70	mouse	WB (1:2000)	Stressgen
aENaC	rabbit	WB (1:100)	Sigma

4.5.2 Secondary antibodies

Antibody	Species	Method	Company
α-mouse	Donkey	WB (1:15000)	Santa Cruz
α-rabbit	Donkey	WB (1:15000)	Santa Cruz
α-rabbit	Donkey	IHC (1:200)	Santa Cruz

4.6 Oligonucleotides

Lyophilized oligonucleotides were purchased at Invitrogen. They were diluted with ddH_2O to 100 µM and stored at -20°C.

4.5.1 Quantitative real-time PCR primer

Gene	Forward primer	Reverse primer
Agtr1a	tggctgaagccagtaccag	tgccagccattttataccaa
Akr1b3	agaagctcaaggagcaggtg	tgcaggtcgctcagtgtct
Aldob	ttgttgccaatgggaagg	atcctttgcaggcggttt
Aqp2	tcgagctgccttctacgtg	gctgttgcattgttgtggag
Atp1a1	gaaccaggtgaaccccaga	tgtgtggtaccgcaagatgt
Dnajc4	cctgcactatgttgccttca	tccggtccttttcatccat
Dnajc12	ggccgactcagtgaaaactt	actgagctggtgaacgtctg
Dnajc14	aaggaggcaatgaacacgat	ccggtccatttcaaacctc
Dnajc15	ccgacatcgaccacacag	aacagctgcaacacctagtcc
Dnajc19	tcagagcctaccaaaatctgc	tccctttattggcagtaggg
Dnajc22/1	aggcaatggctgttctgaag	tggagggtcatccttaggc
Dnajc22/2	gtcggaggtcctggcttc	tcttcattagttgctccttctgg
Dnajc25	cagtgtgtgtgccatttcaa	tggctaggtagctgattgctt
Hprt	tcccagcgtcgtgattagcgatga	aatgtgatggcctcccatctccttcatgacat
Hsp70.1	tccgcaacagtgtcaatagc	cgctagagagtacggattcctg
Nfat5	tcacagacttttcatagagctgga	cagatgtttctctaggtggaggtaa
Ren1	ggaggaagtgttctctgtctactaca	gctacctcctagcaccacctc
Scnn1a	ccaagggtgtagagttctgtga	agaaggcagcctgcagttta
Scnn1b	ttcaactggggcatgacag	ccgatgtccaggatcaactt
Scnn1g	ctgcaatatcaacccctacaagt	gtctagaacatctttgaccccatac
Sgk1	ggactacattaatggtggagagc	agaatcgagcccgtggtt
Slc9a3	tccatgagctgaatttgaagg	tacttggggagcgaatgaag
Slc12a1	catggcattcattctcatcg	aggcatggaaacaggagaaa
Slc12a2	ttgtcggattcgcagagac	aatggctccaataattcggata
Slc12a3	aaggctatggcaagaacagg	gggcgatggtgttaagttca
Slc14a2	cccacagtggagctctttg	gaccatggagctctgaatcc
Slc26a7	tggagacctagacaccgaaaa	ctggccttgctcaaattctt

4.5.2 Primer for cloning

Name	Sequence
5'-ApaI-mC22	tagggccccaccatggccaaagggctgctgatg
mC22-no stop BamHI-3'	tggatccgcggatgctctaggcttcttggg

4.5.3 Genotyping primer

Name	Sequence
geno_F	acctcagcacttgaggaggtaggg
geno_R1	taggtcatcagcagccccttggcc
geno_R2	ccggtggtgcagatgaacttcagg
3'ES_F	agcaaagaccccaacgagaaga
3'ES_R	ggttctcagtgtctcaggggta

4.6 Plasmids

Name	Origin
CD3δ-CFP	H. Lorenz, NIH, Maryland
DNAJC22-GFP	A. Aschenbrenner
Dnajc22 targeting vector	A. Aschenbrenner
pMJ-Green	AG Willecke, Bonn
mini-phage λ	extracted from DY380 after heat-induction
YFP-CD3δ	H. Lorenz, NIH, Maryland

4.7 Bacterial strains

Name	Genotype	Origin
DH5α	F- endA1 deoR (φ80lacZΔM15) recA1 gyrA (Nalr) thi-1 hsdR17(rK-, mK+) supE44 relA1 Δ(lacZYA-argF)U169	Stratagene
DH10B	F- mcrA Δ(mrr-hsdRMS-mcrBC) φ80lacZΔM15 ΔlacX74 recA1 endA1 araD139 Δ(ara, leu)7697 galU galK λ-rpsL nupG	Geneservice Limited (BAC host strain)
DY380	as DH10B, λ-Red+	kindly provided by Joachim Degen (AG Willecke)
EL350	as DY380, araC-P_{BAD}-Cre	
EL250	as DY380, araC-P_{BAD}	

4.8 Cell lines

M-1 cells were obtained from the European Collection of Cell Cultures (Catalogue number 95092201).

HM-1 embryonic stem cells were kindly provided by AG Willecke.

5 Methods

5.1 Working with bacteria

The standard bacteria strain (DH5α) was cultured at 37°C. Recombination-competent strains, as DY380, EL 250, EL350, or strains transfected with the mini-phage λ, were maintained at 32°C. A 15 min heat shock at 42°C, followed by cooling in ice water, is used to induce the recombination functions.

5.1.1 Photometric quantitation of bacteria

Using a spectrophotometer, the concentration of a bacterial culture can be determined by measuring the optical density at 600 nm (OD_{600nm}) relative to plain culture medium.

5.1.2 Preparation of electrocompetent bacteria

After an overnight pre-incubation of a single colony of the desired bacterial strain in 5 ml LB medium containing appropriate antibiotics, the pre-culture is inoculated in 100 ml fresh, LB selection medium until an OD_{600nm} = 0.6-0.8 is reached. If Cre- or FLP-induction is desired (EL350 and EL250 strain, respectively), the bacteria are cultured with 0.1% (w/v) L-arabinose from OD_{600nm} = 0.4 onwards. When needed, the mini-phage λ was activated at OD_{600nm} = 0.6-0.8 by a 15 min incubation at 42°C, followed by cooling in ice water. Otherwise, the culture is directly cooled in ice water for 20 min. In series of centrifugation steps, the bacteria are washed with a 10% glycerol solution (10 min at 2900 g, 4000 g, 5750 g, 7250, and 9000g, 4°C). After the last centrifugation step, the pellet is resuspended 150 µl 50% glycerol solution, aliquoted (25µl), frozen in liquid nitrogen, and stored at -80°C.

5.1.3 Transformation

5.1.3.1 Electroporation

Electrocompetent bacteria are thawed on ice and carefully mixed with the precooled, diluted DNA (50 to 100 ng, salt-free!). Electroporation is executed in a pre-cooled, 1 cm cuvette at 1.8 kV. The afterwards displayed time should not exceed 3 ms. After resuspension of the bacteria in 1 ml ice-cold LB medium, incubated at 32°C for one hour (shaking), streaked out on LB agar plates containing the appropriate antibiotics, and incubated over night at 32°C.

5.1.3.1 Chemical transformation of competent DH5α

Competent DH5α are thawed on ice and carefully mixed with the pre-cooled DNA (10-20 µl). After a 5-30 min incubation on ice, a 42°C-heat shock is performed for 45 s, followed by an

15 min incubation on ice. After the addition of 400 µl LB medium, the suspension is cultured (shaking) at 37°C for one hour, subsequently streaked out on LB agar plates containing the corresponding antibiotic, and incubated overnight at 37°C.

5.1.4 Preparation of glycerol stocks

150 µl glycerol are added to 850 µl bacterial culture and frozen in liquid nitrogen. These stocks can be stored at -80°C.

5.2 Working with nucleic acids

5.2.1 RNA extraction

The isolation of RNA was performed using the NucleoSpin RNA II kit from Macherey & Nagel following the manufacturers' instructions.

5.2.2 Reverse transcription of RNA into cDNA

cDNA synthesis was performed using the Qiagen QuantiTect reverse transcription kit including rDNaseI treatment following the manufacturer's instructions. 500 ng RNA were used in a 10 µl reaction that was afterwards filled up to 50 µl with ddH_2O.

5.2.2 DNA extraction

5.2.2.1 Isolation of plasmid DNA from bacteria

Single bacterial colonies are inoculated in 2-3 ml of LB medium containing the appropriate antibiotics and incubated overnight at 37°C with vigorous shaking. 1.5 ml of the culture are transferred to a reaction tube and centrifuged at maximum speed for 30 s at 4°C on the next day. The supernatant is completely removed and the pellet thoroughly resuspended in 100 µl of ice-cold solution I. Next, 200 µl of freshly prepared solution II are added and gently mixed by inverting several times. 150 µl of solution III are added and the mixture is inverted several times again. After an 3-5 min incubation on ice, it is centrifuged at maximum speed for 5 min (4°C) and the supernatant transferred to a fresh reaction tube. The DNA is precipitated with 900 µl Ethanol and centrifuged at maximum speed for 30 min (4°C). The DNA pellet is washed once with 70% ethanol, air-dried and resuspended in 50 µl ddH_2O.

For the isolation of larger amounts of plasmid DNA, the NucleoSpin Plasmid kits from Macherey & Nagel (midi or maxi) were used according the manufacturers' instructions.

5.2.2.2 Genomic DNA preparation from tissue culture cells

Pre-warmed (37°C) 1.5 ml proteinase K buffer are added to the cells in a T25 flask. After a 30-60 min incubation on a shaker at room temperature, the suspension is transferred into a

falcon and incubated for another 20-24 h at 55°C (slowly rocking). 2.4 ml phenol/chloroform (1:1) are added, the suspension is gently mixed and centrifuged for 5 min at 4300 rpm. The supernatant is transferred to a new reaction tube and the phenol/chloroform extraction is repeated. Then, the aqueous phase is extracted twice with 0.8 Vol chloroform. The DNA is precipitated by adding 1/10 Vol 3M NaOAc and 0.7 Vol isopropanol. After an 5-10 min centrifugation at 4300 rpm, the pellet is washed twice with 1 ml 70% ethanol, air-dried, resuspended overnight in a 55°C water bath in 0.5 ml TE, and stored at 4°C.

DNA exptraction from ES cell clones is performed with one third of the cells when splitting from 48 to 24 wells. The cells are pelleted and incubated with 50 µl proteinase K buffer overnight in a 55°C water bath.

5.2.2.3 Genomic DNA extraction from tail tips

Murine tail tips are incubated overnight in 400 µl Laird buffer in a 55°C water bath. The next day, after a 5min centrifugation at full speed, the supernatant is transferred into a new tube and the DNA is precipitated by addition of 900 µl isopropanol. The DNA pellet is washed with 1 ml 70% ethanol, air-dried and resuspended in 100µl ddH_2O in a 55°C water bath.

5.2.2.3 DNA extraction from agarose gel

The NucleoSpin Extract II Kit (Macherey-Nagel) was used according to the manufacturers' manual to purify DNA from agarose gels. Briefly, the bands containing the desired DNA are excised, melted in binding buffer, and added to the column. After a 1 min centrifugation at 11000 rpm, the column is washed, dried, and the DNA subsequently eluted in an appropriate amount of ddH_2O (15-50 µl).

5.2.3 Quantitation of nucleic acids

1 µl of a RNA or DNA solution is measured with a microvolume spectrophotometer (1 µl ddH_2O serves as blank).

5.2.4 PCR-based methods

5.2.4.1 Cloning PCR

For amplification of DNA fragments for subsequent cloning the proof-reading *Pfu* polymerase was used. The reaction was set up according to the manufacturer's specifications

Component	Vol / 25 µl reaction
Template DNA	25 pg-0.5 µg
10 mM dNTPs	0.5 µl
Forward primer	0.05-0.5 µM
Reverse primer	0.05-0.5 µM
10x *Pfu* buffer	2.5 µl
Pfu Polymerase	0.6-1.25 U
H_2O	variable

and the PCR performed after the following program:

Step	Temp. C°	Time	Cycles
Initial denaturation	95	1-3 min	1
Denaturation	95	30 s	
Annealing	T_m-5	30 s	25-35
Extension	72	2 min / kb	
Final extension	72	5-15 min	1

Using genomic or genomic or BAC DNA as a template, 30 to 35 cycles are performed whereas for an amplification from a vector 25 cycles are sufficient.

After the PCR, DNA fragments are separated by gel electrophoresis, purified from the agarose gel and used for cloning.

5.2.4.2 Genotyping PCR

For genotyping PCRs of tail DNA samples, the GoTaq polymerase is used in the following protocol:

Component	Vol / 25 µl reaction
Tail DNA	1 µl
dNTPs (10 mM)	0.15 µl
Forward primer (100µM)	0.12 µl
Reverse primer (100µM)	0.12 µl
5x GoTaq buffer	5 µl
GoTaq Polymerase (5U/µl)	0.08 µl
H_2O	16.53 µl

and the PCR performed after the following program:

Step	Temp. C°	Time	Cycles
Initial denaturation	95	3 min	1
Denaturation	95	30 s	
Annealing	66.6	30 s	25-35
Extension	72	30 s	
Final extension	72	2 min	1
Storage	12	∞	

Primer for *Dnajc22* genotyping: geno_F & geno_R1 for the WT allele (438 bps) / presence of the 5' loxP site (525 bps), geno_F & geno_R2 for the KO allele (654 bps)

5.2.4.3 Quantitative real-time PCR

Primers for quantitative real-time PCR were designed with the Universal ProbeLibrary Assay Design Center from Roche Applied Science for use at an annealing temperature at 59°C, and tested for efficiency before use.

Condition	Range	Optimum
Primer length	18-25 bp	20 bp
Product length	75-150 bp	120 bp
Melting temperature	57-61 °C	59 °C
% GC (of total)	40-60	50

A dilution series of cDNA to 1:125 was tested as template and primers, which were used later on, showed an efficiency of at least 80%. To verify that no primer dimer formation disturbs the quantification by SYBR Green signal, melt curve analysis were performed for each primer pair. Quantitative real-time experiments were performed with the BioRad I-cycler and IQ5 optical system. Samples were tested in duplicates in a reaction volume of 25 µl. Expression was analyzed using the BioRad IQ5 system software. Expression is calculated according to the ΔΔCt-method, normalized to expression of the housekeeping gene *Hprt*, and depicted as relative to a control condition.

Component	Vol / 25 µl reaction
cDNA	1 µl
Forward primer (20µM)	0.5 µl
Reverse primer (20µM)	0.5 µl
SYBR-Green Supermix	11.5 µl
ddH_2O	10.5 µl

and the PCR performed after the following program:

Step	Temp. C°	Time	Cycles
Initial denaturation	95	5 min	1
Denaturation	95	30 s	
Annealing	59	20 s	40
Extension	72	20 s	
Melt Curve	55 to 95 °C (+0.5 °C increase per cycle)	30 s	81

5.2.5 Separation of DNA fragments via gel electrophoresis

0.8-1.5% agarose gels were used to separate DNA according to their size. The agarose is boiled in 1x TAE buffer until it is completely dissolved. SYBR Safe is mixed into the slightly cooled gel (1:10000) and the liquid is poured into the form. The polymerized gel is placed into an electrophoresis chamber, the nucleic acid samples are mixed with the loading dye and loaded into the pockets of the gel. A DNA ladder is run concomitantly to serve as a marker of size. After sufficient separation (midi gel 30-45 min at 100V), the DNA can be visualized under UV light.

5.2.6 Cloning of DNA fragments

5.2.6.1 Digestion of DNA with restriction endonucleases

1-2 µg DNA are incubated with the restriction endonuclease (3-5 U / µg DNA) and the corresponding buffer in a total volume of 20-30 µl at the indicated incubation temperature, mostly 37°C. After an 2-4 h incubation, the DNA sample is separated by gel electrophoresis and documented or subsequently purified from the agarose. For double digestion with two different enzymes, the buffer recommendations from the manufacturer were used.

5.2.6.2 Dephosphorylation

In order to prevent re-ligation of the linearized vector, the fragments are dephosphorylated by shrimp alkaline phosphatase. The DNA is incubated with 1 U enzyme and the reaction buffer for 30 min at 37°C, followed by a heat-inactivation of the shrimp alkaline phosphatase for 15 min at 65°C.

5.2.6.3 Ligation

The prepared vector and insert are used in molar ratios between 1:2 to 1:5. The reaction is carried out in 20 µl including 1 U T4 Ligase as well as the corresponding ligation buffer and incubated over night at 15°C. The ligation sample is subsequently used for transformation of *E. coli*.

5.2.6.4 DNA sequencing

Sequencing was performed by GATC Biotech. The DNA was prepared according to the requirements of the company and sent in for analysis.

5.2.7 Southern blot

DNA of positive ES cell clones or genomic DNA from mice (liver) were digested with the desired restriction endonuclease (700 ng DNA per digest) and separated by gel electrophoresis (0.7% agarose, midi gel, 40 V). The resulting band pattern was documented next to a fluorescent ruler. The gel was subsequently depurinated for 10 min in 0.25 M HCl (shaking), washed briefly with water, and denatured for 30 min in 1.5 M NaCl + 0.5 M NaOH (shaking). The DNA was then transferred onto a nitrocellulose membrane (Hybond N^+, Amersham). After the blotting, the membrane was washed briefly in 2x SSC and air-dried. For lableling the probes with ^{32}P, approximately 1 µg was cut out of its vector, separated via agarose gel electrophoresis, and purified from the gel (in 30 µl). The labeling reaction was carried out with 50 ng of the probe using the Multiprime-DNA labeling system according to the manufacturer's manual. Afterwards the probe was purified on a Sephadex G50 column, boiled for 5 min and applied to the membranes, which were pre-hybridized for 1 hour at 68°C in 10 ml QuickHyb (Stratagene (rotating)). After a 90 min incubation, the membranes were washed with SSC containing 0.1% SDS in a 68°C water bath (shaking), starting with a 2x solution and lowering the concentration to 0.1x. The radioactivity of the washing solution and the membrane itself is monitored with the Geiger-Müller counter after each washing step until the signal from the membrane is reduced to 200 to 300 cpm. The membrane is then shrinkwrapped and placed in a developing cassette with an itensifying screen in-between two x-ray films and incubated over night at -80°C. Films were developed in a Curix60 developer.

5.3 Working with proteins

5.3.1 Protein extraction

The Precellys homogenizer was used to lyse 1-5 mg tissue in200-500 µl of cold RIPA buffer with complete protease inhibitors. by. After a 10 min centrifugation of the homogenate at maximum speed (4 °C), the supernatant was transferred to a fresh 1.5 ml tube, and stored at -80 °C.

5.3.2 Determining protein concentration (BCA test)

Protein concentrations were determined from crude samples following the manuals instructions of the Pierce BCA Protein Assay Kit. Parts of the samples were incubated with the freshly prepared assay solution, incubated for 30 min at 37°C and measured via OD_{562nm}.

5.3.3 Separation of proteins via SDS-PAGE

SDS polyacrylamide gel electrophoresis under denaturing conditions is used to separate proteins according to their size.

	5% stacking gel (1 ml)
30% acrylamide	0.17 ml
1 M Tris pH 6.8	0.13 ml
10% SDS	10 µl
APS	10 µl
TEMED	1 µl

	12% stacking gel (5ml)
30% acrylamide	1.7 ml
1 M Tris pH 8.8	1.3 ml
10% SDS	50 µl
APS	50 µl
TEMED	3 µl

Loading buffer was added to the lysates, resulting in 1x concentration, and samples were boiled for 5 min, and let cool to room temperature before loading on the gel. Electrophoresis was carried out at 60-90 V.

5.3.4 Western blotting and immunodetection

Proteins were transferred after separation from the SDS gels to PVDF membranes. The membranes were activated in methanol for 1-2 min and equilibrated in transfer buffer before assembling the blot. The membrane and gel sandwich was placed between 2 Whatman paper and sponges on each side and placed in the blotting chamber, in a way that the membrane was oriented towards the anode. An ice-block was added to the tank, the

chamber filled up with buffer, and electro blotting was performed at 100 V for 60 min at 4 °C. After the procedure membranes were stained with Ponceau S to confirm protein transfer. ddH_2O was used for destaining. Membranes were subsequently blocked with 5% milk powder in TBST for at least 60 min at room temperature. Primary antibodies were applied to the membrane in 5% milk powder in TBST and incubated overnight at 4 °C. Next, membranes were washed three times 10 min in TBST and incubated with the second antibody for one hour at room temperature. Membranes were washed again with TBST three times. Signals generated by the HRP-coupled secondary antibody after addition of the ECL substrate were captured on x-ray films and developed in a Curix60 developer.

5.4 Cell culture

M-1 cells were cultured in a 1:1 mixture of DMEM and Ham's F12 containing 5% FCS, 2 mM L-glutamine, and 5 µM dexamethasone at 37 °C and 5% CO_2. Sub-confluent cultures were split 1:5 using 0.25% trypsin/EDTA.

To induce hyperosmotic stress 100 mM NaCl (or other solutes) were added to the medium (control: corresponding amount of water). After an 6 h incubation, the medium was aspirated, lysis was directly applied to the well and RNA was extracted from the cells as described. All wells in the furosemide and amiloride experiments contained the same amount of solvent (DMSO).

5.4.1 Live cell imaging

Cells were grown in 8-well chamber slides. Soluble GFP or DNAJC22-GFP constructs were transfected using Lipofectamine2000 following the manual instructions. After 8-16 hours, cells were treated with Mitotracker, ER-Tracker, or LysoTracker according to the manufacturer's suggestions and cells were imaged at the Zeiss LSM710. For the phalloidin staining, cells were grown and transfected on glass coverslips, fixed at the desired timepoint for 10 min with 4% PFS, washed twice for 10 min in PBS, followed by an incubation with phalloidin-TRITC for 30 min. After two more 10 min washes in PBS, the glass coverslips were mounted with DAPI-Fluoromount G.

5.4.1.1 Fluorescence protease protection assay (FPP)

The CD3δ-YFP and YFP-CD3δ constructs were kindly provided by Holger Lorenz. The assay was performed as published[79]. Trypsin was used at 4 mM, digitonin at 100 µM.

5.4.2 Homologous recombination in ES cell culture

HM-1 embryonic stem (ES) cells were cultured in dishes coated with 0.1% gelatin. Medium was exchanged every 24 hours and cultures were maintained by splitting approximately every three days at 1:4 – 1:6 ratios. Cells are washed twice with PBS before incubation with

trypsin for 5 min at 37°C. Incubations are stopped with full medium and the suspension is for 5 min at 800 rpm. The cell pellet is resuspended in fresh medium and plated on new gelatin-coated dishes (volumes see below).

Trypsinization:

dish	0.1% gelatine	medium	PBS	trypsin	medium to stop
48-Well	100 µl	0.5 ml	0.5 ml	100 µl	0.5 ml
24-Well	250 µl	1.5 ml	1 ml	250 µl	1 ml
12-Well	500 µl	2.5 ml	2 ml	400 µl	1 ml
6-Well	1 ml	6 ml	3 ml	1 ml	4 ml
T 25	3 ml	7 ml	4 ml	1.5 ml	5 ml
T 75	6 ml	25 ml	8 ml	3 ml	7 ml
10 cm	6 ml	10 ml			

5.4.2.1 Electroporation of ES cells

For homologous recombination, ES cells from one confluent grown T75 flask were transfected with 200-350 µg of the linearized targeting construct via electroporation. The cells were counted, diluted to $30x10^6$ per 800 µl, transferred with the DNA to the cuvette and electroporated at 0.8 kV and 3 µF. Cells were left to rest for 10 min at room temperature and subsequently plated on 22 10 cm dishes:

10 cm dish	ml of electroporated cells	cell number
1-4	0.5 ml	750000
5-16	1.0 ml	$1.5 x10^6$
17-20	1.5 ml	$2.2 x10^6$
21 (control)	0.1 ml	$4.0 x10^6$
22 (control)	0.05 ml	$2.0 x10^6$

5.4.2.2 Picking and screening of ES cell clones

From 24 hours after the electroporation onwards, the cells were kept in medium containing 350 µg/ml G418 for negative selection. Untransfected HM-1 cells were plated in control dishes #21+22 and received normal and G418 medium, respectively. Medium was changed every 2-3 days.

Within two weeks ES cell clones grew to a size, at which they were picked with a 200 µl pipet by simultaneous scratching and sucking and transferred into a 48-well plate. Clones were consequently expanded to bigger dishes. At the first splitting to 24-well plates one third of each clone was used for isolation of genomic DNA and PCR screening (see 5.2.2.2).

Component	Vol / 25 µl reaction
ES cell DNA	10 µl
Forward primer (100µM)	0.1 µl
Reverse primer (100µM)	0.1 µl
5x GoTaq buffer	5 µl
10 mM dNTPs	0.2 µl
ddH_2O	10.5 µl

and the PCR performed after the following program:

Step	Temp. C°	Time	Cycles
Initial denaturation	95	3 min	1
Denaturation	95	30 s	
Annealing	61	20 s	40
Extension	72	2 min	
Final extension	72	10 min	1
Storage	12	∞	

ES cell clones were analyzed for the integration of the 5' loxP site and in a second PCR over the 3' homology arm for the correct integration in the genome. Clones that were positive in both PCRs were expanded to several T25 and further analyzed by Southern blot and karyotyping.

5.4.2.3 Karyotyping

One T25 flask of ES cells was incubated with 2 µg/ml colcemid for 1 hour in the incubator and then washed, trypsinized, pelleted, and resuspended in 0.56% KCl. After an incubation for 10 min at room temperature, the cells were washed twice in ice-cold methanol/acetic acid (3:1). Subsequently, cells were dropped from a height of 10-30 cm onto slides causing the nuclei to burst. After air-drying of the slides, they were stained with Giemsa. Chrosmosomes of at least 15 cells per clone were counted to verify the presence of the correct number of chromosomes (40 chromosomes).

Positive ES cell clones were injected into blastocysts by Jürgen Schmidt, HET, University hospital Bonn.

5.5 Histochemistry

Organs slices were fixed in 4% PFA overnight at 4 °C, immersed in 30% sucrose until the tissue sank to the bottom of the tube, and frozen in O.C.T. Tissue-Tek. 8-10 µm cryosections were postfixed in 4% PFA for 5-10 min and washed extensively in PBS. Sections were blocked for endogenous peroxidase activity with 1.2% H_2O_2 in PBS, washed twice for 5 min in PBS, blocked at least 60 min at room temperature with 5% donkey serum in PBS before the first antibody was applied in 2% donkey serum in PBS over night at 4 °C. Subsequently, sections were washed three times for 10 min in PBS followed by incubation with an HRP-secondary antibody for 45-60 min at room temperature. After three 10 min washes with PBS, signal is developed using the NovaRed Peroxidase Substrate Kit for Vector laboratories according to manufacturer's instructions. Sections were briefly counterstained with hematoxylin, washed for 3-5 min in tap water, followed by another 5 min wash in ddH_2O.

5.6 Working with *Mus musculus*

5.6.1 Animal housing

Mice were kept under standard SPF housing conditions with a 12 hour light/dark cycle. Food and water were given *ad libitum*. Genotyping was performed on genomic DNA from tail tips taken at the age of 3-5 weeks at weaning. Primers for genotyping of the *Dnajc22* locus were geno_F, geno_R1, and geno_R2. (Wildtype: 438 bp, flox: 525 bp, knockout: 654 bp).
Control diet contains ~0.2% sodium. For the high salt diet, mice were fed a diet containing >3% sodium for 14 days while receiving water *ad libitum*. Body weight, food and water intake were monitored on day 0 – 3, day 7, and day 14.

5.6.2 Metabolic cages

Mice were house in metabolic cages (Techniplast) for the collection of 24h-urine. Urine was collected under mineral oil to avoid evaporation. Blood was collected while prepping the mice by heart puncture. After incubation at room temperature for 10-15 min, samples were centrifuged for 10 min at 1000 g, and the supernatant taken for analysis. For potassium measurements it was important that the samples were clear, indicating that no red blood cell lysis had occurred. Electrolyte concentrations in serum and urine were measured by the clinical chemistry laboratory of the university hospital.

5.6.3 Blood pressure measurements

Male wildtype and knockout littermates from heterozygous matings were used for these experiments. Blood pressure measurements were performed by Paul Markowski. Briefly, mice were anesthetized with 2-3% isofluran/oxygen (flow 500 ml/min), intubated and mechanically ventilated. The carotic artery is dissected and the pressure-volume loop catheter (Millar instruments) is inserted via a small incision. Peripheral measurements are taken from the aortic arch, while the catheter is inserted further past the aortic valve into the left ventricle for recording intraventricular values.

This methods section was in parts adapted from my diploma thesis[77].

6 References

1. Silbernagl, S. & Despopoulos, A. *Taschenatlas der Physiologie*. 170+280 (Thieme, 2003).

2. Uchida, S., Nakanishi, T., Kwon, H. M., Preston, A. S. & Handler, J. S. Taurine behaves as an osmolyte in Madin-Darby canine kidney cells. Protection by polarized, regulated transport of taurine. *J. Clin. Invest.* **88,** 656–62 (1991).

3. Silbernagl, S. & Despopoulos, A. *Taschenatlas der Physiologie*. 148 (Thieme, 2003).

4. Geddes, C. C. & Baxter, G. M. Renal impairment. *Imaging* **17,** 1–18 (2005).

5. Silbernagl, S. & Despopoulos, A. *Taschenatlas der Physiologie*. 162 (Thieme, 2003).

6. Silbernagl, S. & Despopoulos, A. *Taschenatlas der Physiologie*. 154–6 (Thieme, 2003).

7. Tse, C. M., Brant, S. R., Walker, M. S., Pouyssegur, J. & Donowitz, M. Cloning and sequencing of a rabbit cDNA encoding an intestinal and kidney-specific Na+/H+ exchanger isoform (NHE-3). *J. Biol. Chem.* **267,** 9340–6 (1992).

8. Ponnuchamy, B. & Khalil, R. A. Cellular mediators of renal vascular dysfunction in hypertension. *Am. J. Physiol. Regul. Integr. Comp. Physiol.* **296,** R1001–18 (2009).

9. Silbernagl, S. & Despopoulos, A. *Taschenatlas der Physiologie*. 180 (Thieme, 2003).

10. Giebisch, G. Renal potassium transport: mechanisms and regulation. *Am. J. Physiol.* **274,** F817–33 (1998).

11. Lifton, R. P., Gharavi, A. G. & Geller, D. S. Molecular mechanisms of human hypertension. *Cell* **104,** 545–56 (2001).

12. Lifton, R. P. Molecular genetics of human blood pressure variation. *Science* **272,** 676–80 (1996).

13. Guyton, A. C. Blood pressure control-special role of the kidneys and body fluids. *Science* **252,** 1813–6 (1991).

14. Schultheis, P. J. *et al.* Renal and intestinal absorptive defects in mice lacking the NHE3 Na+/H+ exchanger. *Nat. Genet.* **19,** 282–5 (1998).

15. Noonan, W. T. *et al.* Blood pressure maintenance in NHE3-deficient mice with transgenic expression of NHE3 in small intestine. *Am. J. Physiol. Regul. Integr. Comp. Physiol.* **288,** R685–91 (2005).

16. Li, H. C. *et al.* Proximal tubule specific knockout of the Na^+/H^+ exchanger NHE3: effects on bicarbonate absorption and ammonium excretion. *J. Mol. Med. (Berl).* **91,** 951–63 (2013).

17. Simon, D. B. *et al.* Bartter's syndrome, hypokalaemic alkalosis with hypercalciuria, is caused by mutations in the Na-K-2Cl cotransporter NKCC2. *Nat. Genet.* **13,** 183–8 (1996).

18. Takahashi, N. *et al.* Uncompensated polyuria in a mouse model of Bartter's syndrome. *Proc. Natl. Acad. Sci. U. S. A.* **97,** 5434–9 (2000).

19. Schultheis, P. J. Phenotype Resembling Gitelman's Syndrome in Mice Lacking the Apical Na+-Cl- Cotransporter of the Distal Convoluted Tubule. *J. Biol. Chem.* **273,** 29150–29155 (1998).

20. Simon, D. B. *et al.* Gitelman's variant of Bartter's syndrome, inherited hypokalaemic alkalosis, is caused by mutations in the thiazide-sensitive Na-Cl cotransporter. *Nat. Genet.* **12,** 24–30 (1996).

21. Chang, S. S. *et al.* Mutations in subunits of the epithelial sodium channel cause salt wasting with hyperkalaemic acidosis, pseudohypoaldosteronism type 1. *Nat. Genet.* **12,** 248–53 (1996).

22. Pradervand, S. *et al.* Salt restriction induces pseudohypoaldosteronism type 1 in mice expressing low levels of the beta-subunit of the amiloride-sensitive epithelial sodium channel. *Proc. Natl. Acad. Sci. U. S. A.* **96,** 1732–7 (1999).

23. McDonald, F. J. *et al.* Disruption of the beta subunit of the epithelial Na+ channel in mice: hyperkalemia and neonatal death associated with a pseudohypoaldosteronism phenotype. *Proc. Natl. Acad. Sci. U. S. A.* **96,** 1727–31 (1999).

24. Barker, P. M. *et al.* Role of gammaENaC subunit in lung liquid clearance and electrolyte balance in newborn mice. Insights into perinatal adaptation and pseudohypoaldosteronism. *J. Clin. Invest.* **102,** 1634–40 (1998).

25. Shimkets, R. A. *et al.* Liddle's syndrome: heritable human hypertension caused by mutations in the beta subunit of the epithelial sodium channel. *Cell* **79,** 407–14 (1994).

26. Hansson, J. H. *et al.* Hypertension caused by a truncated epithelial sodium channel gamma subunit: genetic heterogeneity of Liddle syndrome. *Nat. Genet.* **11,** 76–82 (1995).

27. Pradervand, S. *et al.* A mouse model for Liddle's syndrome. *J. Am. Soc. Nephrol.* **10,** 2527–33 (1999).

28. Kahle, K. T. *et al.* WNK4 regulates the balance between renal NaCl reabsorption and K+ secretion. *Nat. Genet.* **35,** 372–6 (2003).

29. Lalioti, M. D. *et al.* Wnk4 controls blood pressure and potassium homeostasis via regulation of mass and activity of the distal convoluted tubule. *Nat. Genet.* **38,** 1124–32 (2006).

30. Kahle, K. T., Ring, A. M. & Lifton, R. P. Molecular physiology of the WNK kinases. *Annu. Rev. Physiol.* **70,** 329–55 (2008).

31. Wilson, F. H. *et al.* Human hypertension caused by mutations in WNK kinases. *Science* **293,** 1107–1112 (2001).

32. Yang, C.-L., Angell, J., Mitchell, R. & Ellison, D. H. WNK kinases regulate thiazide-sensitive Na-Cl cotransport. *J. Clin. Invest.* **111,** 1039–45 (2003).

33. Shibata, S., Zhang, J., Puthumana, J., Stone, K. L. & Lifton, R. P. Kelch-like 3 and Cullin 3 regulate electrolyte homeostasis via ubiquitination and degradation of WNK4. *Proc. Natl. Acad. Sci. U. S. A.* **110,** 7838–43 (2013).

34. Boyden, L. M. *et al.* Mutations in kelch-like 3 and cullin 3 cause hypertension and electrolyte abnormalities. *Nature* **482,** 98–102 (2012).

35. Jose, P. A., Soares-da-Silva, P., Eisner, G. M. & Felder, R. A. Dopamine and G protein-coupled receptor kinase 4 in the kidney: role in blood pressure regulation. *Biochim. Biophys. Acta* **1802,** 1259–67 (2010).

36. Kusche-Vihrog, K. & Oberleithner, H. An emerging concept of vascular salt sensitivity. *F1000 Biol. Rep.* **4,** 20 (2012).

37. Titze, J. & Machnik, A. Sodium sensing in the interstitium and relationship to hypertension. *Curr. Opin. Nephrol. Hypertens.* **19,** 385–92 (2010).

38. Jeggle, P. *et al.* Epithelial sodium channel stiffens the vascular endothelium in vitro and in Liddle mice. *Hypertension* **61,** 1053–9 (2013).

39. Wiig, H. *et al.* Immune cells control skin lymphatic electrolyte homeostasis and blood pressure. *J. Clin. Invest.* **123,** 2803–15 (2013).

40. Machnik, A. *et al.* Macrophages regulate salt-dependent volume and blood pressure by a vascular endothelial growth factor-C-dependent buffering mechanism. *Nat. Med.* **15,** 545–52 (2009).

41. Machnik, A. *et al.* Mononuclear phagocyte system depletion blocks interstitial tonicity-responsive enhancer binding protein/vascular endothelial growth factor C expression and induces salt-sensitive hypertension in rats. *Hypertension* **55,** 755–61 (2010).

42. Silbernagl, S. & Despopoulos, A. *Taschenatlas der Physiologie*. 377 (Thieme, 2003).

43. Brocker, C., Thompson, D. C. & Vasiliou, V. The role of hyperosmotic stress in inflammation and disease. *Biomol. Concepts* **3,** 345–364 (2012).

44. Burg, M. B., Ferraris, J. D. & Dmitrieva, N. I. Cellular response to hyperosmotic stresses. *Physiol. Rev.* **87,** 1441–74 (2007).

45. Alfieri, R. R. & Petronini, P. G. Hyperosmotic stress response: comparison with other cellular stresses. *Pflugers Arch.* **454,** 173–85 (2007).

46. McManus, M. L., Churchwell, K. B. & Strange, K. Regulation of cell volume in health and disease. *N. Engl. J. Med.* **333,** 1260–6 (1995).

47. Yancey, P. H. Organic osmolytes as compatible, metabolic and counteracting cytoprotectants in high osmolarity and other stresses. *J. Exp. Biol.* **208,** 2819–30 (2005).

48. Beck, F.-X. & Neuhofer, W. Response of renal medullary cells to osmotic stress. *Contrib. Nephrol.* **148,** 21–34 (2005).

49. Miyakawa, H., Woo, S. K., Dahl, S. C., Handler, J. S. & Kwon, H. M. Tonicity-responsive enhancer binding protein, a rel-like protein that stimulates transcription in response to hypertonicity. *Proc. Natl. Acad. Sci. U. S. A.* **96,** 2538–42 (1999).

50. Woo, S. K., Lee, S. Do, Na, K. Y., Park, W. K. & Kwon, H. M. TonEBP/NFAT5 stimulates transcription of HSP70 in response to hypertonicity. *Mol. Cell. Biol.* **22,** 5753–60 (2002).

51. Shim, E.-H. *et al.* Targeted disruption of hsp70.1 sensitizes to osmotic stress. *EMBO Rep.* **3,** 857–61 (2002).

52. Cohen, D. M., Wasserman, J. C. & Gullans, S. R. Immediate early gene and HSP70 expression in hyperosmotic stress in MDCK cells. *Am. J. Physiol.* **261,** C594–601 (1991).

53. Nylandsted, J., Jäättelä, M., Hoffmann, E. K. & Pedersen, S. F. Heat shock protein 70 inhibits shrinkage-induced programmed cell death via mechanisms independent of effects on cell volume-regulatory membrane transport proteins. *Pflugers Arch.* **449,** 175–85 (2004).

54. Lee, J.-S., Lee, J.-J. & Seo, J.-S. HSP70 deficiency results in activation of c-Jun N-terminal Kinase, extracellular signal-regulated kinase, and caspase-3 in hyperosmolarity-induced apoptosis. *J. Biol. Chem.* **280,** 6634–41 (2005).

55. Garcia-Perez, A. *et al.* Molecular cloning of cDNA coding for kidney aldose reductase. Regulation of specific mRNA accumulation by NaCl-mediated osmotic stress. *J. Biol. Chem.* **264,** 16815–16821 (1989).

56. Cowley, B. D., Ferraris, J. D., Carper, D. & Burg, M. B. In vivo osmoregulation of aldose reductase mRNA, protein, and sorbitol in renal medulla. *Am. J. Physiol.* **258,** F154–61 (1990).

57. Yamauchi, A. *et al.* Cloning of a Na(+)- and Cl(-)-dependent betaine transporter that is regulated by hypertonicity. *J. Biol. Chem.* **267,** 649–52 (1992).

58. Uchida, S., Yamauchi, A., Preston, A. S., Kwon, H. M. & Handler, J. S. Medium tonicity regulates expression of the Na(+)- and Cl(-)-dependent betaine transporter in Madin-Darby canine kidney cells by increasing transcription of the transporter gene. *J. Clin. Invest.* **91,** 1604–7 (1993).

59. Kwon, H. M. *et al.* Cloning of the cDNa for a Na+/myo-inositol cotransporter, a hypertonicity stress protein. *J. Biol. Chem.* **267,** 6297–301 (1992).

60. Yamauchi, A., Uchida, S., Preston, A. S., Kwon, H. M. & Handler, J. S. Hypertonicity stimulates transcription of gene for Na(+)-myo-inositol cotransporter in MDCK cells. *Am J Physiol Ren. Physiol* **264,** F20–23 (1993).

61. Caplan, A. J., Cyr, D. M. & Douglas, M. G. Eukaryotic homologues of Escherichia coli dnaJ: a diverse protein family that functions with hsp70 stress proteins. *Mol. Biol. Cell* **4,** 555–63 (1993).

62. Kampinga, H. H. & Craig, E. A. The HSP70 chaperone machinery: J proteins as drivers of functional specificity. *Nat. Rev. Mol. Cell Biol.* **11,** 579–92 (2010).

63. Cheetham, M. E. & Caplan, A. J. Structure, function and evolution of DnaJ: conservation and adaptation of chaperone function. *Cell Stress Chaperones* **3,** 28–36 (1998).

64. Hageman, J. & Kampinga, H. H. Computational analysis of the human HSPH/HSPA/DNAJ family and cloning of a human HSPH/HSPA/DNAJ expression library. *Cell Stress Chaperones* **14,** 1–21 (2009).

65. Ohtsuka, K. & Hata, M. Mammalian HSP40/DNAJ homologs: cloning of novel cDNAs and a proposal for their classification and nomenclature. *Cell Stress Chaperones* **5,** 98–112 (2000).

66. Hennessy, F., Cheetham, M. E., Dirr, H. W. & Blatch, G. L. Analysis of the levels of conservation of the J domain among the various types of DnaJ-like proteins. *Cell Stress Chaperones* **5,** 347–58 (2000).

67. Vos, M. J., Hageman, J., Carra, S. & Kampinga, H. H. Structural and functional diversities between members of the human HSPB, HSPH, HSPA, and DNAJ chaperone families. *Biochemistry* **47,** 7001–11 (2008).

68. Kampinga, H. H. *et al.* Guidelines for the nomenclature of the human heat shock proteins. *Cell Stress Chaperones* **14,** 105–11 (2009).

69. Rauch, J. N. & Gestwicki, J. E. Binding of Human Nucleotide Exchange Factors to Heat Shock Protein 70 (Hsp70) Generates Functionally Distinct Complexes In Vitro. *J. Biol. Chem.* (2013). doi:10.1074/jbc.M113.521997

70. Behr, M., Wingen, C., Wolf, C., Schuh, R. & Hoch, M. Wurst is essential for airway clearance and respiratory-tube size control. *Nat. Cell Biol.* **9,** 847–53 (2007).

71. Stümpges, B. & Behr, M. Time-specific regulation of airway clearance by the Drosophila J-domain transmembrane protein Wurst. *FEBS Lett.* **585,** 3316–21 (2011).

72. Wingen, C., Aschenbrenner, A. C., Stümpges, B., Hoch, M. & Behr, M. The Wurst protein: a novel endocytosis regulator involved in airway clearance and respiratory tube size control. *Cell Adh. Migr.* **3,** 14–8 (2009).

73. Hummler, E. *et al.* Early death due to defective neonatal lung liquid clearance in alpha-ENaC-deficient mice. *Nat. Genet.* **12,** 325–8 (1996).

74. Olver, R. E., Walters, D. V & M Wilson, S. Developmental regulation of lung liquid transport. *Annu. Rev. Physiol.* **66,** 77–101 (2004).

75. Liu, L., Johnson, W. a & Welsh, M. J. Drosophila DEG/ENaC pickpocket genes are expressed in the tracheal system, where they may be involved in liquid clearance. *Proc. Natl. Acad. Sci. U. S. A.* **100,** 2128–33 (2003).

76. Ensembl database. at <http://www.ensembl.org/Mus_musculus/Gene/Compara_Ortholog?db=core;g=ENSMUSG00000038009;r=15:99093170-99104737>

77. Aschenbrenner, A. C. Functional Analysis of the Novel Endocytosis Regulator Wurst in Murine and Human Cell Systems. (2008).

78. Vihervaara, A. *et al.* Transcriptional response to stress in the dynamic chromatin environment of cycling and mitotic cells. *Proc. Natl. Acad. Sci. U. S. A.* **110,** E3388–97 (2013).

79. Lorenz, H., Hailey, D. W., Wunder, C. & Lippincott-Schwartz, J. The fluorescence protease protection (FPP) assay to determine protein localization and membrane topology. *Nat. Protoc.* **1,** 276–9 (2006).

80. Court, D. L. *et al.* Mini-λ: a tractable system for chromosome and BAC engineering. *Gene* **315,** 63–69 (2003).

81. Lallemand, Y., Luria, V., Haffner-Krausz, R. & Lonai, P. Maternally expressed PGK-Cre transgene as a tool for early and uniform activation of the Cre site-specific recombinase. *Transgenic Res.* **7,** 105–12 (1998).

82. McMahon, A. P. *et al.* GUDMAP: the genitourinary developmental molecular anatomy project. *J. Am. Soc. Nephrol.* **19,** 667–71 (2008).

83. Harding, S. D. *et al.* The GUDMAP database--an online resource for genitourinary research. *Development* **138,** 2845–53 (2011).

84. Woo, S. K., Lee, S. D., Na, K. Y., Park, W. K. & Kwon, H. M. TonEBP/NFAT5 Stimulates Transcription of HSP70 in Response to Hypertonicity. *Mol. Cell. Biol.* **22,** 5753–5760 (2002).

85. Ares, G. R., Caceres, P. S. & Ortiz, P. A. Molecular regulation of NKCC2 in the thick ascending limb. *Am. J. Physiol. Renal Physiol.* **301,** F1143–59 (2011).

86. Lee, E. C. *et al.* A highly efficient Escherichia coli-based chromosome engineering system adapted for recombinogenic targeting and subcloning of BAC DNA. *Genomics* **73,** 56–65 (2001).

87. Yu, D. *et al.* An efficient recombination system for chromosome engineering in Escherichia coli. *Proc. Natl. Acad. Sci. U. S. A.* **97,** 5978–83 (2000).

88. Knepper, M. A., Saidel, G. M., Hascall, V. C. & Dwyer, T. Concentration of solutes in the renal inner medulla: interstitial hyaluronan as a mechano-osmotic transducer. *Am. J. Physiol. Renal Physiol.* **284,** F433–46 (2003).

89. Davidson, A. J. Mouse kidney development. at <www.stembook.org>

90. Randrianarison, N. *et al.* Low expression of the beta-ENaC subunit impairs lung fluid clearance in the mouse. *Am. J. Physiol. Lung Cell. Mol. Physiol.* **294,** L409–16 (2008).

91. Schild, L. The epithelial sodium channel and the control of sodium balance. *Biochim. Biophys. Acta* **1802,** 1159–65 (2010).

92. Snyder, P. M. *et al.* Mechanism by which Liddle's syndrome mutations increase activity of a human epithelial Na+ channel. *Cell* **83,** 969–78 (1995).

93. Staub, O. *et al.* WW domains of Nedd4 bind to the proline-rich PY motifs in the epithelial Na + channel deleted in Liddle ' s syndrome. **15,** 2371–2380 (1996).

94. Staub, O. *et al.* Regulation of stability and function of the epithelial Na+ channel (ENaC) by ubiquitination. *EMBO J.* **16,** 6325–36 (1997).

95. Ronzaud, C. *et al.* Renal tubular NEDD4-2 deficiency causes NCC-mediated salt-dependent hypertension. *J. Clin. Invest.* **123,** 657–65 (2013).

96. Brooks, H. L. *et al.* Profiling of renal tubule Na+ transporter abundances in NHE3 and NCC null mice using targeted proteomics. *J. Physiol.* **530,** 359–66 (2001).

97. Hadchouel, J. *et al.* Decreased ENaC expression compensates the increased NCC activity following inactivation of the kidney-specific isoform of WNK1 and prevents hypertension. *Proc. Natl. Acad. Sci. U. S. A.* **107,** 18109–14 (2010).

98. Yu, L. *et al.* WNK4 inhibition of ENaC is independent of Nedd4-2-mediated ENaC ubiquitination. *Am. J. Physiol. Renal Physiol.* **305,** F31–41 (2013).

99. Kunzelmann, K. & Mall, M. Electrolyte transport in the mammalian colon: mechanisms and implications for disease. *Physiol. Rev.* **82,** 245–89 (2002).

100. Zeissig, S. *et al.* Altered ENaC Expression Leads to Impaired Sodium Absorption in the Noninflamed Intestine in Crohn's Disease. *Gastroenterology* **134,** 1436–1447 (2008).

101. Wilson, F. H. *et al.* Human hypertension caused by mutations in WNK kinases. *Science* **293,** 1107–12 (2001).

102. Staub, O. *et al.* WW domains of Nedd4 bind to the proline-rich PY motifs in the epithelial Na+ channel deleted in Liddle's syndrome. *EMBO J.* **15,** 2371–80 (1996).

103. Wang, X., Armando, I., Upadhyay, K., Pascua, A. & Jose, P. A. The regulation of proximal tubular salt transport in hypertension: an update. *Curr. Opin. Nephrol. Hypertens.* **18,** 412–20 (2009).

104. Zhang, M.-Z. *et al.* Intrarenal dopamine deficiency leads to hypertension and decreased longevity in mice. *J. Clin. Invest.* **121,** 2845–54 (2011).

105. Zeng, C. *et al.* Dysregulation of dopamine-dependent mechanisms as a determinant of hypertension: studies in dopamine receptor knockout mice. *Am. J. Physiol. Heart Circ. Physiol.* **294,** H551–69 (2008).

106. Bacic, D. *et al.* Dopamine acutely decreases apical membrane Na/H exchanger NHE3 protein in mouse renal proximal tubule. *Kidney Int.* **64,** 2133–41 (2003).

107. Albrecht, F. E. *et al.* Role of the D1A dopamine receptor in the pathogenesis of genetic hypertension. *J. Clin. Invest.* **97,** 2283–8 (1996).

108. Gomes, P. & Soares-da-Silva, P. Upregulation of apical NHE3 in renal OK cells overexpressing the rodent alpha(1)-subunit of the Na(+) pump. *Am. J. Physiol. Regul. Integr. Comp. Physiol.* **290,** R1142–50 (2006).

109. Fahlke, C. & Fischer, M. Physiology and pathophysiology of ClC-K/barttin channels. *Front. Physiol.* **1,** 155 (2010).

110. Estévez, R. *et al.* Barttin is a Cl- channel beta-subunit crucial for renal Cl- reabsorption and inner ear K+ secretion. *Nature* **414,** 558–61 (2001).

111. Jeck, N., Waldegger, P., Doroszewicz, J., Seyberth, H. & Waldegger, S. A common sequence variation of the CLCNKB gene strongly activates ClC-Kb chloride channel activity. *Kidney Int.* **65,** 190–7 (2004).

112. Jeck, N. *et al.* Activating mutation of the renal epithelial chloride channel ClC-Kb predisposing to hypertension. *Hypertension* **43,** 1175–81 (2004).

113. Geller, D. S. A genetic predisposition to hypertension? *Hypertension* **44,** 27–8 (2004).

114. Kokubo, Y. *et al.* Association analysis between hypertension and CYBA, CLCNKB, and KCNMB1 functional polymorphisms in the Japanese population--the Suita Study. *Circ. J.* **69,** 138–42 (2005).

115. Barlassina, C. *et al.* Common genetic variants and haplotypes in renal CLCNKA gene are associated to salt-sensitive hypertension. *Hum. Mol. Genet.* **16,** 1630–8 (2007).

116. Wall, S. M. *et al.* NaCl restriction upregulates renal Slc26a4 through subcellular redistribution: role in Cl- conservation. *Hypertension* **44,** 982–7 (2004).

117. Verlander, J. W. *et al.* Dietary Cl(-) restriction upregulates pendrin expression within the apical plasma membrane of type B intercalated cells. *Am. J. Physiol. Renal Physiol.* **291,** F833–9 (2006).

118. Sindić, A., Chang, M.-H., Mount, D. B. & Romero, M. F. Renal physiology of SLC26 anion exchangers. *Curr. Opin. Nephrol. Hypertens.* **16,** 484–90 (2007).

119. Pedrosa, R., Jose, P. A. & Soares-da-Silva, P. Defective D1-like receptor-mediated inhibition of the Cl-/HCO3- exchanger in immortalized SHR proximal tubular epithelial cells. *Am. J. Physiol. Renal Physiol.* **286,** F1120–6 (2004).

120. Pradervand, S. Dysfunction of the Epithelial Sodium Channel Expressed in the Kidney of a Mouse Model for Liddle Syndrome. *J. Am. Soc. Nephrol.* **14,** 2219–2228 (2003).

121. Van Huysse, J. W., Amin, M. S., Yang, B. & Leenen, F. H. H. Salt-induced hypertension in a mouse model of Liddle syndrome is mediated by epithelial sodium channels in the brain. *Hypertension* **60,** 691–6 (2012).

122. Rubera, I., Hummler, E. & Beermann, F. Transgenic mice and their impact on kidney research. *Pflugers Arch.* **458,** 211–22 (2009).

123. Miyakawa, H., Rim, J. S., Handler, J. S. & Kwon, H. M. Identification of the second tonicity-responsive enhancer for the betaine transporter (BGT1) gene. *Biochim. Biophys. Acta - Gene Struct. Expr.* **1446,** 359–364 (1999).

124. Lee, S. Do *et al.* TonEBP stimulates multiple cellular pathways for adaptation to hypertonic stress: organic osmolyte-dependent and -independent pathways. *Am. J. Physiol. Renal Physiol.* **300,** F707–15 (2011).

125. Lee, H.-W. *et al.* Sequential expression of NKCC2, TonEBP, aldose reductase, and urea transporter-A in developing mouse kidney. *Am. J. Physiol. Renal Physiol.* **292,** F269–77 (2007).

126. Burg, M. B., Garcia-Perez, A. & Burg, B. How tonicity regulates gene expression. *J. Am. Soc. Nephrol.* **3,** 121–7 (1992).

127. Uchida, S., Garcia-Perez, A., Murphy, H. & Burg, M. Signal for induction of aldose reductase in renal medullary cells by high external NaCl. *Am. J. Physiol.* **256,** C614–20 (1989).

128. Lee, S. Do, Choi, S. Y. & Kwon, H. M. Distinct cellular pathways for resistance to urea stress and hypertonic stress. *Am. J. Physiol. Cell Physiol.* **300,** C692–6 (2011).

129. Tian, W. & Cohen, D. M. Urea inhibits hypertonicity-inducible TonEBP expression and action. *Am J Physiol Ren. Physiol* **280,** F904–912 (2001).

130. Cai, Q., Ferraris, J. D. & Burg, M. B. Greater tolerance of renal medullary cells for a slow increase in osmolality is associated with enhanced expression of HSP70 and other osmoprotective genes. *Am. J. Physiol. Renal Physiol.* **286,** F58–67 (2004).

131. Zhang, Z., Yang, X. Y. & Cohen, D. M. Urea-associated oxidative stress and Gadd153/CHOP induction. *Am. J. Physiol.* **276,** F786–93 (1999).

132. Santos, B. C., Chevaile, A., Hébert, M. J., Zagajeski, J. & Gullans, S. R. A combination of NaCl and urea enhances survival of IMCD cells to hyperosmolality. *Am. J. Physiol.* **274,** F1167–73 (1998).

133. Michea, L. *et al.* Cell cycle delay and apoptosis are induced by high salt and urea in renal medullary cells. *Am. J. Physiol. Renal Physiol.* **278,** F209–18 (2000).

134. Cohen, D. M. & Gullans, S. R. Urea selectively induces DNA synthesis in renal epithelial cells. *Am. J. Physiol.* **264,** F601–7 (1993).

135. Tian, W. & Cohen, D. M. Urea stress is more akin to EGF exposure than to hypertonic stress in renal medullary cells. *Am. J. Physiol. Renal Physiol.* **283,** F388–98 (2002).

136. Zhao, H., Tian, W., Xu, H. & Cohen, D. M. Urea signalling to immediate-early gene transcription in renal medullary cells requires transactivation of the epidermal growth factor receptor. *Biochem. J.* **370,** 479–87 (2003).

137. Xu, H. *et al.* EphA2: expression in the renal medulla and regulation by hypertonicity and urea stress in vitro and in vivo. *Am. J. Physiol. Renal Physiol.* **288,** F855–66 (2005).

138. Marciniak, S. J. & Ron, D. Endoplasmic reticulum stress signaling in disease. *Physiol. Rev.* **86,** 1133–49 (2006).

139. Cai, Q., Ferraris, J. D. & Burg, M. B. Greater tolerance of renal medullary cells for a slow increase in osmolality is associated with enhanced expression of HSP70 and other osmoprotective genes. *Am. J. Physiol. Renal Physiol.* **286,** F58–67 (2004).

140. Zhang, Z., Yang, X.-Y. & Cohen, D. M. Urea-associated oxidative stress and Gadd153/CHOP induction. *Am J Physiol Ren. Physiol* **276,** F786–793 (1999).

141. Eickelberg, O., Geibel, J., Seebach, F., Giebisch, G. & Kashgarian, M. K+-induced HSP-72 expression is mediated via rapid Ca2+ influx in renal epithelial cells. *Am J Physiol Ren. Physiol* **281,** F280–287 (2001).

142. Kleyman, T. R. & Cragoe, E. J. Amiloride and its analogs as tools in the study of ion transport. *J. Membr. Biol.* **105,** 1–21 (1988).

143. Nahm, O., Woo, S. K., Handler, J. S. & Kwon, H. M. Involvement of multiple kinase pathways in stimulation of gene transcription by hypertonicity. *Am. J. Physiol. Cell Physiol.* **282,** C49–58 (2002).

144. Christian, M. *et al.* Targeting DNA double-strand breaks with TAL effector nucleases. *Genetics* **186,** 757–61 (2010).

145. Miller, J. C. *et al.* A TALE nuclease architecture for efficient genome editing. *Nat. Biotechnol.* **29,** 143–8 (2011).

146. Mali, P. *et al.* RNA-guided human genome engineering via Cas9. *Science* **339,** 823–6 (2013).

147. Cho, S. W., Kim, S., Kim, J. M. & Kim, J.-S. Targeted genome engineering in human cells with the Cas9 RNA-guided endonuclease. *Nat. Biotechnol.* **31,** 230–2 (2013).

148. Vos, M. J., Hageman, J., Carra, S. & Kampinga, H. H. Structural and functional diversities between members of the human HSPB, HSPH, HSPA, and DNAJ chaperone families. *Biochemistry* **47,** 7001–11 (2008).

149. Butterworth, M. B. Regulation of the epithelial sodium channel (ENaC) by membrane trafficking. *Biochim. Biophys. Acta* **1802,** 1166–77 (2010).

150. Bermak, J. C., Li, M., Bullock, C. & Zhou, Q. Y. Regulation of transport of the dopamine D1 receptor by a new membrane-associated ER protein. *Nat. Cell Biol.* **3,** 492–8 (2001).

151. Kuang, Y.-Q. *et al.* Dopamine receptor-interacting protein 78 acts as a molecular chaperone for CCR5 chemokine receptor signaling complex organization. *PLoS One* **7,** e40522 (2012).

152. Bermak, J. C. & Zhou, Q. Y. Accessory proteins in the biogenesis of G protein-coupled receptors. *Mol. Interv.* **1,** 282–7 (2001).

153. Go, W. Y., Liu, X., Roti, M. A., Liu, F. & Ho, S. N. NFAT5/TonEBP mutant mice define osmotic stress as a critical feature of the lymphoid microenvironment. *Proc. Natl. Acad. Sci. U. S. A.* **101,** 10673–8 (2004).

154. Lim, S. R., Gooi, B.-H. & Gam, L. H. Identification of low abundance proteins in colorectal cancer tissues. *Cancer Biomark.* **12,** 185–98 (2012).

155. Nguyen, H., Odelola, O. A., Rangaswami, J. & Amanullah, A. A review of nutritional factors in hypertension management. *Int. J. Hypertens.* **2013,** 698940 (2013).

156. World Health Organization | Global Health Observatory: Risk factors for Noncommunicable diseases - Raised blood pressure. at <http://www.who.int/gho/ncd/risk_factors/blood_pressure_prevalence_text/en/>

157. Stolarz-Skrzypek, K. *et al.* Fatal and nonfatal outcomes, incidence of hypertension, and blood pressure changes in relation to urinary sodium excretion. *JAMA* **305,** 1777–85 (2011).

158. Carey, R. M. *et al.* Salt sensitivity of blood pressure is associated with polymorphisms in the sodium-bicarbonate cotransporter. *Hypertension* **60,** 1359–66 (2012).

159. Ehret, G. B. *et al.* Genetic variants in novel pathways influence blood pressure and cardiovascular disease risk. *Nature* **478,** 103–9 (2011).

160. Felder, R. A., White, M. J., Williams, S. M. & Jose, P. A. Diagnostic tools for hypertension and salt sensitivity testing. *Curr. Opin. Nephrol. Hypertens.* **22,** 65–76 (2013).

161. Wadei, H. M. & Textor, S. C. The role of the kidney in regulating arterial blood pressure. *Nat. Rev. Nephrol.* **8,** 602–9 (2012).

7 List of figures

8 List of abbreviations

Akr1b3	aldo-keto reductase family 1, member B3 (encodes aldose reductase)
Amp	Ampicillin
AR	aldose reductase (encoded by Akr1b3)
ATF	activating transcription factor
ATP	adenosine triphosphate
AT_1R	angiotensin II receptor type 1
BAC	bacterial artificial chromosome
BCA	bicinchoninic acid assay
BGT1	betaine/γ-aminobutyric acid transporter (encoded by *Slc6a12*)
bp	base pair
BW	body weight
Cas	CRISPR-associated
C22	short for DNAJC22
CFP	cyan fluorescent protein
CD	cluster of differentiation
cDNA	copy DNA
CDS	coding sequence
Cl	chloride
CLC-K	chloride channel, voltage-sensitive, type K
CRISPR	clustered regularly interspaced short palindromic repeats
ctrl	control
CUL3	Cullin 3
DBP	diastolic blood pressure
ddH_2O	double distilled water
D.m.	*Drosophila melanogaster*
DMEM	Dulbecco's Modified Eagle Medium
DNA	desoxyribonucleic acid
DNAJC22	J protein, subfamily C, member 22
dNTPs	deoxyribonucleotide triphosphate
DTA	diphtheria toxin A
dist	distal
e.g.	for expample
EGF	epidermal growth factor
Egr	early growth resonse
ENaC	epithelial sodium channel (encoded by *Scnn1a,b,c*)

ER	endoplasmic reticulum
ES	embryonic stem
F	phenylalanine
FLP	Flippase
FPP	fluorescence protease protection
G	glycine
gDNA	genomic DNA
GFP	green fluorescent protein
GPCR	G protein coupled receptor
GRK4	G protein-coupled receptor kinase type 4
GRP78	78 kDa glucose-regulated protein
H	hydrogen
H_2O	water
HEK	human embryonic kidney
het	heterozygous
HIF	hypoxia inducible factor
HPD	catalytic tripeptide of the J domain (histidine / proline / aspartic acid)
Hprt	*hypoxanthine guanine phosphoribosyl transferase*
HR	homologous region
HRP	horseradish peroxidase
H.s.	*Homo sapiens*
HSC	heat shock cognate protein
HSD	high salt diet
HSF	heat shock factor
HSP	heat shock protein
id	identity
K	potassium
kDa	kilo Dalton
kb	kilobase
KCl	potassium chloride
KO	knockout
KLHL3	Kelch-like 3
KS	kidney-specific
kV	kilovolt
MEFs	mouse embryonic fibroblasts
$MgCl_2$	magnesium chloride
M.m.	*Mus musculus*
mmHg	millimeter mercury
mRNA	messenger RNA
Na	sodium
NaCl	sodium chloride

$NaHCO_3$	sodium bicarbonate
NCC	Na^+-Cl^--symporter (encoded by *Slc12a3*)
n.d.	non-detectable
NEDD4	neural precursor cell expressed, developmentally down-regulated 4
Neo	Neomycin
NFAT5	nuclear factor of activated T cells
NF-κB	nuclear factor of kappa light polypeptide gene enhancer in B cells
NHE3	Na^+/H^+-exchanger 3 (encoded by *Slc9a3*)
NKCC1	Na^+-$2Cl^-$-K^+-symporter 1 (encoded by *Slc12a2*)
NKCC2	Na^+-$2Cl^-$-K^+-symporter 2 (encoded by *Slc12a1*)
n.t.	not tested
OD	optical density
OE-PCR	overlap extension PCR
osm	osmoles
PBS	phosphate buffered saline
PCR	polymerase chain reaction
PGK	phosphoglycerate kinase
PFA	paraformaldehyde
PHA	pseudohypoaldosteronism
Ppk	pickpocket genes (*Drosophila* orthologs of ENaC)
prox	proximal
RNA	ribonucleic acid
RNAi	RNA interference
rpm	rounds per minute
ROMK	renal outer medullary potassium channel
SBP	systolic blood pressure
Scnn1a	sodium channel non-neuronal 1 (encodes α subunit of the ENaC)
Scnn1b	sodium channel non-neuronal 1 (encodes β subunit of the ENaC)
Scnn1c	sodium channel non-neuronal 1 (encodes γ subunit of the ENaC)
SD	standard derivation
SDS	sodium dodecyl sulfate
SEM	standard error of the mean
Sgk1	*serum/glucocorticoid regulated kinase 1*
sim	similarity
siRNA	small interfering RNA
Slc6a12	Solute carrier family 6, member 12 (encodes BGT1)
Slc9a1	Solute carrier family 9, member 1 (encodes NHE1)
Slc9a3	Solute carrier family 9, member 3 (encodes NHE3)
Slc12a1	Solute carrier family 12, member 1 (encodes NKCC2)
Slc12a2	Solute carrier family 12, member 2 (encodes NKCC1)
Slc12a3	Solute carrier family 12, member 3 (encodes NCC)

Slc14a2	Solute carrier family 14, member 2 (encodes rea transporter A1)
Slc26a4	Solute carrier family 26, member 4 (encodes Pendrin)
Slc26a6	Solute carrier family 26, member 6
SMIT	sodium/*myo*-inositol transporter
STAT	signal transducer and activator of transcription
TAUT	taurine transporter
TBS	Tris buffered saline
Temp	temperature
T_m	melting temperature
U	unit
UPR	unfolded protein response
UTR	untranslated region
VEGFC	vascular endothelial growth factor C
v.s.	versus
WNK	with no lysine (K)
WT	wildtype
w/v	weight per volume
YFP	yellow fluorescent protein
Zn	zinc